CR-152354

(NASA-CR-152345) INTRODUCTORY STUDY OF THE CHEMICAL BEHAVIOR OF JET EMISSIONS IN PHOTOCHEMICAL SMOG Final Report (Systems Applications, Inc.) 115 p HC A06/MF A01 CSCL 13B G3/45

N80-21891

Unclas
18200

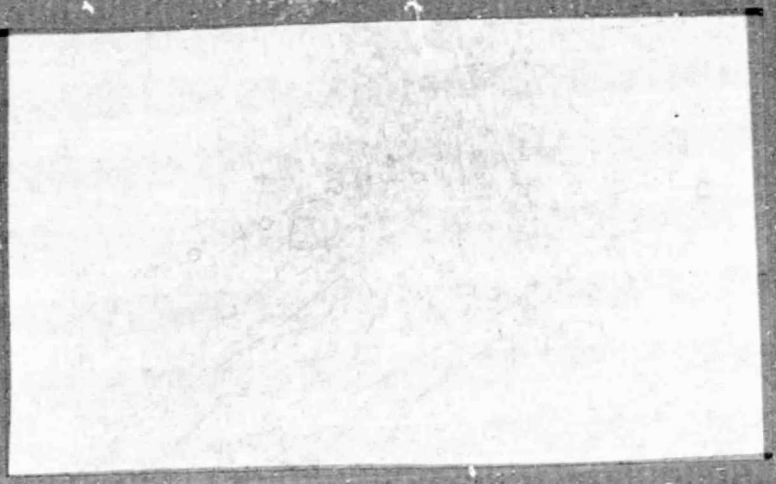

PREPARED BY

SYSTEMS APPLICATIONS, INC.

CR-152354

Final Report

INTRODUCTORY STUDY OF THE CHEMICAL BEHAVIOR OF JET EMISSIONS IN PHOTOCHEMICAL SMOG

Contract No. NAS2-8821

EF76-04R

May 1976

by

Gary Z. Whitten
Henry Hogo

Systems Applications, Incorporated
950 Northgate Drive
San Rafael, California 94903

Prepared for

Ames Research Center
National Aeronautics and Space Administration
Moffett Field, California 94035

and

Federal Aviation Administration
Washington, D. C.

CONTENTS

SUMMARY

The chemical behavior of jet aircraft emissions in the atmosphere was studied using computer simulations of static well mixed air parcels. Emissions data contained in the literature indicate that 85 to 95 percent of the hydrocarbons emitted from jet aircraft in the vicinity of airports are associated with the taxi-idle mode. The types and amounts of compounds present are listed below:

Type	Percent (by volume)	Average Carbon Number
Paraffins	50-60	8
Olefins	15-30	3
Aromatics	7-30	8
Aldehydes	1-17	2

Nitrogen oxide emissions are associated primarily (80 to 90 percent) with the takeoff and climbout modes, and we estimate a 9:1 mole ratio of nitric oxide to nitrogen dioxide. Most significantly, the literature data show that the ratio of hydrocarbons to nitrogen oxides averages nearly 42 moles of carbon (C) per mole of nitrogen oxides (NO_x). Observations at airports confirm this emissions ratio; those data average about 45 moles C per mole NO_x.

The emissions data were used as initial conditions for a series of computer simulations of photochemical smog formation in static air. The chemical kinetics mechanism used in these simulations was an updated version of the Hecht, Seinfeld, and Dodge (1974) mechanism.

This kinetics mechanism contains certain parameters which are designed to account for hydrocarbon reactivity. These parameters were varied to simulate the reaction rate constants and average carbon numbers associated with the jet emissions. The roles of surface effects, variable light sources, NO/NO_2

ratio, continuous emissions, and untested mechanistic parameters were also assessed.

The results of these calculations indicate that the present jet emissions are capable of producing oxidant by themselves. The hydrocarbon/NO_x ratio of present jet aircraft emissions is much higher than that of automobiles. These two ratios appear to bracket the hydrocarbon/NO_x ratio that maximizes ozone production. Hence an enhanced effect is seen in the simulations when jet exhaust emissions are mixed with automobile exhaust emissions.

ILLUSTRATIONS

TABLES

I INTRODUCTION

The formation of photochemical oxidant has long been known to be related to interactions of two classes of primary pollutants, the hydrocarbons and the nitrogen oxides. These pollutants are normally associated with the use of fossil fuels: hydrocarbons from incomplete combustion or fuel leakage and nitrogen oxides from exposure of air to high temperatures. The automobile is recognized as a major source of these primary pollutants in urban areas. However the control of automobile emissions has increased the relative importance of other sources of primary pollutants, such as airports. It is now possible to estimate quantitatively the relative importance of emissions from these other sources because of our understanding of the photochemical processes that lead to oxidant formation. Perhaps more importantly, this new knowledge makes it possible to assess the effects of the mixing of pollutants from a number of sources. Production or destruction of oxidant may be enhanced in an air parcel between two pollutant sources. Knowledge of such enhancement effects would be important for consideration of control strategies proposed for either source or for consideration of the location of sources in an airshed area.

The ratio of hydrocarbons to nitrogen oxides can be an important factor in the production of ozone. Very high or very low ratios can lead to low ozone concentrations. At an intermediate ratio much more ozone can be generated from similar amounts of pollutants. In addition to differing from automobile emissions in hydrocarbon composition, jet aircraft emissions (especially from the idle-taxi mode) have a higher hydrocarbon/NO_x ratio. This report shows that ozone enhancement effects are seen for the combined emissions of jets and automobiles.

The chemical behavior of jet emissions in the production of photochemical smog is to be assessed in this study. However, chemical effects

alone are examined; the impact on air quality of physical processes such as transport, dispersion, and dilution was not studied. The main elements of the effort were:

- Estimation of emissions of jet aircraft--a literature survey of the types of compounds and their relative abundance.
- Simulation of the dynamics of photochemical smog--computer simulations using a generalized kinetic mechanism in static, continuously irradiated air.
- Evaluation and assessment of the sensitivity of the kinetic mechanism--assessment of the impact on oxidant formation of variations in composition of emitted hydrocarbons; determination of sensitivity of prediction to variations in highly uncertain kinetic rate parameters.
- Estimation of ozone formation in air parcels containing mixtures of auto and jet emissions--computer simulations that show enhanced ozone formation resulting from chemical interaction in some cases.

II EXHAUST EMISSIONS IN THE VICINITY OF AN AIRPORT

Major fractions of the local hydrocarbons and nitrogen oxides observed in the vicinity of airports are attributable to emissions from aircraft (see Table 1). Aircraft emit other compounds as well, such as water, carbon monoxide, and hydrogen, but at typical concentration levels these compounds do not affect the formation of photochemical oxidant and are not considered in this study.

Before the effects of aircraft emissions on local air quality can be examined the published data on aircraft exhaust emissions must be converted into concentrations of pollutant species in air. The following data are required:

- The rate of emission of total hydrocarbons, NO, and NO_2 from aircraft engines in the idle, landing, and takeoff modes (the LTO cycle).
- The time spent in each of the modes of operation by different aircraft at typical airports.
- The fraction of the total hydrocarbons represented by each type of hydrocarbon (alkane, alkene, or aromatic).

A. THE LTO CYCLE

Aircraft operations in the immediate vicinity of an airport can be separated into three modes:

- Approach from the inversion base* to landing.
- Landing, idling, and takeoff operations at the airport.
- Climbout from the airport to the inversion base.

*Recent studies by Segal (1975) have shown that a typical worst case height of the inversion base is 150 meters. One kilometer is the value assumed by the Environmental Protection Agency.

Table 1

PORTION OF POLLUTANTS ATTRIBUTABLE TO JET AIRCRAFT EMISSIONS

Airport	Hydrocarbons	Nitrogen Oxides	Reference
Atlanta, Georgia	69 %	78 %	Cirillo et al.(1975)
Los Angeles International	72	---	LAAPCD(1971)
O'Hare International, Chicago*	69.4	74.7	Rote et al.(1973)

*O'Hare International Airport, one of the busiest airports in the world, serves as a central stopping point for passengers making transfers to other flights. Because transfers do not involve automobiles, we expect that the percentage of pollutants due to automobiles should be low compared to other airports. Rote et al. estimated the access vehicle percent at 10 percent.

In order to prevent detonation from a cold running engine, aircraft use an enriched fuel-air mixture during idle and taxi modes. The emissions from aircraft in these modes have high hydrocarbon concentrations and low nitrogen oxide (NO_x) concentrations. During flight, combustion of a normal fuel-air mixture in a hot engine produces emissions having low hydrocarbon concentrations and high NO_x concentrations. Table 2 shows the emissions from different engines in various modes. Although one of the ways to qualitatively characterize an operational mode can be by a hydrocarbon/NO_x ratio, the values of this ratio differ widely for different engines operating in the same mode. The ratio of total hydrocarbon emissions (THC) to NO_x emissions in the taxi mode ranges from 8.0 for an Allison 501-DB engine to 140.0 for a Pratt and Whitney JT-3D engine. A detailed discussion of these ratios will be presented in a later section.

An examination of Table 2 reveals that for most of the engines the largest amounts of hydrocarbon are emitted during the taxi-idle and approach modes. In Table 3, the typical time spent in each of the different opera-

Table 2

EMISSION LEVELS FROM AIRCRAFT ENGINES
IN VARIOUS OPERATIONAL MODES

Engine	Mode	Pollutant Species: HC (moles Carbon per engine)	Pollutant Species: NO_x (moles NO_2 per engine)	THC/NO_x*
Pratt & Whitney	Taxi	617.42	4.16	145
JT-3D	Idle	51.52	0.39	130
	Takeoff	0.76	8.12	0.09
	Approach	181.82	19.3	9.25
Pratt & Whitney	Taxi	67.05	3.58	18.4
JT-8D	Idle	5.68	0.29	19.2
	Takeoff	2.65	4.93	0.53
	Approach	12.12	11.90	1.00
Pratt & Whitney	Taxi	46.97	2.13	21.6
JT-12	Idle	3.79	0.19	19.6
	Takeoff	0.38	1.45	0.26
	Approach	1.14	2.13	0.53
Allison	Taxi	36.36	4.26	8.4
501-DB	Idle	2.65	0.29	8.97
	Takeoff	3.03	0.77	3.87
	Approach	11.74	4.84	2.39
Pratt & Whitney	Taxi	245.45	2.13	113.12
R-2800	Idle	16.29	--	--
	Takeoff	189.39	--	--
	Approach	1091.29	1.74	615.72
Continental	Taxi	18.94	0.19	97.86
IO-520-A	Idle	2.27	--	--
	Takeoff	4.17	--	--
	Approach	25.76	1.74	14.5
General Electric	Taxi	16.29	0.68	23.7
CT-58	Idle	1.14	0.10	11.2
	Takeoff	--	--	--
	Approach	2.27	4.74	0.47

*Ratio of total carbon in moles to total moles of NO_2.

Source: Northern Research (1968)

Table 3

TYPICAL TIME IN MODE FOR LANDING TAKEOFF CYCLE AT A METROPOLITAN AIRPORT

Aircraft	Time in mode--minutes				
	Taxi-idle	Takeoff	Climbout	Approach	Taxi-idle
Jumbo jet	19.00	0.70	2.20	4.00	7.00
Long range jet	19.00	0.70	2.20	4.00	7.00
Medium range jet	19.00	0.70	2.20	4.00	7.00
Air carrier turboprop	19.00	0.50	2.50	4.50	7.00
Business jet	6.50	0.40	0.50	1.60	6.50
General aviation turboprop	19.00	0.50	2.50	4.50	7.00
General aviation piston	12.00	0.30	4.98	6.00	4.00
Piston transport	6.50	0.60	5.00	4.60	6.50
Helicopter	3.50	0	6.50	6.50	3.50
Military transport	19.00	0.50	2.50	4.50	7.00
Military jet	6.50	0.40	0.50	1.60	6.50
Military piston	6.50	0.60	5.00	4.60	6.50

Source: U.S. Environmental Protection Agency (1973).

tional modes is tabulated for different aircraft classes. The table shows that aircraft spend the most operating time at airports in the taxi-idle modes. The data presented in Tables 2 and 3 show that most hydrocarbons emitted from aircraft in the vicinity of an airport are from the taxi-idle modes.

B. HYDROCARBON COMPOSITION OF AIRCRAFT EMISSIONS

The rate of formation of oxidants in photochemical smog depends on the reactivity of the mix of hydrocarbons emitted by the various sources of pollutants. Whereas data on total hydrocarbon emissions from jet engines are plentiful, very little information is available on the quantities of

individual hydrocarbons in the emissions. The most complete examination of hydrocarbon emissions of which we are aware is that of Conkle, Lackey, and Miller (1975). They used a combustor test rig designed to simulate the operating conditions of the T-56 engine used on the C-130 transport. Different operating conditions were simulated by varying the combustor inlet temperature and pressure as shown in Table 4. At a constant inlet pressure, exhaust hydrocarbon compositions were measured for different types of fuels. Table 5 shows these measurements of hot exhaust gas. There can be substantial differences in exhaust emissions from use of the various fuels. The amount of paraffins emitted varied from 1.6 percent for JP8 fuel to 23 percent for JP4 fuel, while aromatics varied from 20 percent fo JP4 fuel to 52 percent for JP5 fuel. Table 6 shows the variation of the percent of the total hydrocarbons in the exhaust under the various operating conditions for JP4 fuel. In most cases, the fraction of the species type varied by less than a factor of 2 over the range of operating conditions for which tests were made. Paraffins, olefins, aromatics, and aldehydes seem to be the major hydrocarbon constituents in the idle mode (corresponding to 15 psig). After adjustment to 100 percent, their respective percentage values are 58, 18, 7, and 17 percent.

Lozano et al. (1968) performed a study on the emissions from T-56-A7, J-57-19W, and TF-33-P5 engines. Their results are presented in Table 7. JP-4 fuel was used throughout their study. The hydrocarbon composition emitted in the idle mode from the T-56 engine contains approximately 62 percent paraffins, 24 percent olefins, 9 percent aromatics, and 5 percent aldehydes. The largest difference between this composition and that reported by Conkle et al. is the percentage of aldehyde, which differs by a factor of 3. The hydrocarbon compositon reported for the exhaust emitted from the J-57 engine in the idle mode contains 49 percent paraffins, 24 percent olefins, 25 percent aromatics, and 2 percent aldehydes. For the TF-33 engine, the corresponding values are 58 percent paraffins, 31 percent olefins, 8 percent aromatics, and 3 percent aldehydes.

Table 4

SINGLE-COMBUSTOR RIG OPERATING CONDITIONS

Nominal Power Setting	Rig Pressure (psig)	Inlet Temp. °C	Fuel/Air Wt. Basis	Fuel
Preliminary	75	93	0.0076	JP4
Moderate PR* Simulated idle	33	166	0.0070	JP4
Low PR Simulated idle	15	93	0.0073	JP4
Moderate PR Simulated idle	33	169	0.0083	JP5
High PR Simulated idle	50	204	0.0079	JP5
Moderate PR Simulated idle	33	164	0.0071	JP4
Moderate PR Simulated idle	33	166	0.0072	JP8
No fuel flow (Background)	33	--	--	--

* PR--pressure ratio.

Source: Conkle, Lackey, and Miller (1975).

Table 5

DISTRIBUTION OF EXHAUST HYDROCARBONS BY LUMPED SPECIES FOR VARIOUS FUELS

	(at 33 PSIG Combustor Pressure)				
Species	JP4*	JP4*	JP5	JP8	No Fuel†
Paraffins	26%	23%	3.4	1.6	0
Olefins	24	20	25	39	0
Diolefins	3.2	0.26	t§	0.45	0
Napthenes	t	2.3	3.8	0.45	0
Aromatics	14	7.2	5.3	2.3	0
Aldehydes	20	21	52	36	0
Alcohols	1.9	3.6	0.57	7.5	82
Ketones	7	7	6.3	10	18
Ethers	1.6	2.1	3.4	2	0
Esters	0	3.1	t	0	0
Nitrogen-containing compounds	1.6	0	0.19	t	0
Halogen-containing compounds	1.6	8.8	0.19	0.23	0
Lactones	0	0	0.19	0.23	
TOTAL HYDROCARBONS	3.17 ppm	3.89 ppm	5.27 ppm	4.41 ppm	0.11 ppm

*Duplicate combustor conditions
†Background sample (no fuel)
§Trace, concentration less than 0.001 ppm

Source: Conkle, Lackey, and Miller (1975)

Table 6

DISTRIBUTION OF EXHAUST HYDROCARBONS BY LUMPED SPECIES AT VARIOUS INLET PRESSURES

Species	Combustor Inlet Pressure (psig) 15	33	33	50	75
Paraffins	51%	23%	26%	31%	27%
Olefins	16	20	24	23	47
Diolefins	0.2	0.2	3	3	t
Napthenes	2	2	t	7	2
Aromatics	6	10	14	5	14
Aldehydes	15	21	20	23	7
Alcohols	2	4	2	0	t
Ketones	3	7	7	t	t
Ethers	1	2	2	3	t
Esters	0	3	0	0	3
Nitrogen-containing compounds	0	0	2	t	0
Halogen-containing compounds	3	9	2	4	t
Lactones	0	0	0	1	0
TOTAL HYDROCARBONS	23.05 ppm	3.87 ppm	3.17 ppm	0.74 ppm	0.59 ppm

Source: Conkle, Lackey, and Miller (1975)

Table 7

POLLUTION EMISSIONS FROM JET AIRCRAFT

Pollutant	Power Setting and Engine Type: Take-off T-56	Take-off J-57	Take-off TF-33	Cruise and approach T-56	Cruise and approach J-57	Cruise and approach TF-33	Idle T-56	Idle J-57	Idle TF-33
Oxygen (%)	--	16.7	17.1	--	17.5	18.0	--	19.0	19.6
Carbon dioxide (%)	4.1	2.3	2.7	3.2	1.5	2.1	2.4	1.0	0.9
Carbon monoxide (ppm)	34	32	7	40	55	30	109	130	195
Oxides of nitrogen as NO_2 (ppm)	43	59	27	27	39	15	12	13	11
Nitric oxide (ppm)	37	44	25	--	30	13	--	8	9
Total hydrocarbons (as C atoms)(ppm)	5.5	5	7	2.5	5	42	101	152	700
Olefins as C atoms (ppm)	--	--	--	--	--	--	25	38	220
Aromatics as C atoms (ppm)	--	--	--	--	--	--	10	39	60
Total aldehydes as HCHO (ppm)	4.1	0.8	0.6	2.0	0.8	0.3	4.8	2.5	21
Formaldehyde (ppm)	1.1	0.5	--	1.9	0.5	--	3.5	2.4	--

Source: Lozano et al. (1968)

In another study (Groth and Robertson, 1974), total and unreactive hydrocarbons were measured under various conditions for several Pratt and Whitney engines currently in operation on many commercial aircraft. The unreactive hydrocarbons consist of paraffins, which are relatively unreactive in smog-producing reactions with NO_x compared to olefins and aldehydes. The results of Groth and Robertson are shown in Tables 8(a) through 8(d). The unreactive hydrocarbons can reach as high as 30 percent during the idle mode (the idle mode is represented by the lower values of engine thrust). Groth and Robertson also determined the percentage of aliphatics, aromatics, and oxygenates in their study. Their results are summarized in Table 9. Since aliphatics contain olefins, alkynes, and diolefins, and oxygenates consist of aldehydes and ketones, we need to know the percentage of alkynes, diolefins, and ketones emitted from these engines. For our study, we assumed the percentages are the same as those for a T-56 engine (Table 6). Using Tables 6 and 9, we calculated the composition of hydrocarbons emitted from a JT-9D engine during the idle mode as 51.3 percent paraffins, 15 percent olefins, 29.4 percent aromatics, and 1.93 percent aldehydes. For a JT-3D engine, the corresponding calculated values are 60.8 percent paraffins, 17.8 percent olefins, 18.3 percent aromatics, and 0.8 percent aldehydes.

The three studies presented in this section are the only studies we were able to find that contained extensive measurements of hydrocarbon compositions. Nevertheless a rather narrow range of hydrocarbon composition is indicated for emissions from different types of engines (e.g., turbojet, turbofan, and conventional jet), different operating conditions (e.g., temperature, fuel-air ratio, and pressure), and different types of fuels (e.g., JP-4, JP-5, and JP-8). In Table 10, we summarize the hydrocarbon compositions from these three studies.

C. AIRCRAFT EMISSIONS OF NITROGEN OXIDES

Aircraft use a higher fuel-air ratio in the taxi-idle mode than in other modes, which leads to low combustion temperatures. Also the amount of nitrogen oxides (NO_x) emitted in the taxi-idle mode is low compared to the amount

Table 8

HYDROCARBON EMISSIONS FROM JET ENGINES AT VARIOUS THRUSTS

(a) JT-9D Engine With JP5 Fuel

Thrust (pounds)	Total Hydrocarbons (ppm)	Unreactive Hydrocarbons	
		ppm	percent
1993 (subidle)	823	361	43.7
2628 (idle)	407	125	30.8
3419	219	58	26.6
9839	89	25	28.1
11236	60	9	15.0
19347	51	7.4	14.5
23165	44	6.5	14.8
28626	36	4.6	12.8

(b) JT-9D Engine With Jet A Fuel

Thrust (pounds)	Total Hydrocarbons (ppm)	Unreactive Hydrocarbons	
		ppm	percent
39622	2.0	0	0
40365	1.5	0	0
42126	1.5	0	0
37568	2.0	0	0
34934	1.8	0	0
15162	3.3	0	0
7100	36.5	4.5	12.3
4000	103.5	15.5	15.0
3040	174	34.5	19.8

(c) JT-3D Engine With Bill Of Materials Burner Cans And JP5 Fuel

Thrust (pounds)	Total Hydrocarbons (ppm)	Unreactive Hydrocarbons	
		ppm	percent
750 (idle)	665	122	18.4
2100	225	53	23.5
7500	30	8	26.7
15800	14	0	0
17900	6	0	0
13000	14	0	0
9950	10	0	0
3000	83	8	9.6
850	655	100	15.3

(d) JT-3D Engine With Smokeless Burner Cans And JP5 Fuel

Thrust (pounds)	Total Hydrocarbons (ppm)	Unreactive Hydrocarbons	
		ppm	percent
750 (idle)	477	125	26.3
2000	110	20	18.2
7500	8	1	12.5
16000	6	0	0
18500	6	0	0
13000	2	0	0
10000	2	0	0
3000	32	8	25.0
850	410	110	26.8

Source: Groth and Robertson (1974).

Table 9

LIQUID CHROMATOGRAPH ANALYSIS OF EXHAUST HYDROCARBONS

Engine Type	Thrust (lb)	Total Hydrocarbons (ppm)	Aliphatics (percent)	Aromatics		Oxygenates	
				$\mu g\ l^{-1}$	(percent)	$\mu g\ l^{-1}$	(percent)
JT-9D	2,702 (sub idle)	155	58.1	61	39.4	3.8	2.5
	27,505	5.4	44.5	2.4	44.4	0.6	11.1
JT-9D	2,700 (sub idle)	170	78.1	33	19.4	4.2	2.5
	12,700	30	43.0	16	53.3	1.1	3.7
JT-3D	700	1200	80.7	220	18.3	12.0	1.0
	3,500	244	78.9	46	18.9	5.3	2.2

* Percent of total hydrocarbons; assumption made that 1 ppm = 1 $\mu l\ l^{-1}$ = 1 $\mu g\ l^{-1}$ for comparison purposes only.

Source: Groth and Robertson (1974).

Table 10

COMPOSITION OF EXHAUST HYDROCARBONS DURING IDLE MODE

(in percent)

Species	Engine Type					
	T-56 Combuster*	T-56-A7†	J-57-19W†	TF-33-P5†	JT-9D§	JT-3D§
Pareffins	58	62	49	58	51.3	60.8
Olefins	18	24	24	31	15	17.8
Aromatics	7	9	25	8	29.4	18.3
Aldehydes	17	5	2	3	1.93	0.8
Fuel used	JP4	JP4	JP4	JP4	JP5	JP5

*Conkle et al. (1975)

†Lozano et al. (1968)

§Groth and Robertson (1974)

of NO_x emitted during the take-off and approach operational modes because of the power requirements involved. Tables 2 and 7 show the amount of NO_x emitted in each of the different operational modes. The combined taxi and idle modes emit the lowest amount of NO_x for the following aircraft engines: Pratt and Whitney JT-3D, Pratt and Whitney JT-8D, and General Electric CT-58. Similar amounts of NO_x are emitted in the different operational modes for the other aircraft classes.

The results of the study by Lozano et al. (1968) (Table 7) show that NO_x emissions are lowest in the idle mode and highest during the take-off mode for the three engines studied. Table 11 presents a summary of emission factors for a number of different aircraft engines compiled by the Environmental Protection Agency (1973). Again, NO_x emissions are lowest during the taxi-idle mode.

As with hydrocarbon compositions, very few studies have been made on the composition of the nitrogen oxides emitted from aircraft engines. The ratio of NO to NO_2 varies between different types of engines. Lozano et al. (1968) reported that most of the NO_x emitted was in the form of nitric oxide (NO); they found that nitric oxide varied from 82 to 93 percent by volume of the total NO_x emitted from a TF-33 engine (Table 7). For the J-57 engine, NO varied from 62 to 76 percent of total NO_x depending on the operational mode. Lozano et al. also found the percent composition of NO was greatest in the take-off mode and lowest in the idle mode.

In a detailed study by Bogdan and McAdams (1971), aircraft exhaust emission measurements performed by different organizations are summarized. NO and NO_2 concentrations were measured individually for many of the test engines. The value of the NO/NO_2 ratio was found to range from approximately 1 to 20 for most engines. Table 12 shows the NO_x emissions for some engines; the average NO/NO_2 ratio is approximately 9.7.

Table 11

MODAL EMISSION FACTORS

Engine mode	Fuel rate lb/hr	Fuel rate kg/hr	Carbon monoxide lb/hr	Carbon monoxide kg/hr	Hydrocarbons lb/hr	Hydrocarbons kg/hr	Nitrogen oxides (NO_x as NO_2) lb/hr	Nitrogen oxides (NO_x as NO_2) kg/hr	Solid particulates lb/hr	Solid particulates kg/hr
Pratt & Whitney JT-9D										
(Jumbo jet)										
Taxi-idle	1,738	788	102.0	46.3	27.3	12.4	6.06	2.75	2.2	1.0
Takeoff	17,052	7,735	8.29	3.76	2.95	1.34	720.0	327.0	3.75	1.7
Climbout	14,317	6,494	11.7	5.31	2.65	1.20	459.0	208.0	4.0	1.8
Approach	5,204	2,361	32.6	14.8	3.00	1.36	54.1	24.5	2.3	1.0
General Electric CF6										
(Jumbo jet)										
Taxi-idle	1,030	467	51.7	23.5	15.4	7.0	3.6	1.63	0.04	0.02
Takeoff	13,449	6,100	6.7	3.04	1.3	0.59	540.0	245.0	0.54	0.24
Climbout†	11,400	5,171	6.6	2.99	1.3	0.59	333.0	151.0	0.54	0.24
Approach	6,204	2,814	18.6	8.44	1.9	0.86	173.0	78.5	0.44	0.20
Pratt & Whitney JT-3D										
(Long range jet)										
Taxi-idle	872	396	109.0	49.4	98.6	44.7	1.43	0.649	0.45	0.20
Takeoff	10,835	4,915	12.3	5.60	4.65	2.11	148.0	67.1	8.25	3.7
Climbout	8,956	4,062	15.3	6.94	4.92	2.23	96.2	43.6	8.5	3.9
Approach	4,138	1,877	39.7	18.0	7.84	3.56	21.8	9.89	8.0	3.6
Pratt & Whitney JT-3C										
(Long range jet)										
Taxi-idle	1,198	543	92.6	42.0	92.2	41.8	2.49	1.13	0.40	0.18
Takeoff	10,183	4,619	9.04	4.10	0.855	0.388	119.0	54.0	6.50	2.9
Climbout	8,509	3,860	16.0	7.26	0.893	0.405	84.7	38.4	6.25	2.8
Approach	4,115	1,867	49.0	22.2	8.26	3.75	23.2	10.5	3.25	1.5
Pratt & Whitney JT-4A										
(Long range jet)										
Taxi-idle	1,389	630	62.8	28.5	64.8	29.4	2.71	1.23	1.2	0.54
Takeoff	15,511	7,036	18.8	8.53	0.674	0.306	236.0	107.0	21.0	9.5
Climbout	13,066	5,927	18.3	8.30	1.27	0.576	155.0	70.3	20.0	9.1
Approach	5,994	2,719	26.3	11.9	3.83	1.74	35.9	16.3	6.0	2.7
General Electric CJ805										
(Long range jet)										
Taxi-idle	1,001	454	63.8	[illegible]	27.3	12.4	1.57	0.712	1.3	0.59
Takeoff	9,960	4,518	29.1	[illegible]	0.556	0.252	111.0	50.3	15.0	6.8
Climbout	8,290	3,760	28.9	[illegible]	0.583	0.264	74.0	33.6	15.0	6.8
Approach	3,777	1,713	42.8	19.4	2.43	1.10	17.8	8.07	5.0	2.3
Pratt & Whitney JT-8D‡										
(Med. range jet)										
Taxi-idle	959	435	33.4	15.2	6.99	3.71	2.91	1.32	0.36	0.16
Takeoff	8,755	3,971	7.49	3.40	0.778	0.353	198.0	89.8	3.7	1.7
Climbout	7,337	3,328	8.89	4.03	0.921	0.418	131.0	59.4	2.6	1.2
Approach	3,409	1,546	18.2	8.26	1.75	0.794	30.9	14.0	1.5	0.68

Table 11 (Concluded)

Engine and mode	Fuel rate lb/hr	Fuel rate kg/hr	Carbon monoxide lb/hr	Carbon monoxide kg/hr	Hydrocarbons lb/hr	Hydrocarbons kg/hr	Nitrogen oxides (NO_x as NO_2) lb/hr	Nitrogen oxides (NO_x as NO_2) kg/hr	Solid particulates lb/hr	Solid particulates kg/hr
Rolls Royce Spey MK511 (Med.range jet)										
Taxi-idle	662	300	60.2	27.3	66.1	30.0	0.849	0.385	0.17	0.077
Takeoff	7,625	3,459	14.2	6.44	Neg	Neg	153.0	69.4	16.0	7.3
Climbout	6,356	2,883	15.3	6.94	0.242	0.110	115.0	52.2	10.0	4.5
Approach	3,052	1,384	39.1	17.7	4.22	1.91	30.4	13.8	1.5	0.68
Allison T56-A15 (Air carrier turboprop; mil. transport)										
Taxi-idle	493	224	8.74	3.96	7.39	3.35	1.23	0.560	1.6	0.73
Takeoff	2,393	1,085	3.77	1.71	0.440	0.200	27.9	12.7	3.7	1.7
Climbout	2,188	992	3.40	1.54	0.399	0.181	22.2	10.1	3.0	1.4
Approach	1,146	520	3.49	1.58	0.326	0.148	7.32	3.32	3.0	1.4
Allison T56-A7 (Air carrier turboprop; mil. transport)										
Taxi-idle	548	249	15.3	6.94	6.47	2.93	2.16	0.980	1.6	0.73
Takeoff	2,079	943	2.15	0.975	0.430	0.195	22.9	10.4	3.7	1.7
Climbout	1,908	865	3.01	1.37	0.476	0.216	21.2	9.62	3.0	1.4
Approach	1,053	478	3.67	1.66	0.517	0.235	7.78	3.53	3.0	1.4
Airesearch TPE-331** (Gen. aviation turboprop)										
Taxi-idle	146	66.2	3.53	1.60	0.879	0.399	0.955	0.433	0.3	0.14
Takeoff	365	166.0	0.393	0.178	0.055	0.025	3.64	1.65	0.8	0.36
Climbout	339	154.0	0.568	0.258	0.053	0.024	3.31	1.50	0.6	0.27
Approach	206	93.4	2.58	1.17	0.240	0.109	1.69	0.767	0.6	0.27
Teledyne/Continental O-200 (Gen. aviation piston)										
Taxi-idle	7.6	3.48	7.52	3.41	0.214	0.097	0.009	0.004	NA††	NA
Takeoff	48.4	22.0	54.6	24.8	0.720	0.327	0.259	0.117	NA	NA
Climbout	48.4	22.0	54.6	24.8	0.720	0.327	0.259	0.117	NA	NA
Approach	21.3	9.66	23.8	10.8	0.380	0.172	0.052	0.024	NA	NA
Lycoming O-320 (Gen. aviation piston)										
Taxi-idle	13.0	5.90	11.1	5.03	0.355	0.161	0.013	0.006	NA	NA
Takeoff	65.7	29.8	70.9	32.2	1.49	0.676	0.214	0.097	NA	NA
Climbout	63.5	28.8	65.8	29.8	1.31	0.594	0.375	0.170	NA	NA
Approach	23.1	10.5	24.3	11.0	0.496	0.225	0.051	0.023	NA	NA

Analysis of Aircraft Exhaust Emission Measurements. Cornell Aeronautical Laboratory, Inc. Buffalo, N.Y. Prepared for the Environmental Protection Agency, Research Triangle Park, N.C., under Contract Number 68-04-0040. October 1971.

†Estimated and/or calculated.

‡"Diluted smokeless" JT-8D. All air carriers scheduled for conversion of JT-8D engines to smokeless by January 1973.

**Similar to the PT-6A engine.

††NA-Not available

Table 12

NO_x EMISSIONS FOR SOME ENGINES

Engine	Thrust (lbs)	NO (ppmV)	NO_2 (ppmV)	Ratio NO/NO_2
Pratt and Whitney JT-3D	1777	7.2	8.6	0.8
	6778	27.9	6.9	4.04
	14628	80.5	2.9	27.8
Pratt and Whitney JT-8D-1	9660	61.0	5.0	12.2
	11480	84.0	5.0	16.8
	800	4.0	7.0	0.57
Pratt and Whitney JT-9D	2482	9.6	11.1	0.9
	3493	13.8	15.3	0.9
	10968	62.4	13.0	4.8
Pratt and Whitney J57-P10	430	7	2.9	2.4
	6080	30	3	10
	7940	43	3	14.3
	9420	67	3	22.3
Pratt and Whitney J-79	275	8.0	3.0	2.8
	6650	39.0	4.0	9.8
	9800	62.0	6.0	10.3
Pratt and Whitney T-56-A7B	2237	71.0	7.0	10.1
	3114	103.0	5.0	20.6
	3443	109.0	5.0	21.8

Source: Bogdan and McAdams (1971).

D. HYDROCARBON/NO_x RATIOS FROM AIRCRAFT EMISSIONS AND AUTOMOBILE EMISSIONS

Computer simulations of the effects of mixing aircraft and automobile emissions require hydrocarbon/NO_x ratios for emissions from aircraft and automobiles. The results of these simulations are presented in Chapter V, but the emissions and HC/NO_x ratios are discussed here for easy comparison with the previous section.

In order to tabulate a consistent set of hydrocarbon/NO_x ratios from available data, the following conditions were imposed:

- All data were converted to moles of carbon for hydrocarbons and moles of NO (or NO_2) for NO_x.
- Ratios of hydrocarbon to NO_x were required for the whole LTO cycle.

Conversion factors are discussed in the Appendix.

1. Hydrocarbon/NO_x Ratios from Aircraft Emissions

Due to the broad range of values for hydrocarbons and NO_x emitted from different aircraft engines using different types of fuel and different operational modes, a comprehensive analysis of reported data was performed. Table 2 presents hydrocarbon/NO_x ratios tabulated for each mode of the LTO cycle from data obtained from Northern Research (1968). Table 13 lists the total hydrocarbon and NO_x emitted during the LTO cycle. These values were obtained by combining the emissions from the different modes. All emissions were multiplied by a time factor taken from Table 3. The time factors were obtained by calculating the relative percentage of time spent in each mode. For the seven classes of engines, the hydrocarbon/NO_x ratios range from $\sim$ 400 to $\sim$ 3.6. For the three engines studied by Lozano et al. (1968), hydrocarbon/NO_x ratios varied from 2.7 for the T-56 engine to 27.0 for the TF-33 engine (Table 14).

Table 13

SUMMARY OF ENGINE EMISSION LEVELS DURING AN LTO CYCLE

Engine	HC (moles of carbon per engine)	NO_x (moles of NO_2 per engine)	THC/NO_x*
Pratt and Whitney JT-3D	851.5	32.0	26.1
Pratt and Whitney JT-8D	87.5	20.7	4.1
Pratt and Whitney JT-12	52.3	5.9	8.7
Allison 501-DB	53.79	10.2	5.2
Pratt and Whitney R-2800	1542.4	3.87	391.0
Continental 10-520-A	51.1	0.39	129.0
General Electric CT-58	19.7	5.5	3.5

*Units of moles of carbon/moles of NO_2

Source: Northern Research (1968)

Table 14

POLLUTION EMISSIONS FROM JET AIRCRAFT DURING AN LTO CYCLE

Engine	HC (ppm as C)	NO_x (ppm as NO_2)	THC/NO_x
T-56	58.2	21.2	2.7
J-57	87.3	27.6	3.14
TF-33	404.9	14.7	27.0

Source: Lozano et al. (1968)

EPA (1973) has reported modal emission factors for 13 different aircraft engines with uses ranging from jumbo jets to air carriers (Table 11). Table 15 shows the emissions during the entire LTO cycle and the hydrocarbon/NO_x ratio for each engine. The values for the hydrocarbon/NO_x ratio range from 3.5 to 70.0 (moles as C/moles as NO_2).

Broderick et al. (1971) performed a survey of aircraft emissions monitoring requirements. Table 16 lists the types of jets and engines considered in their study. Table 17 shows the emission index of the jets listed in Table 16. These values were cited by Broderick et al. from a study by Northern Research (1968). Again, there is a broad range of values for the hydrocarbon/NO_x ratios--from 33.0 to 137 (units of moles of carbon per moles of NO_2).

Naugle (1974) surveyed the measurements of exhaust emissions from military aircraft. Table 18 summarizes some of the aircraft emissions data tabulated by Naugle. This table lists the emissions during the entire LTO cycle. The hydrocarbon/NO_x ratios range from 2.4 to 22.4 for the four engines studied. Table 19 lists emissions per touch-and-go cycle. The touch-and-go operations are used as training methods at many Air Force bases. According to Naugle, these operations can give emissions "nearly as great as from landings and takeoffs at some airbases." The hydrocarbon/NO_x ratios are low compared with the ratios in Table 18.

Rote et al. (1973) reported emissions of aircraft at O'Hare International Airport. Table 20 lists their observations. The hydrocarbon/NO_x ratios range from 4.0 for the superjets to 76.0 for long range jets.

The six studies cited in this section report a broad range of values for the hydrocarbon/NO_x ratios. Therefore, for the computer simulations, an averaged hydrocarbon/NO_x ratio was used. The averaged value for the hydrocarbon/NO_x ratio is approximately 41.4.

The hydrocarbon/NO_x ratios tabulated for emissions during the LTO cycle provide one measure of the hydrocarbon/NO_x ratio, but the gross amounts of

Table 15

EPA MODAL EMISSIONS FACTORS DURING LTO CYCLE

Engine	Hydrocarbons (kg hr^{-1})	NO_x (as NO_2) (kg hr^{-1})	Ratio of Total Hydrocarbons to NO_x (ppm as C/ppm as NO_2)
Pratt and Whitney JT-9D	10.7	12.1	3.4
General Electric DF-6	6.07	16.5	1.41
Pratt and Whitney JT-3D	38.5	3.18	46.5
Pratt and Whitney JT-3C	36.0	3.41	40.6
Pratt and Whitney JT-4A	25.2	5.30	18.3
General Electric CJ-805	10.7	2.66	15.5
Pratt and Whitney JT-8D	3.26	4.74	2.64
Rolls Royce Sprey MK 511	25.8	3.51	28.3
Allison T56-A15	2.84	1.22	8.95
Allison T56-A7	2.5	1.56	6.17
Airesearch TPE-331	0.35	0.51	2.64
Teledyne/Continental O-200	0.12	0.01	46.1
Lycoming O.320	0.18	0.01	69.2

Source: EPA (1973).

Table 16

AIRCRAFT CONSIDERED IN BRODERICK'S STUDY

Type	Example	Engine
Long-Range Jet	707, DC8	Pratt & Whitney JT-3D
Medium-Range Jet	727, 737, DC9	Pratt & Whitney JT-8D
Turboprop	Electra	Allison 501-DB
Piston	DC6, Corvair 440	Rolls Royce R2800
Superjet	747	Pratt & Whitney JT-9D

Table 17

EMISSION INDEX CITED FROM BRODERICK'S STUDY

Type	Fuel Usage ($lb\ hr^{-1}$)	HC (1000 lb fuel)	NO_x (1000 lb fuel)	Ratio of Hydrocarbons to NO_x (ppm as C/ppm as NO_2)
Long-Range Jet	1090	54.6	1.56	134
Medium-Range Jet	920	12.7	1.46	33.5
Turboprop	587	9.7	2.18	17.1
Superjet		13.4	1.55	33.3

Table 18

EMISSIONS PER LTO CYCLE

Aircraft	Engine	Hydrocarbon (lbs/cycle)	NO_x (lbs/cycle)	HC/NO_x (moles as C/moles as NO_2)
F-4	J-79	9.8	14	2.7
F-104	J-79	4.4	7.3	2.4
T-37	J-85	19	3.7	19.7
T-38	J-85	25	4.3	22.4
B-52H	TF-33	680	170	15.4
KC-135A	J-57	198	61	12.5

Source: Naugle (1974)

Table 19

EMISSIONS PER TOUCH-AND-GO CYCLE

Aircraft	Engine	Hydrocarbon (lbs/cycle)	NO_x (lbs/cycle)	HC/NO_x (moles as C/moles as NO_2)
F-4	J-79	0.22	5	0.17
F-104	J-79	0.15	3	0.20
T-37	J-85	5.8	2.8	7.96
T-38	J-85	4.6	2.4	7.37
B-52H	TF-33	6	52	0.44
KC-135A	J-57	6	25	0.92

Source: Naugle (1974)

Table 20

EMISSION RATES PER LTO CYCLE

Aircraft	Engine	Hydrocarbons lb hr^{-1} engine^{-1}	NO_x lb hr^{-1} engine^{-1}	HC/NO_x (moles as C/ moles as NO_2)
Jumbo	JT-9D	32.7	30.7	4.1
Long Range	JT-3D	144.6	7.3	76.2
Medium Range	JT-8D	15.4	8.7	6.8
	CJ-805-3A	46.2	7.9	22.5
Short Range	A-501-D13	10.3	4.9	8.1
	SPEY 511	107.7	8.7	47.6

Source: Rote et al. (1973)

hydrocarbons and NO_x emitted by all aircraft at an airport can provide another measure. Northern Research (1968) reported the total emissions from all aircraft operating at FAA-controlled fields as follows: hydrocarbons--415 tons/day; NO_x--42.8 tons/day. The hydrocarbon/NO_x ratio for these values is 37.3 (moles as C/moles as NO_2). Rote et al. (1973) reported emissions of 5.074 x 10^3 tons/year for hydrocarbons (moles as C/moles as NO_2) and 0.2931 x 10^3 tons/year for NO_x, for a hydrocarbon/NO_x ratio of 66.6. LAAPCD (1971) reported the following emissions at the Los Angeles International Airport: 10,685 tons/year of hydrocarbons and 1105 tons/year of NO_x. The hydrocarbon/NO_x ratio is 37.2 (moles as C/moles as NO_2). Averaging the ratio found for the individual engines with the three ratios of gross emissions yields a value of 45.7 (in units of moles as carbon/moles of NO_2).

2. Hydrocarbon/NO_x Ratios For Automobile Exhaust Emissions

Unlike aircraft engine operations during the taxi-idle mode, automobile engines (from 1972 to the present) run on a "lean" fuel-air mixture. Automobile exhaust emissions have low hydrocarbon concentrations and high NO_x concentrations. This is the opposite of aircraft emissions. Table 21 presents the results of a Bureau of Mines study (1973) on ten 1970-1973 automobiles using a 40 percent aromatic fuel. The HC/NO_x ratios are low compared with the ratios for jet aircraft (Table 10). The EPA studies (Table 22) show slightly higher hydrocarbon/NO_x ratios for average emissions in a given year. An important feature shown in Table 22 is that greater amounts of hydrocarbons are emitted at the slower speed than at the higher speed.

Of the ten automobiles studied by the Bureau of Mines (Table 21), only the 1971 Vega shows a very high hydrocarbon/NO_x ratio. Excluding the Vega, the range of values is very narrow compared with the wide range of values found for aircraft emissions. The average hydrocarbon/NO_x ratio for automobile emissions from these cars is approximately 2.2 (excluding the Vega). The higher ratios reported by the EPA (Table 22) have an average hydrocarbon/NO_x ratio of approximately 4.

Table 21

EMISSIONS FROM 1970 - 1973 AUTOMOBILES

Vehicle	Total Hydrocarbons (grams/mile)	NO_x (grams/mile)	HC/NO_x [§]
1972 Oldsmobile (car 151)	1.79	5.01	1.4
1971 Ford Galaxie (car 707)	4.88	7.34	2.6
1971 Plymouth Fury (car 76)	3.22	8.52	1.45
1972 Ford Torino (car 769)	2.16	4.32	1.92
1970 Chevrolet Impala (car 595)	3.58	4.37	3.15
1970 Pontiac (car 400)	5.86	9.36	2.44
1970 Volkswagen (car 365)	2.44	6.09	1.54
1971 Vega (car 68)	4.92	1.88	10.1
1973 Ford Torino (car 146)	2.79	4.17	2.57
1973 Impala (car 110)	2.16	2.66	3.12

Note: Fuel used was 40 percent aromatic.

[§]Moles C per mile / moles NO_2 per mile.

Source: Bureau of Mines (1973)

Table 22

AUTOMOBILE EMISSIONS BY YEAR AND NATIONAL AVERAGE EMISSIONS

Vehicle	Total Hydrocarbons (grams/mile)	NO_x (as NO_2) (grams/mile)	HC/NO_x [§]
1971 Models*	7.2	5.4	5.14
1971 (California)*	2.9	3.5	3.19
1972 Models*	6.6	5.4	4.7
National Average [+]			
@ 45 mph	4.7	8.0	2.3
@ 19.6 mph	14.6	4.6	12.2

* Source: EPA (1973)
[+] Source: EPA (1975)

[§]Moles C per mile / moles NO_2 per mile.

III COMPUTER SIMULATIONS OF PHOTOCHEMICAL SMOG

An important part of this study is the prediction of oxidant formation given an initial set of conditions. Ozone is considered to be the principal component of photochemical oxidants. The method for the measurement of oxidants is specific for ozone (EPA, 1971). Therefore, this study was confined to the ozone behavior predicted by the kinetic mechanism. Predictions were made by numerical integration of a set of differential rate equations that describe the kinetics of photochemical smog. The numerical integrations were performed using the CHEMK program developed by G. Z. Whitten of Systems Applications, Incorporated on the CDC 7600 computer located at the Lawrence Berkeley Laboratories.

A. THE GENERALIZED KINETIC MECHANISM

The kinetic mechanism used as a starting point for the computer simulations in this study is an updated version of the generalized 39-step mechanism developed by Hecht, Seinfeld, and Dodge (1974). The mechanism is presented in Table 23. This kinetic mechanism has been validated by Hecht et al. (1974a,b) using data collected in smog chamber experiments performed at the University of California at Riverside (UCR). The emissions data surveyed in the present study were used as starting conditions, as in a smog chamber experiment, for the computer simulations. The computer program (CHEMK) is capable of simulating up to 200 rate expressions containing up to 50 species. The CHEMK program has been previously employed in the validation of kinetic mechanisms by Durbin et al. (1975) using UCR smog chamber data. Simulating using the emissions data as if in a smog chamber experiment can be considered as an illustrative situation, because the system remains static, i.e., there is no loss or gain of products or reactants due to dilution or replenishment of the system, and

Table 23
THE SMOG MECHANISM

Reaction	Rate Constant (ppm^{-1} min^{-1})
NO_x, O_3 inorganic chemistry	
$O + O_2 + M \rightarrow O_3 + M$	2.08×10^{-5} ppm^{-2} min^{-1}
$O_3 + NO \rightarrow NO_2 + O_2$	25.2
$O + NO_2 \rightarrow NO + O_2$	1.34×10^{4}
$O_3 + NO_2 \rightarrow NO_3 + O_2$	0.05
$NO_3 + NO \rightarrow 2NO_2$	1.3×10^{4}
$NO_3 + NO_2 \rightarrow N_2O_5$	5.6×10^{3}
$N_2O_5 + M \rightarrow NO_3 + NO_2$	2.4×10^{-5}
$OH + NO_2 \rightarrow HNO_3$	1.0×10^{4}
$OH + NO \rightarrow HNO_2$	3.0×10^{3}
$HO_2 + NO \rightarrow NO_2 + OH$	8.0×10^{2}
HO_2-HO_2 recombination	
$HO_2 + HO_2 \rightarrow H_2O_2$	6.0×10^{3}
Organic oxidation reactions	
Alkane + $OH \rightarrow RO_2 + H_2O$	3.4×10^{3}
Alkane + $O \rightarrow RO_2 + OH$	64
Alkene + $OH \rightarrow$ Aldehyde + $\alpha HO_2 + (1 - \alpha)RO_2$	2.5×10^{4}
Alkene + $O_3 \rightarrow OH$ + Aldehyde + $\beta RCO_3 + (1 - \beta)HO_2 + (1 - \beta)CO$	0.02
Alkene + $O \rightarrow RO_2 + \gamma HO_2 + \gamma CO + (1 - \gamma)RCO_3$	5.3×10^{3}
Aromatic + $OH \rightarrow RO_2 + H_2O$	9.0×10^{3}
Aromatic + $O \rightarrow RO_2 + OH$	120
Aldehyde + $OH \rightarrow \delta HO_2 + (1 - \delta)RO_2$	2.1×10^{4}
Reactions of lumped species	
$RO_2 + NO \rightarrow$ Aldehyde + $0.5(1 + \epsilon)HO_2 + 0.5(1 + \epsilon)CO + 0.5(1 - \epsilon)RO_2 + NO_2$	1.0×10^{3}
$RCO_3 + NO \rightarrow RO_2 + CO_2 + NO_2$	1.0×10^{3}
$RCO_3 + NO_2 \rightarrow PAN$	3.0×10^{2}
$PAN \rightarrow RO_2 + CO_2 + NO_3$	3.0×10^{-3} min^{-1}
$RO_2 + HO_2 \rightarrow RO_2H + O_2$	3.0×10^{3}
$RCO_3 + HO_2 \rightarrow RCO_3H + O_2$	3.0×10^{3}

Table 23 (Concluded)

Reaction	Rate Constant (ppm^{-1} min^{-1})
CO oxidation	
$CO + OH \rightarrow CO_2 + HO_2$	250
Photochemistry	
$NO_2 + h\nu \rightarrow NO + O$	k_1 min^{-1}
$H_2O_2 + h\nu \rightarrow 2OH$	0.036 k_1 min^{-1}
Aldehyde + $h\nu \rightarrow$ Products	0.0045 k_1 min^{-1}
Aldehyde + $h\nu \rightarrow (1 + \delta)HO_2 + (1 - \delta)RO_2 + CO$	0.0045 k_1 min^{-1}
$HNO_2 + h\nu \rightarrow OH + NO$	0.07 k_1
Surface reactions*	
$NO + NO_2 + H_2O \rightarrow 2HNO_2$	2.6×10^{-7} ppm^{-2} min^{-1}
$2HNO_2 \rightarrow NO + NO_2 + H_2O$	0.26
$N_2O_5 + H_2O \rightarrow 2HNO_3$	5×10^{-6}
$O_3 \rightarrow$ Products	0.001 min^{-1}

α = split between $RO \rightarrow RO_2$ + Aldehyde and $RO + O_2 \rightarrow HO_2$ + Aldehyde = 0.6.

β = split between pathways for o-p biradical decomposition = 0.33.

γ = split between internal and terminal O addition = 0.5.

δ = fraction of aldehydes that are formaldehyde = 0.5.

ϵ = fraction of RO_2 that is MeO_2 = 0.5.

*These depend on the surface/volume and the nature of the surface.

Note: δ and ϵ are empirical "closure parameters." The present values were determined from simulations of UCR data and the data themselves. α, β, and γ are functions of olefin. Their values were assigned on the basis of propylene values.

Sources:

Hampson and Garvin (1975)
Atkinson and Pitts (1975)
Davis (1975)
Durbin et al. (1975)
Hecht et al. (1974b)

solar radiation is held constant for a 12-hour period. The hydrocarbons used in the validations of smog chamber data are butane, propylene, and toluene, which represent their respective general groups (e.g., butane represents the alkanes in the reactions involving alkanes) for our initial simulations. The closure parameters, α, β, γ, δ, and ϵ are determined by the specific hydrocarbons used in the mechanism. For example, the closure parameter δ represents the fraction of the aldehyde produced which is formaldehyde. If the alkane and alkene molecules are longer chain molecules, then the fraction of formaldehyde produced is expected to be smaller. The value of δ was determined from smog chamber data on a propylene/NO_x system obtained at the University of California at Riverside. The parameters α, β, and γ are functions of the alkene.

The parameter α is determined by the split between the unimolecular decomposition of alkoxyl radicals (RO·) and the oxidation of alkoxyl radicals. Although the individual rates of these reactions are of little importance in the kinetic mechanism, their ratio, α, is important in determining the course of the overall reaction. The parameter β is determined by the pathways for the oxyperoxy biradical decomposition. The mechanism for this decomposition, developed by O'Neal and Blumstein (1973), is now given (assuming the alkene is propylene):

(1)

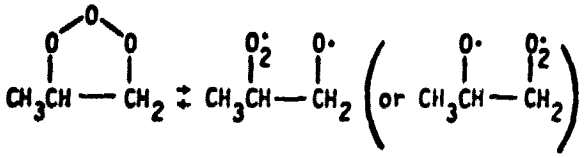

(2)

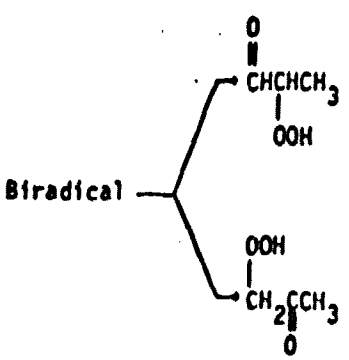

(3a)

(3b)

Whether reaction (3a) or (3b) occurs depends on the nature of the biradical intermediate. The α-keto hydroperoxide formed in Reaction (3) is in an excited state. Its fractionation leads to the following overall reaction:

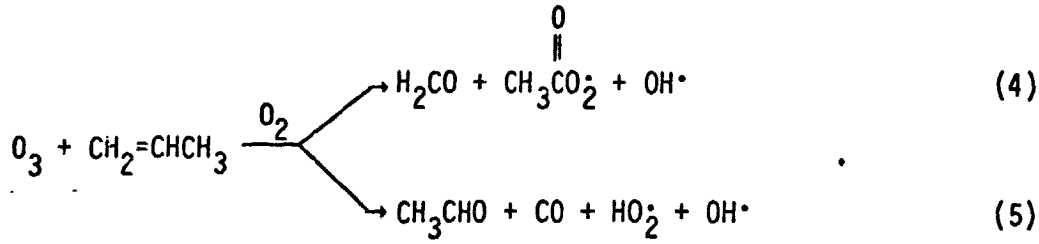

(4)

(5)

The split between Reactions (4) and (5) is determined by which hydroperoxide is formed in Reaction (2). Durbin et al. (1975) used a value of 0.33 for β to fit smog chamber data from University of California at Riverside. The parameter γ is the fraction of carbons attached to the double bond in a monoolefin that are not terminal carbons on the chain. Consider the reactions of oxygen atoms with propylene and 2-butene:

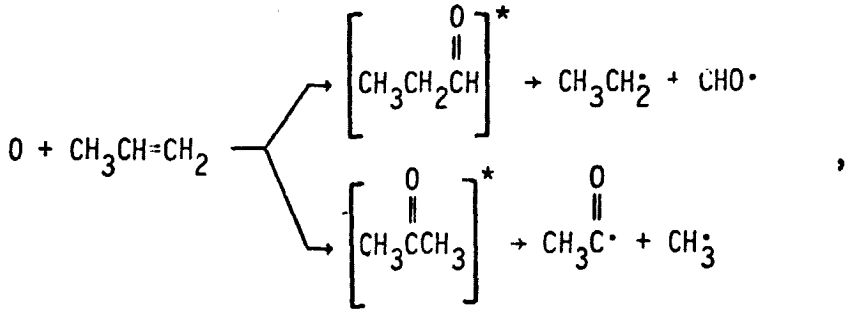

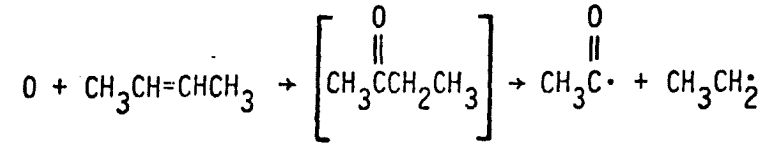

If we assume that the oxygen atom will react with equal probability with either of the carbon atoms in the double bond, γ = 0.5 for propylene and γ = 1.0 for 2-butene.

For the simulations performed in this chapter, we assumed a value of the NO_2 photolysis rate constant k_1 of 0.25 ppm^{-1} min^{-1} (an average value of k_1 for a typical solar spectrum). Some of the surface reactions listed in Table 23 have been shown to be very sensitive to changes in reactant concentrations and changes in rate constants (Durbin et al., 1975). These surface (or heterogeneous) reactions will be discussed in a later section.

B. RESULTS OF THE COMPUTER SIMULATIONS

A necessary input to the kinetic mechanism is a set of initial concentrations of various groups of hydrocarbons. Four mixtures with different relative concentrations of alkanes, alkenes, and aromatics were constructed to represent the range of hydrocarbon compositions in jet exhaust emissions (Table 24). One of these mixtures and a value for the total hydrocarbon concentration were used in each computer simulation. The initial concentrations of hydrocarbons and NO_x used in the simulations are shown in Figure 1. For each mixture in Table 24, computer simulations were performed using each point in Figure 1 as an initial condition. Ozone profiles as a function of time were computed for each point. Isopleths of ozone concentrations were then constructed as a function of the hydrocarbon and NO_x concentrations at intervals of 1, 2, 4, 8, and 12 hours. Due to the limited number of simulations, some interpolation was necessary in constructing the isopleths.

Since the computer program is coded to accept initial concentrations (in ppm) of specific molecules, hydrocarbon concentrations reported as ppm of carbon had to be converted before the simulations could be performed. Assuming that the compositions of Table 10 are representative of hydrocarbon exhaust emissions for most aircraft engines, the average composition of exhaust is 57 percent alkane, 22 percent alkene, 16 percent aromatic, and 5 percent aldehydes. From the values of Table 10 an average molecular weight of 89 g $mole^{-1}$ can be determined. This molecular weight is close to that of a six-carbon molecule, so a six-carbon molecule was used in the computer simulation.

Table 24

HYDROCARBON COMPOSITIONS OF MIXTURES USED IN SIMULATIONS

	Relative Concentration		
Mixture	Alkanes	Alkenes	Aromatics
1	25%	55%	20%
2	50	40	10
3	55	25	20
4	33	33	33

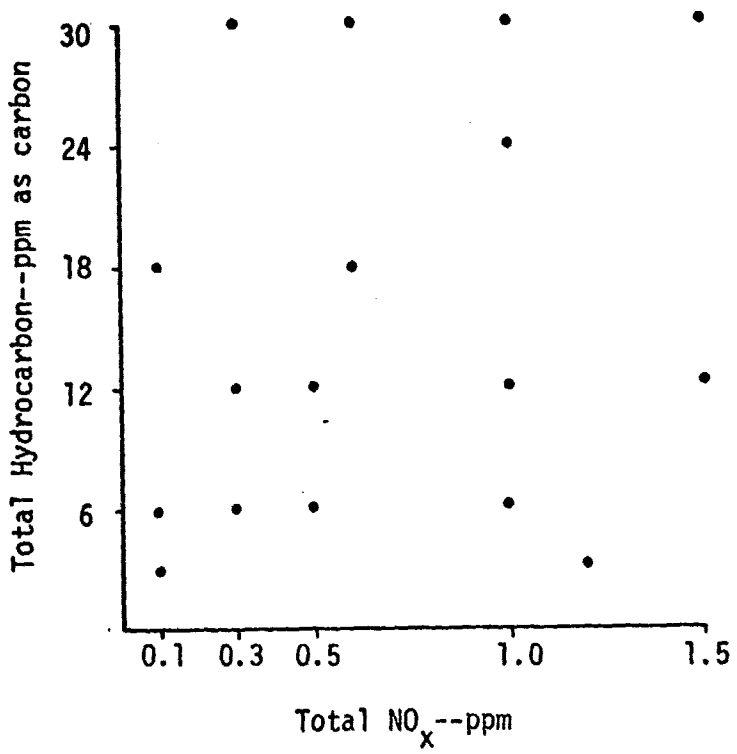

FIGURE 1. INITIAL CONCENTRATIONS USED IN SIMULATIONS

Figures 2 to 11 show the ozone isopleths for Mixtures 1 and 3 listed in Table 24. Ozone concentration curves are given in intervals of 0.1 ppm (solid lines) or 0.01 ppm (dashed lines). These isopleths show that Mixture 1, which contained the highest concentration of alkenes, was the most reactive producer of ozone. Mixture 3, which contained the lowest percentage of alkenes, was the least reactive producer of ozone. Of the different mixtures, Mixture 3 is the mixture most representative of typical aircraft mixtures. However, the data base did not seem sufficient to warrant a study relating airplane population to ozone production.

The isopleths in general show a distinctive evolutionary pattern; the region of maximum ozone moves toward the upper right corner with time. A diagonal line along the ridge of any isopleth divides it into two regions. Varying the hydrocarbon (HC) concentration at a constant NO_x concentration would have a significant effect on ozone concentration in the lower right region of an isopleth. Varying HC would have a minimal effect in the upper left region. Conversely, varying the NO_x concentration at a constant hydrocarbon concentration would have a more pronounced effect in the upper left region than in the lower right region. The kinetic mechanism has never been validated at hydrocarbon concentrations greater than 18 ppm (as carbon). Reactions that are insignificant at lower hydrocarbon concentrations may become important at the higher concentrations. Therefore, there is some uncertainty in the region from 18 ppm (as carbon) to 30 ppm (as carbon) hydrocarbon concentration.

Isopleths of one and eight hour simulations of Mixtures 2 and 4 are presented in Figures 12 to 15. Since Mixtures 2 and 4 contain approximately the same amount of alkenes, their isopleths are very similar. Mixture 2 is slightly more reactive since it contained a little more alkene than Mixture 4.

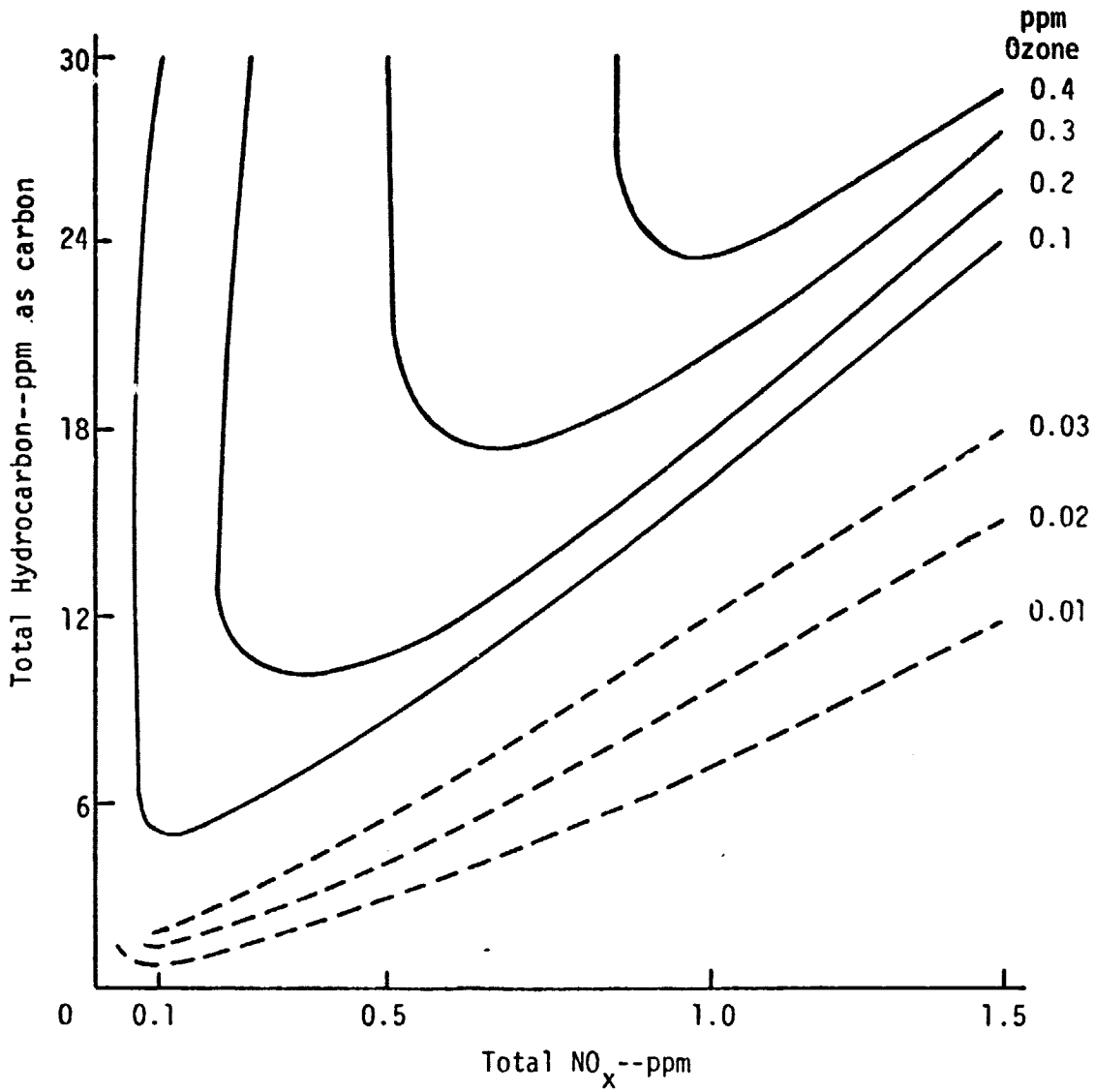

FIGURE 2. OZONE ISOPLETH FOR A SIMULATION OF MIXTURE 1 AFTER A ONE-HOUR PERIOD

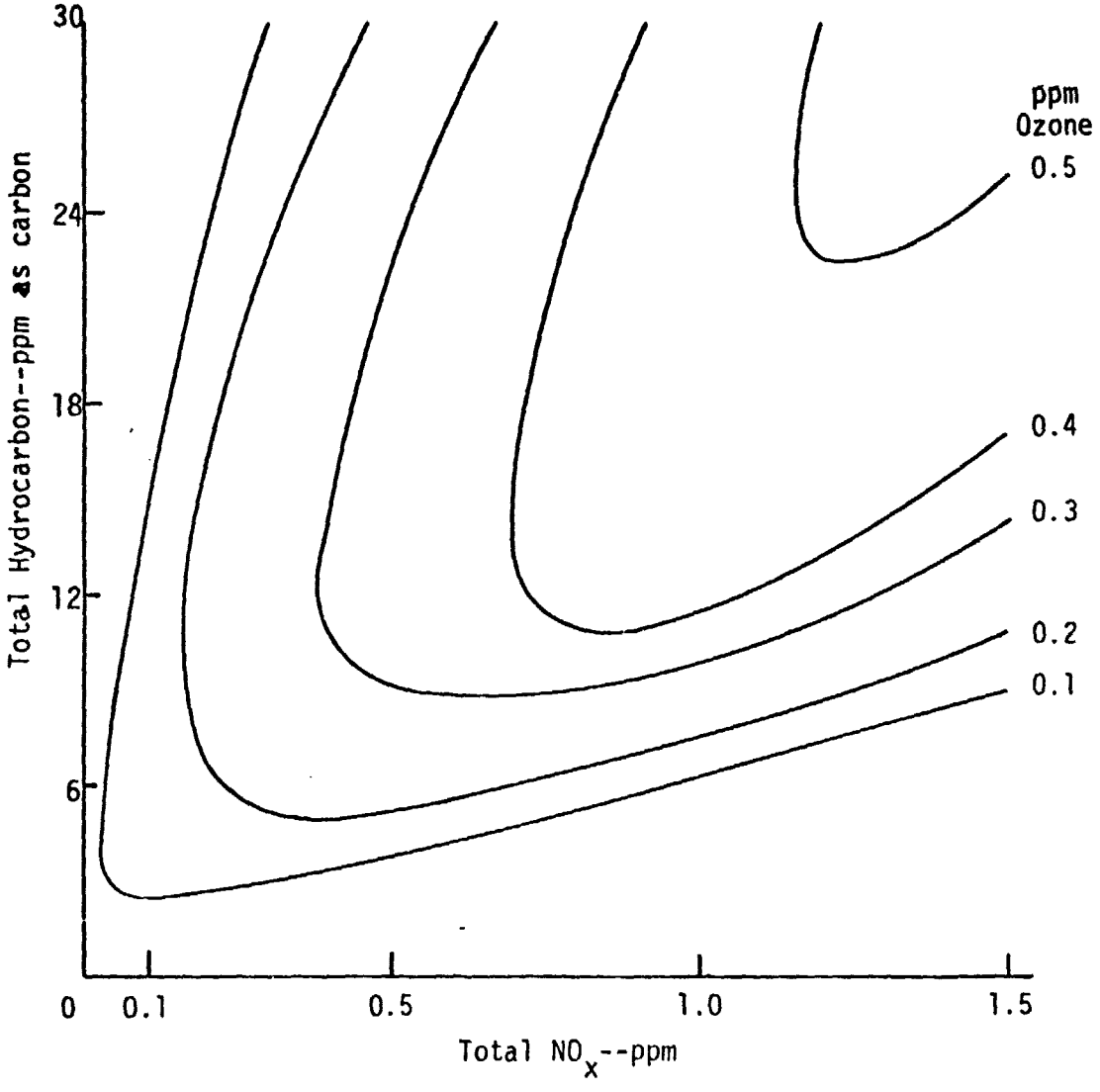

FIGURE 3. OZONE ISOPLETH FOR A SIMULATION OF MIXTURE 1 AFTER A TWO-HOUR PERIOD

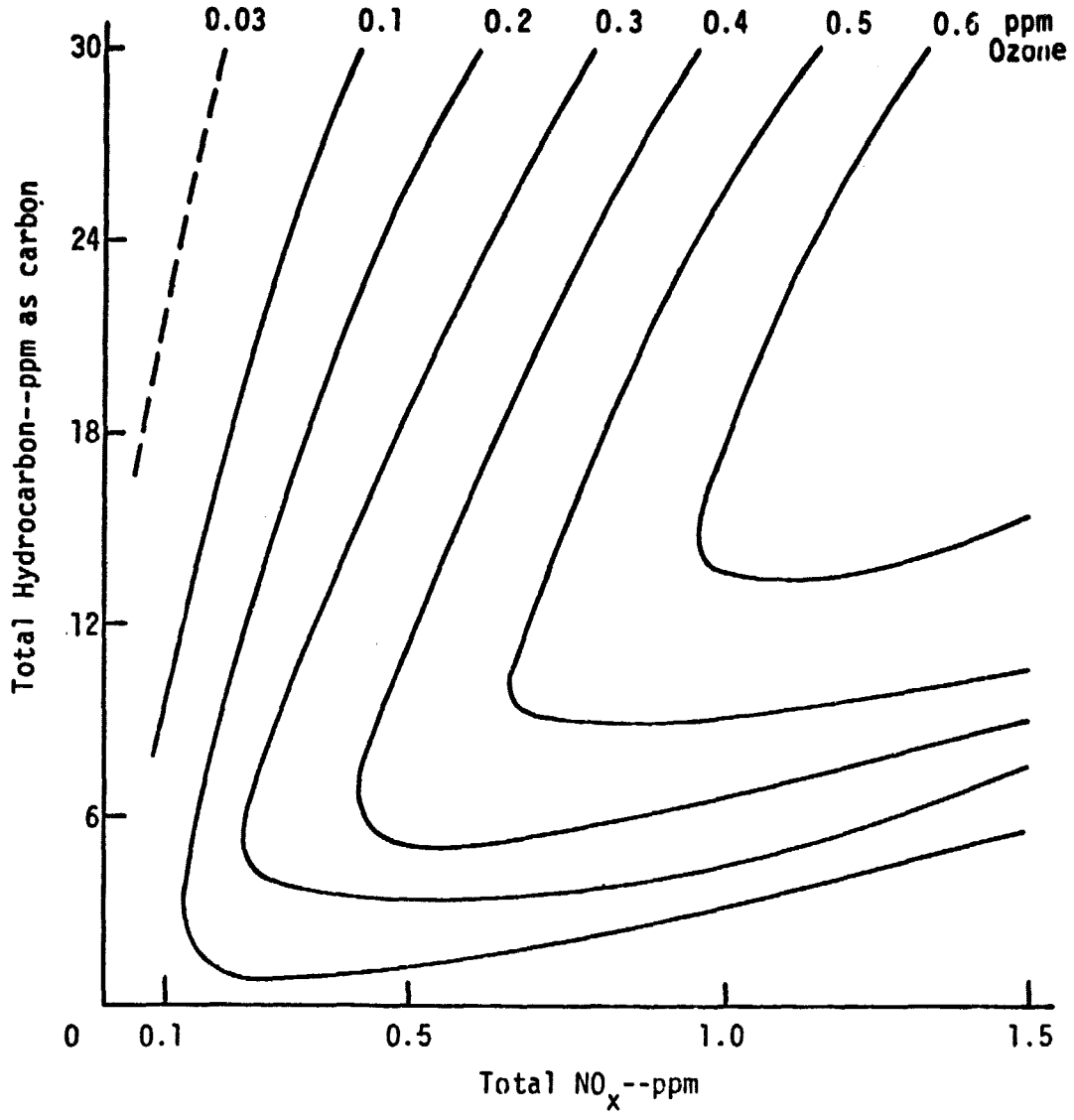

FIGURE 4. OZONE ISOPLETH FOR A SIMULATION OF MIXTURE 1 AFTER A FOUR-HOUR PERIOD

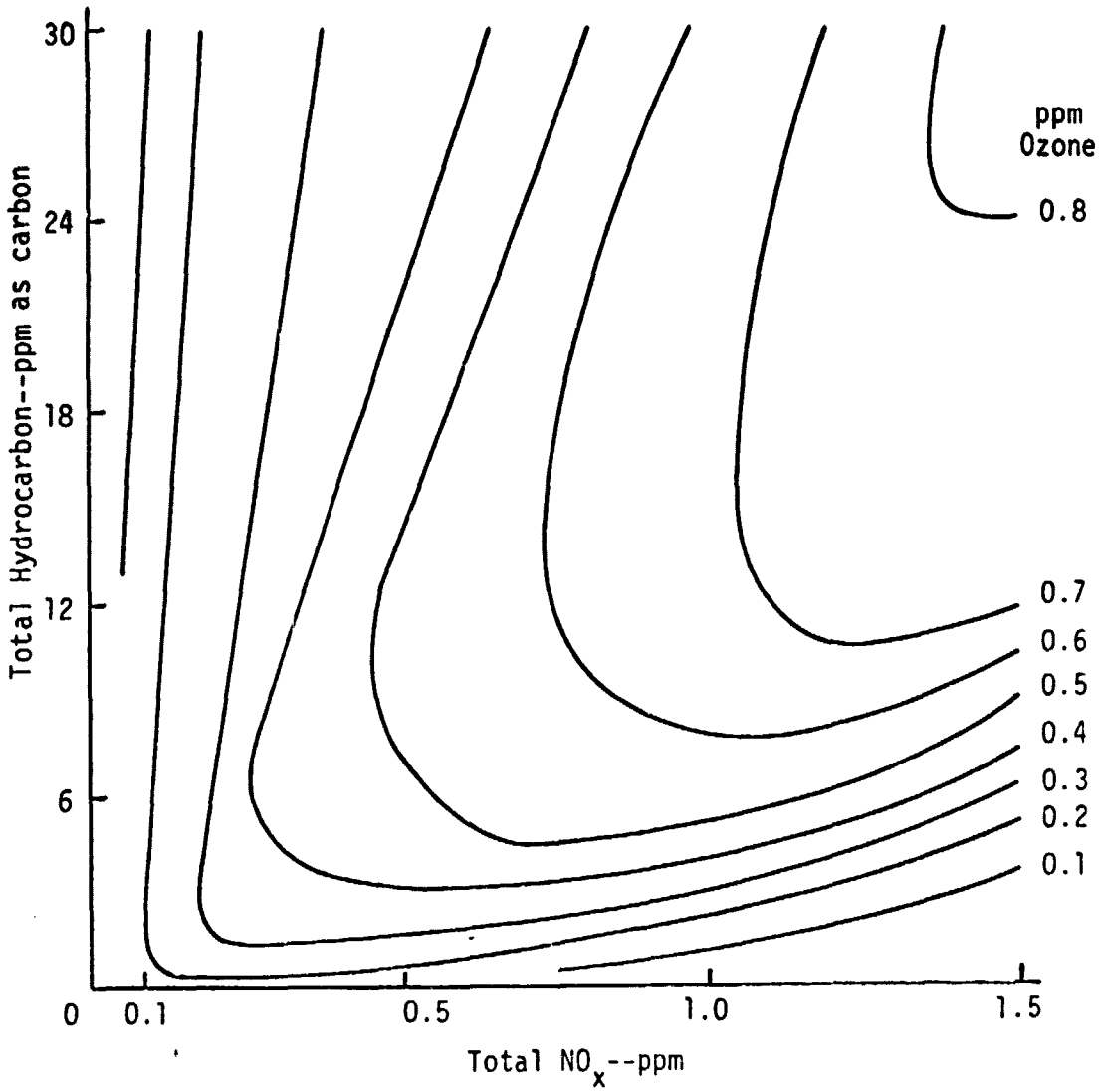

FIGURE 5. OZONE ISOPLETH FOR A SIMULATION OF MIXTURE 1 AFTER AN EIGHT-HOUR PERIOD

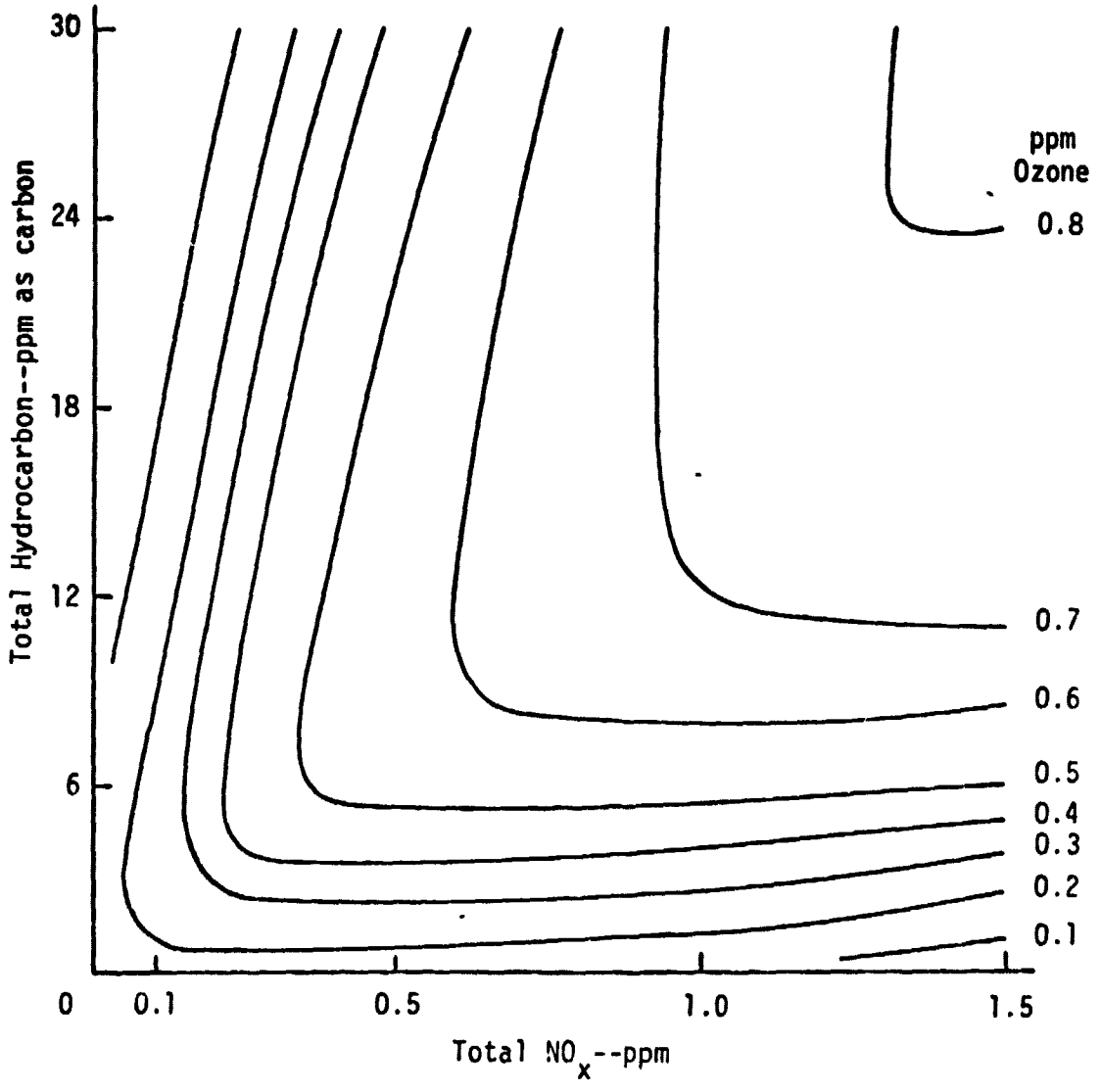

FIGURE 6. OZONE ISOPLETH FOR A SIMULATION OF MIXTURE 1 AFTER A TWELVE-HOUR PERIOD

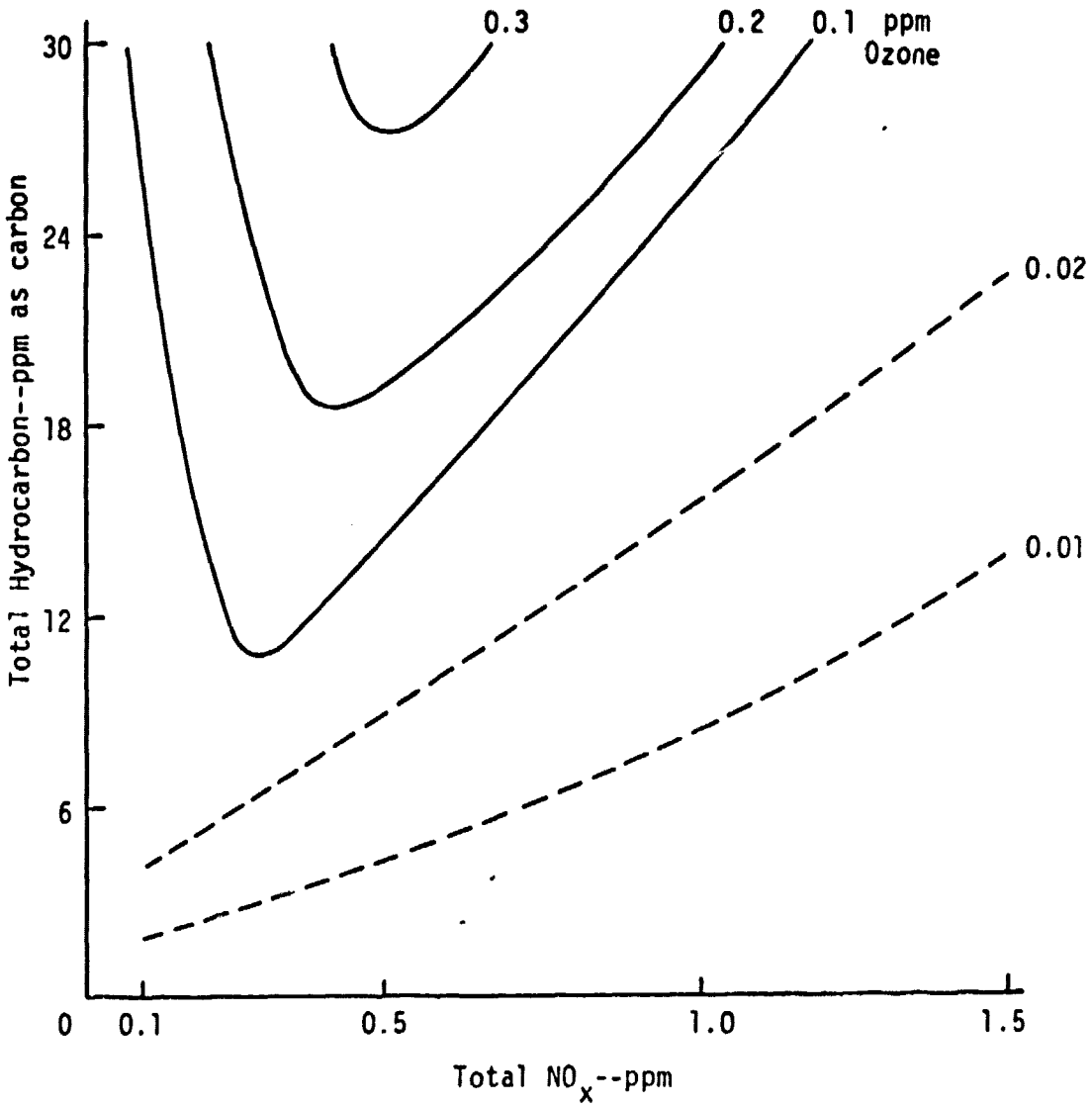

FIGURE 7. OZONE ISOPLETH FOR A SIMULATION OF MIXTURE 3 AFTER A ONE-HOUR PERIOD

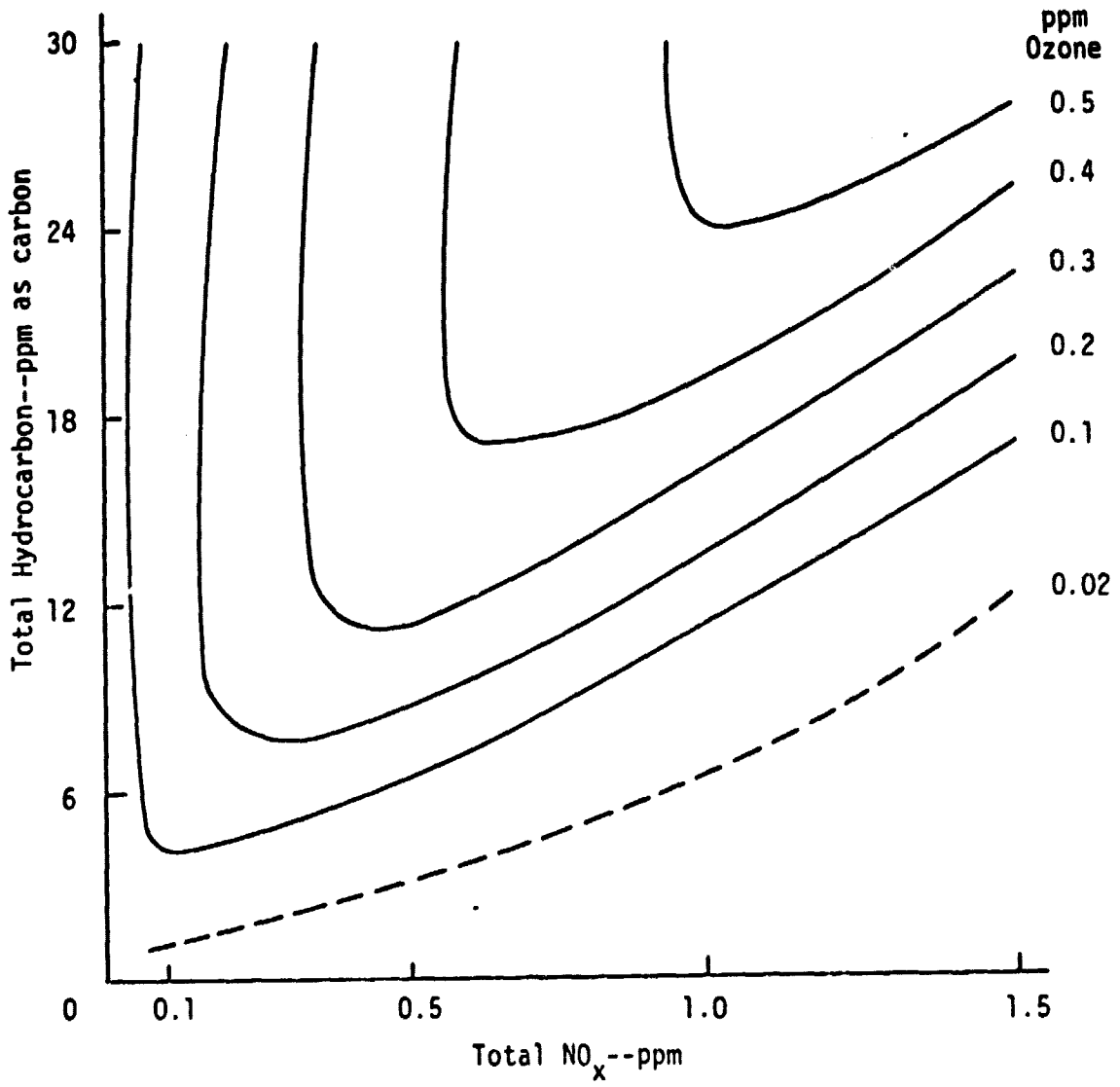

FIGURE 8. OZONE ISOPLETH FOR A SIMULATION OF MIXTURE 3 AFTER A TWO-HOUR PERIOD

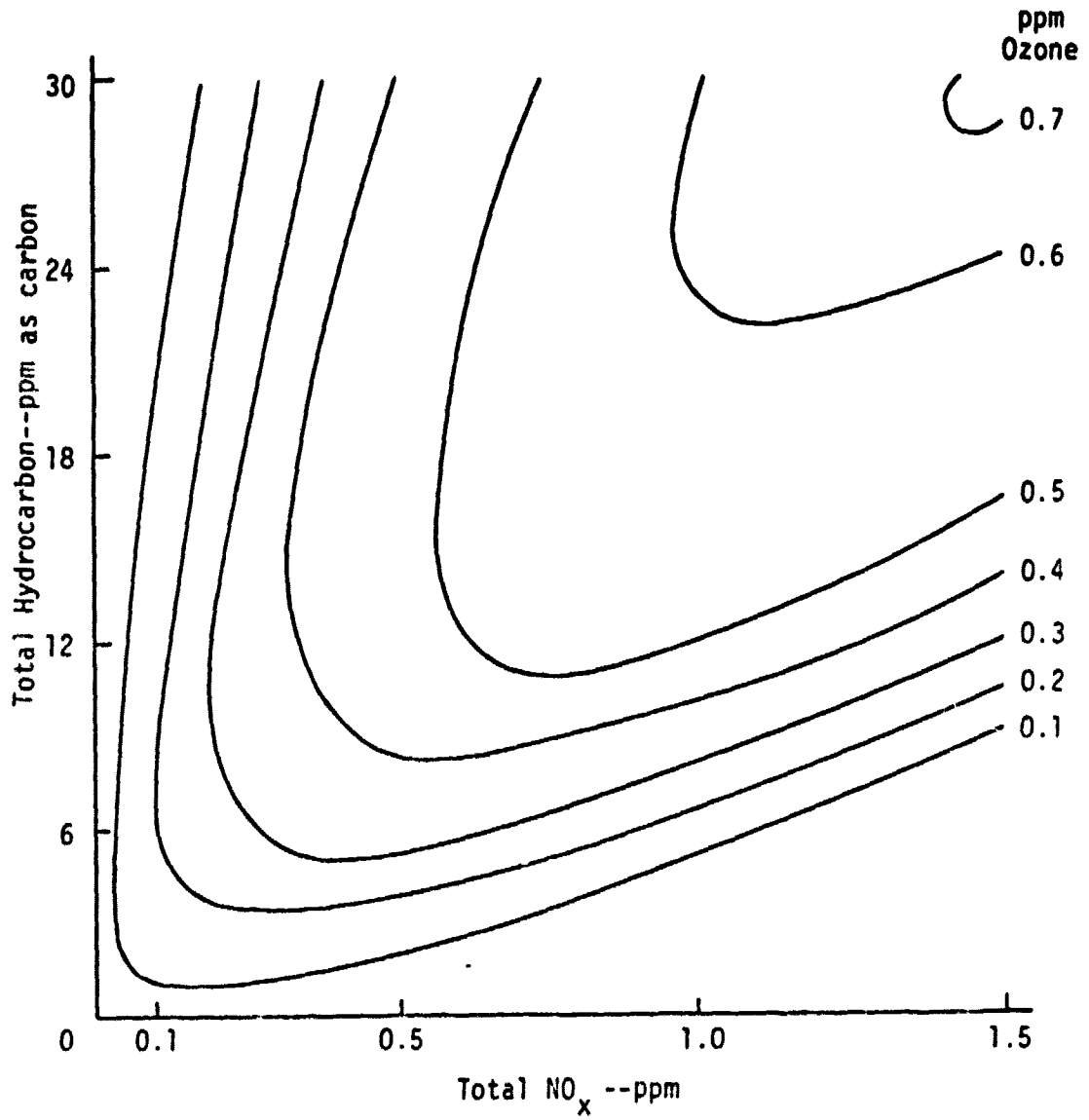

FIGURE 9. OZONE ISOPLETH FOR A SIMULATION OF MIXTURE 3 AFTER A FOUR-HOUR PERIOD

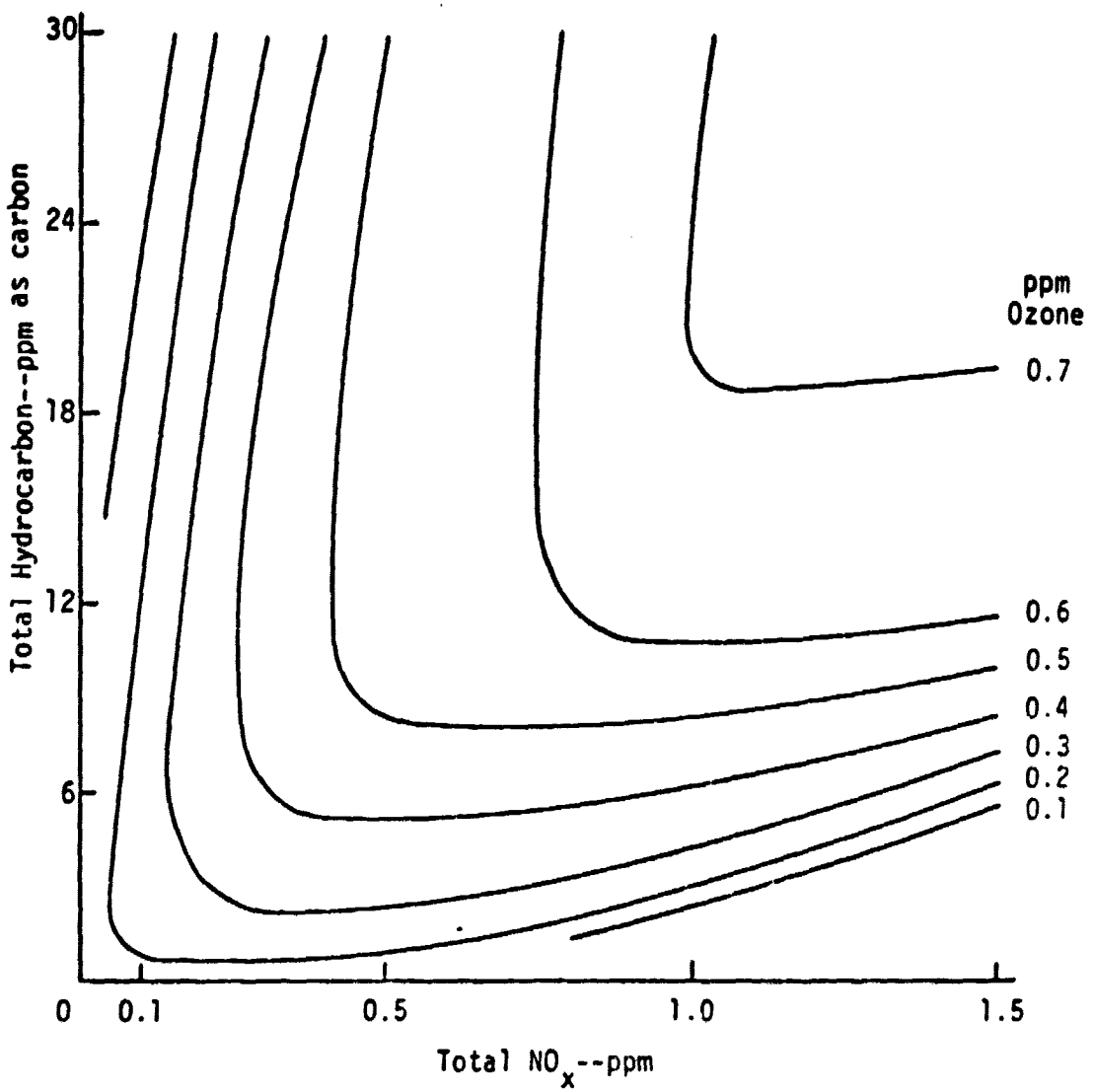

FIGURE 10. OZONE ISOPLETH FOR A SIMULATION OF MIXTURE 3 AFTER AN EIGHT-HOUR PERIOD

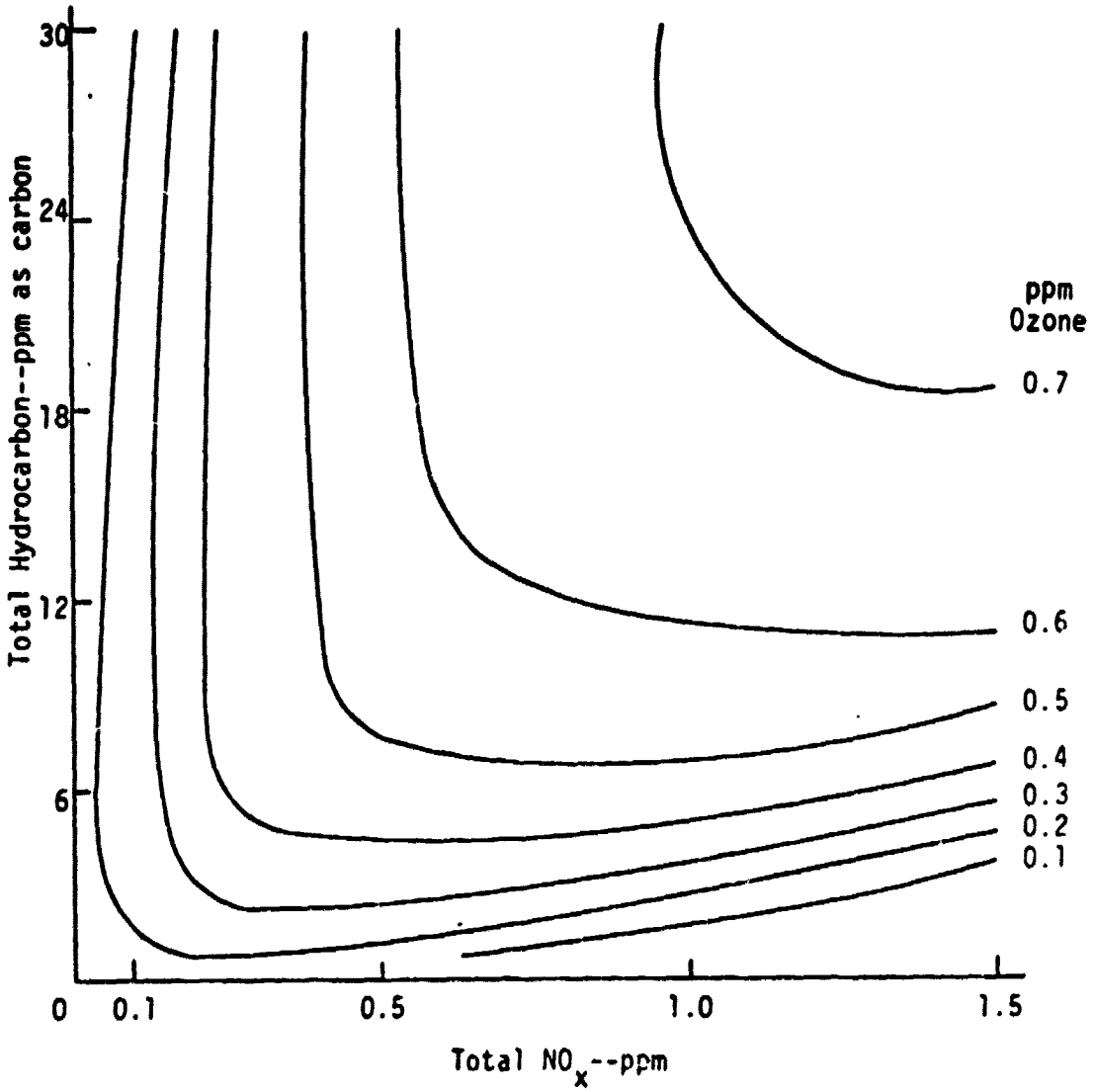

FIGURE 11. OZONE ISOPLETH FOR A SIMULATION OF MIXTURE 3 AFTER A TWELVE-HOUR PERIOD

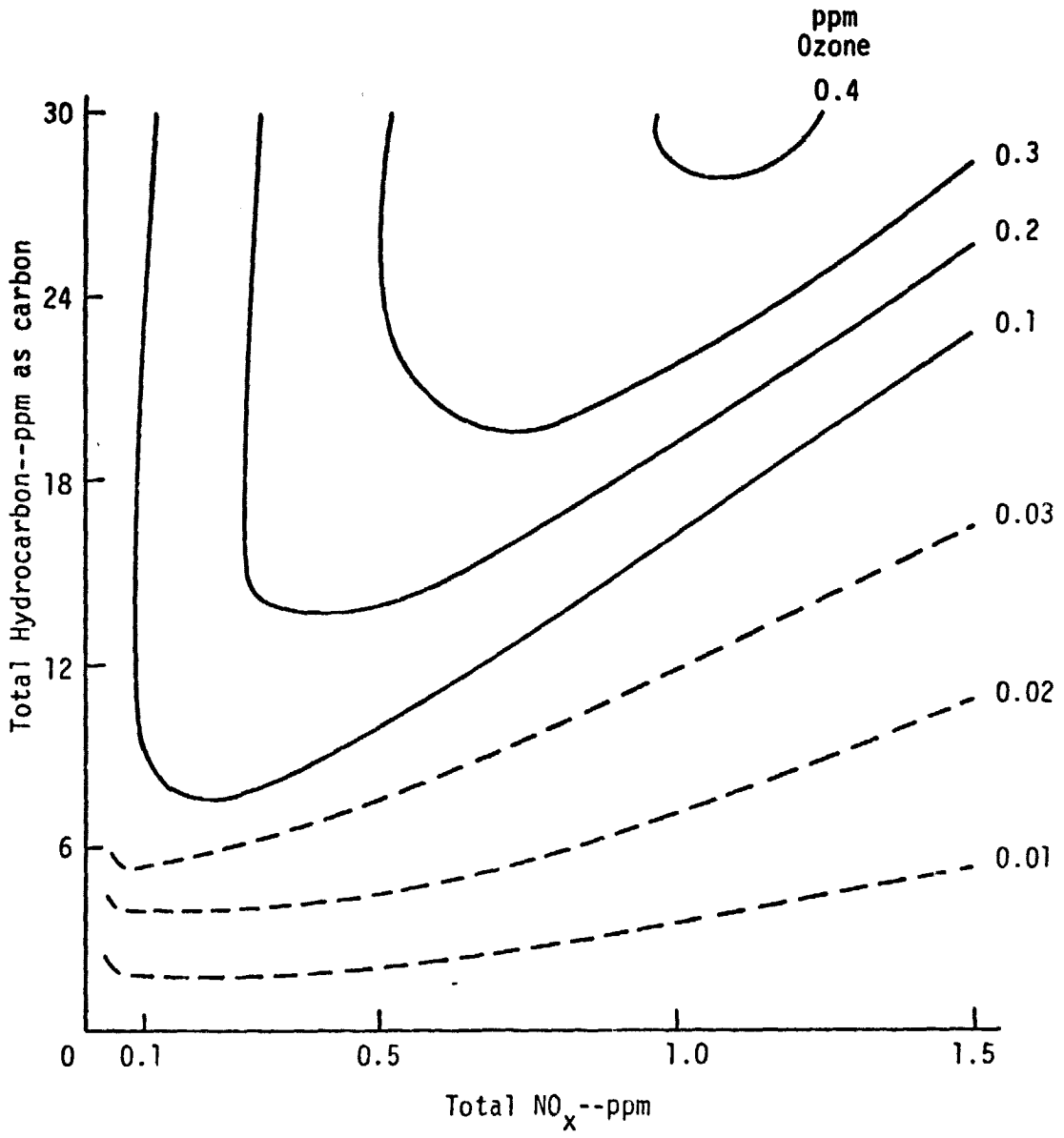

FIGURE 12. OZONE ISOPLETH FOR A SIMULATION OF MIXTURE 2 AFTER A ONE-HOUR PERIOD

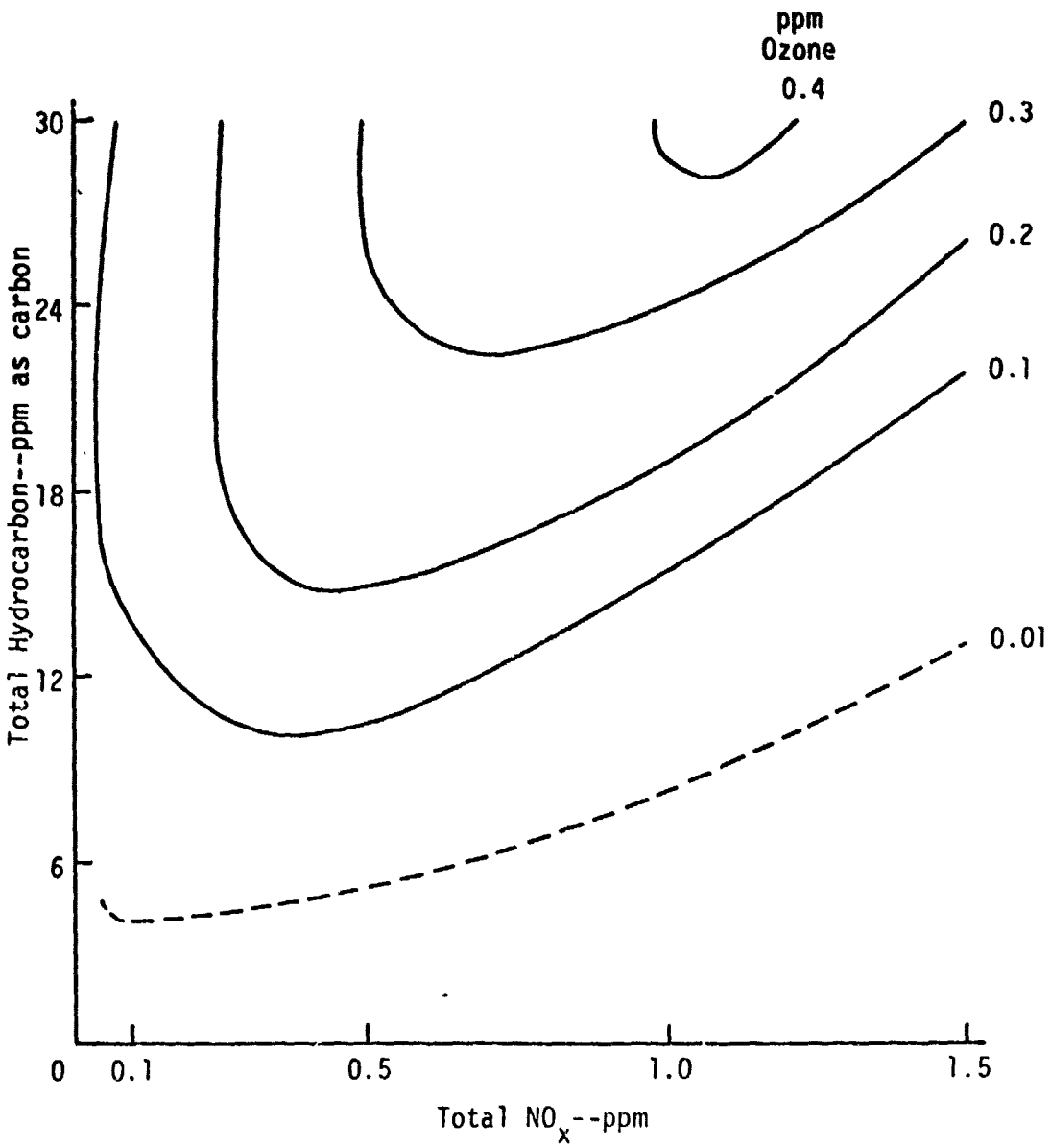

FIGURE 13. OZONE ISOPLETH FOR A SIMULATION OF MIXTURE 4 AFTER A ONE-HOUR PERIOD

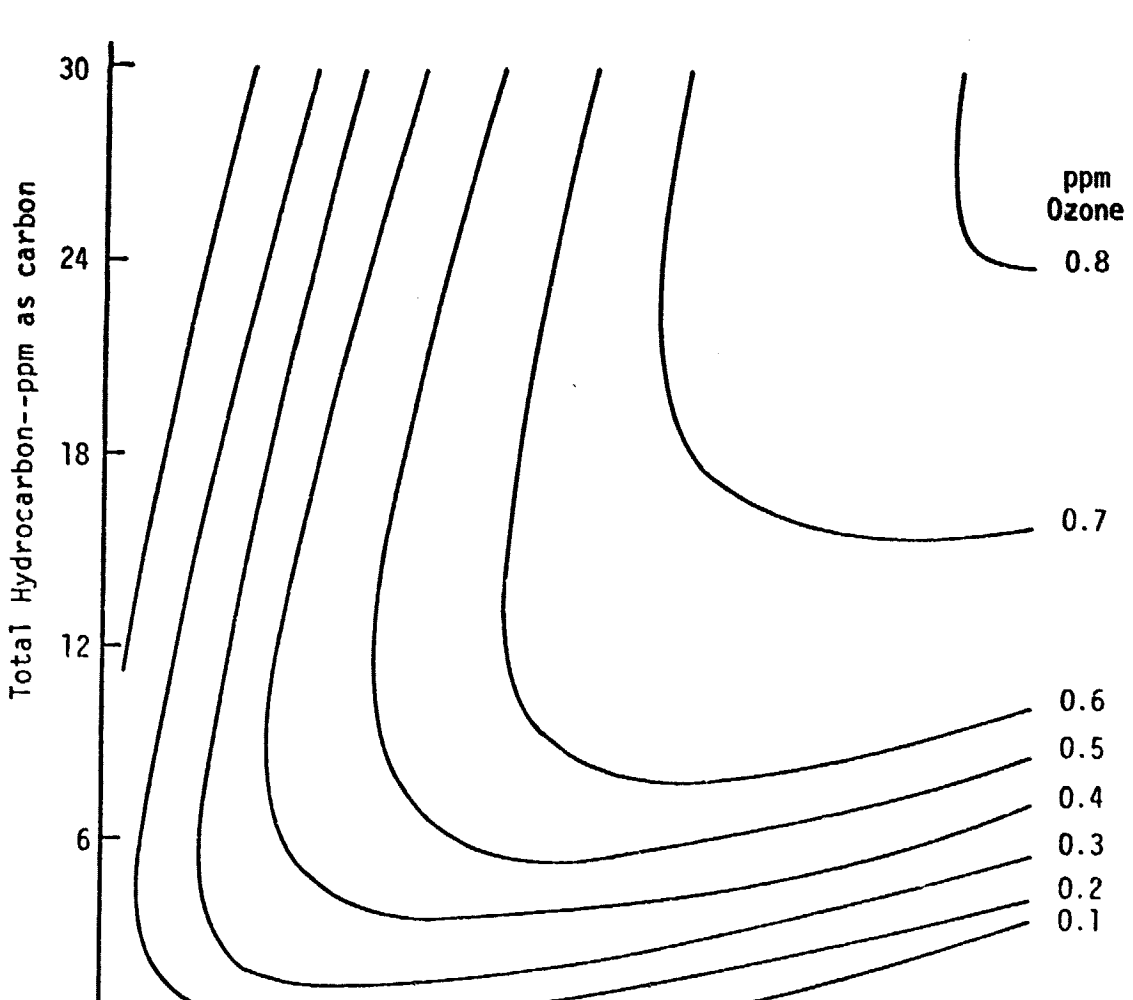

FIGURE 14. OZONE ISOPLETH FOR A SIMULATION OF MIXTURE 2 AFTER AN EIGHT-HOUR PERIOD

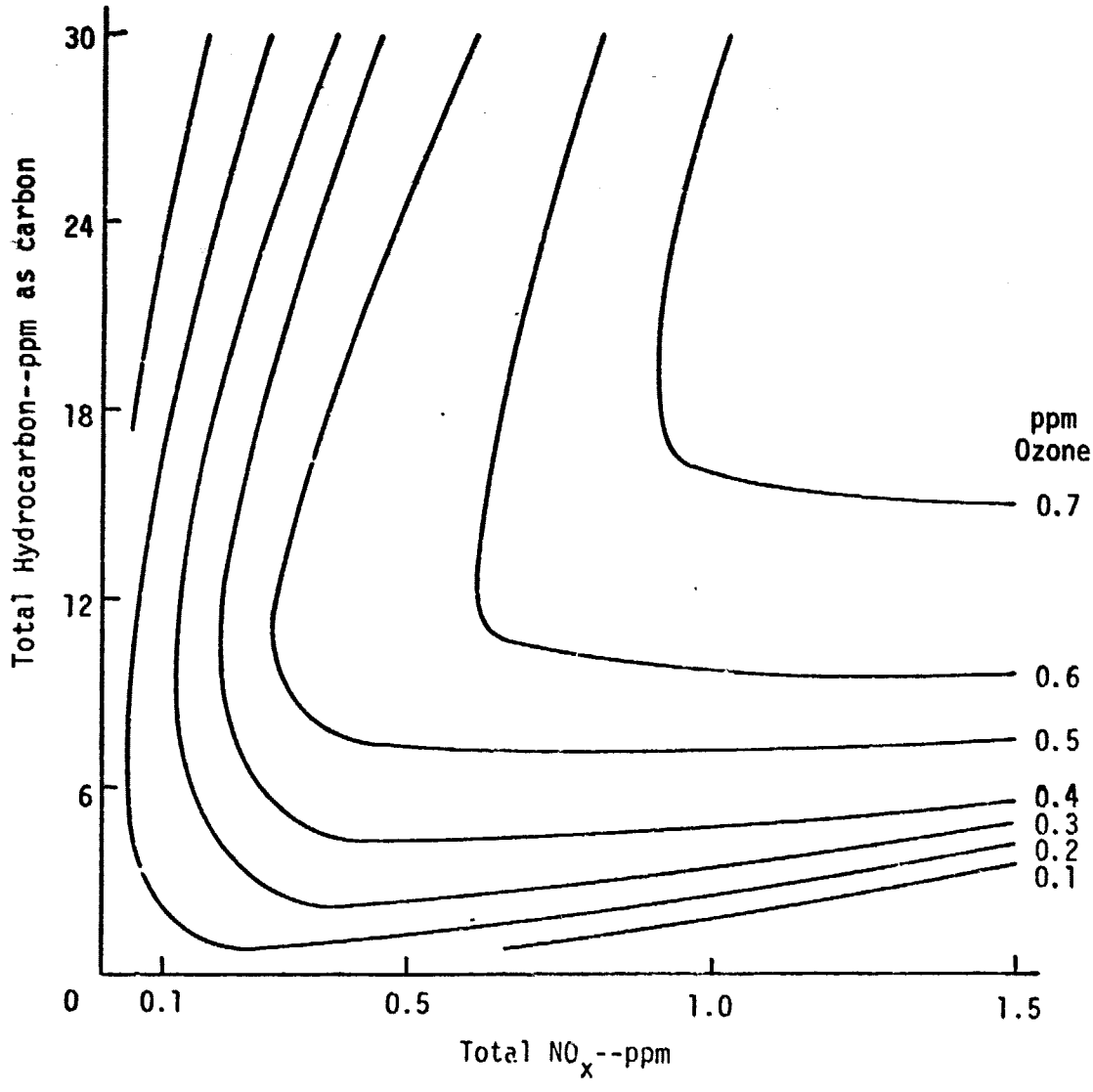

FIGURE 15. OZONE ISOPLETH FOR A SIMULATION OF MIXTURE 4 AFTER AN EIGHT-HOUR PERIOD

C. COMPUTER SIMULATIONS WITH AUTOMOBILE EMISSIONS

The reactions of a hydrocarbon mixture typical of automobile emissions were simulated for comparison with the results of the aircraft mixture simulations. The Bureau of Mines (1973) performed an extensive study of hydrocarbon and NO_x emissions from ten 1970-1973 automobiles. The results of their study are presented in Table 25. The hydrocarbon distributions are presented as weight percent of total hydrocarbon. Converting from weight percent to moles of carbon for the 40 percent aromatic fuel, one finds that the C_2-C_5 group is most representative of paraffins, the C_3-C_5 group is most representative of the olefins, and the C_7+ group is most representative of the aromatics. Therefore, in the computer simulations, butane is used for the alkane reactions, propylene for the alkene reactions, and toluene for the aromatic reactions. The percentages of the alkane, alkene, and aromatic groups from Table 25 are approximately 20 percent, 45 percent, and 35 percent, respectively. Computer simulations were performed using hydrocarbon and NO_x initial concentrations in Figure 1 and a NO/NO_2 ratio of 9:1. The ozone isopleths obtained from these simulations are shown in Figures 16 and 17. The hydrocarbon mixture from automotive emissions is very similar to Mixture 1 of the aircraft mixtures. A comparison of the ozone isopleths of Mixture 1 with the ozone isopleths of the automobile mixture shows similar trends in ozone behavior. Also, both of these mixtures show approximately the same hydrocarbon reactivity upon comparing the isopleths at any given time.

Table 25

HYDROCARBON DISTRIBUTION IN AUTOMOBILE EXHAUST
(in weight percent)

Automobile	Total Hydrocarbons (grams/mile)	Paraffins			Olefins			Aromatics		Acetylenes
		Methane	C_2-C_5	C_6^+	Ethylene	C_3-C_5	C_6^+	Benzene	C_7^+	
1972 Oldsmobile 98 with a 455-CID Engine	1.79	3.0	8.8	17.4	9.6	9.0	2.1	4.5	39.4	6.2
1971 Ford Galaxie with a 351-CID Engine	4.88	8.7	7.4	12.6	8.4	9.6	1.5	4.8	35.2	11.8
1971 Plymouth Fury III with a 360-CID Engine	3.22	3.6	8.3	12.5	10.6	12.7	1.2	5.1	40.1	5.9
1972 Ford Torino with a 351-CID Engine	2.16	10.9	7.7	8.9	10.8	8.4	0.8	6.0	31.2	15.3
1970 Chevrolet Impala with a 350-CID Engine	3.58	6.3	7.0	11.4	10.0	10.4	1.1	5.5	40.6	7.7
1970 Pontiac with a 400-CID Engine	5.86	3.7	10.1	21.7	8.0	12.8	3.1	3.9	21.7	5.0
1970 Volkswagon with a 1,600-CC Engine	2.44	6.6	7.3	12.8	9.4	8.6	1.1	5.2	39.8	9.2
1971 Chevrolet Vega with a 2,300-CC Engine	4.92	7.4	9.4	19.9	7.9	8.8	2.8	3.8	30.9	9.1
1973 Ford Torino with a 351-CID Engine	2.79	4.7	8.1	11.5	11.0	13.1	1.2	5.3	38.5	6.6
1973 Chevrolet Impala with a 350-CID Engine	2.16	6.1	8.8	14.3	10.6	10.3	1.6	5.2	36.7	6.4

Notes: Fuel--typical clear III; 40 percent aromatic. Data weighted in accordance with the 1975 Federal test procedure. All tests conducted at 75°F ambient temperature.

Source: Bureau of Mines (1973)

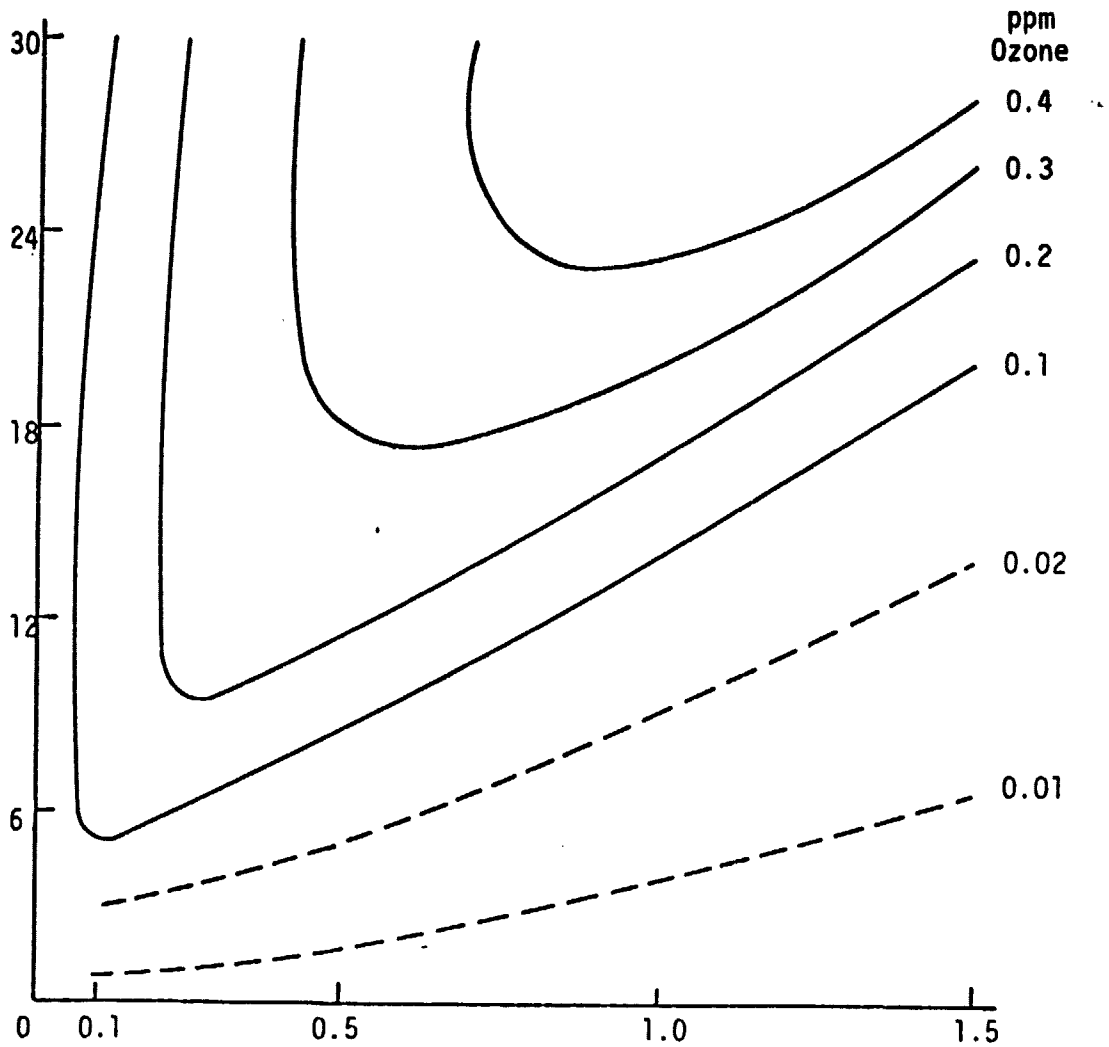

FIGURE 16. OZONE ISOPLETH FOR A SIMULATION OF AN AUTOMOBILE MIXTURE AFTER A ONE-HOUR PERIOD

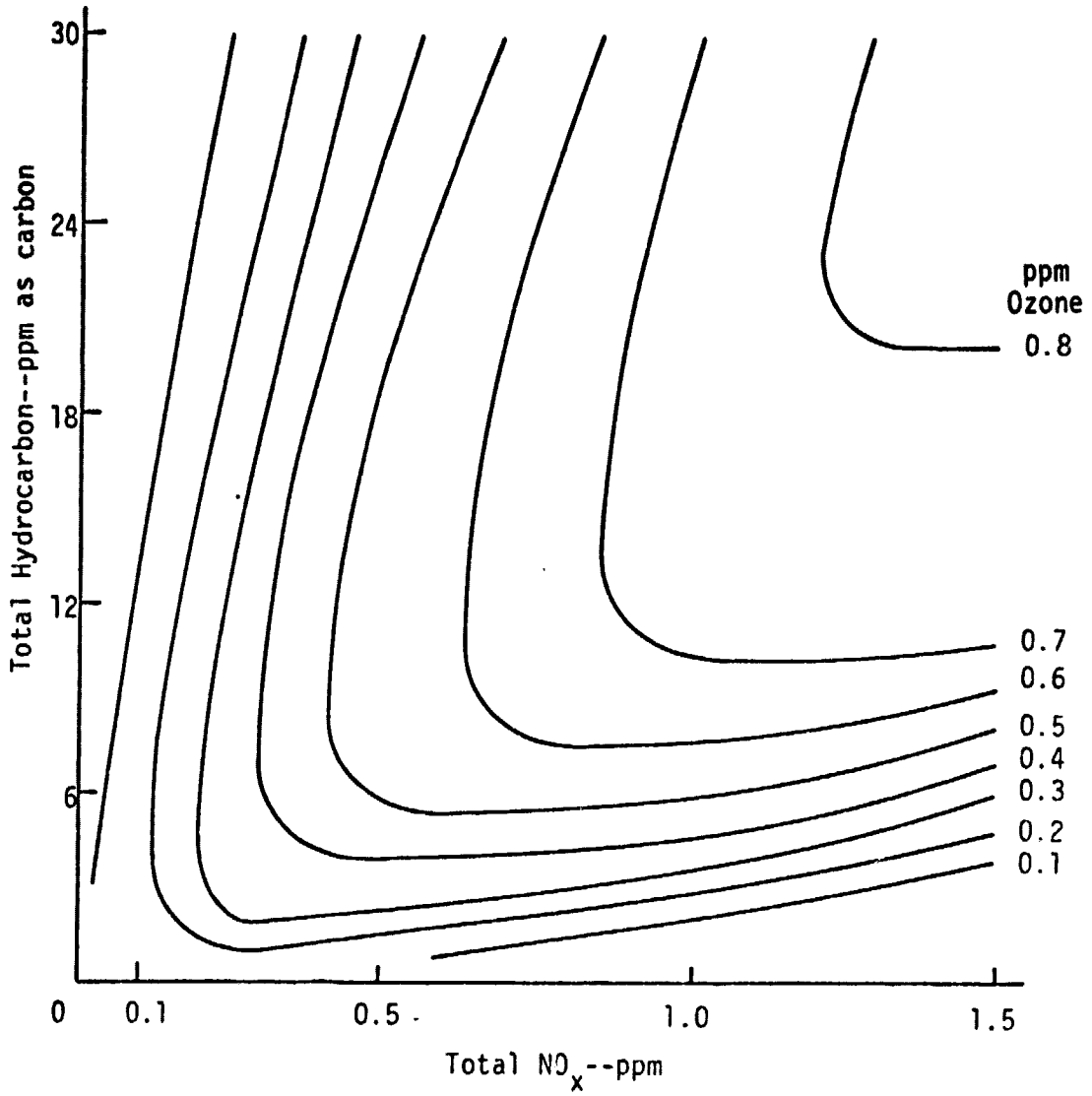

FIGURE 17. OZONE ISOPLETH FOR A SIMULATION OF AN AUTOMOBILE MIXTURE AFTER A EIGHT-HOUR PERIOD

IV SENSITIVITY RUNS AND EVALUATION OF THE KINETIC MECHANISM

As with all theoretical formulations, some uncertainties are inherent in the kinetic mechanism. These uncertainties may be due to the inaccuracy of the rate constants or the omission of important reactions. Minimization of these uncertainties is a major goal of the experimentalist. Yet, the evaluation of the kinetic mechanism for the reliability of predictions must be left to others.

The Hecht, Seinfeld, and Dodge general kinetic mechanism was evaluated by Hecht et al. (1974a). They found that predictions of the kinetic mechanism are strongly dependent on the production of radicals ($HO_2^{\cdot}$, $O\cdot$, $RO_2^{\cdot}$, $OH\cdot$, and $RO\cdot$). Without these radicals to initiate the reactions, oxidant levels will be very low. The following reactions are the main sources of radicals:

$$NO_2 + h\nu \rightarrow NO + O\cdot$$

$$\text{Aldehyde} + h\nu \rightarrow (1 + \delta)HO_2^{\cdot} + (1 - \delta)RO_2^{\cdot} + CO$$

$$HNO_2 + h\nu \rightarrow NO + OH\cdot \quad .$$

Unless a small concentration of aldehydes is used as an initial condition, the photolysis of aldehydes cannot occur until after they are formed through reactions involving hydrocarbons. In all the computer simulations previously mentioned, the initial aldehyde concentrations were assumed to be zero. However, aldehydes may compose up to 15 percent of the total hydrocarbons emitted from aircraft engines. To investigate the effects of the presence of aldehydes at the start of the simulation, we performed computer simulations with initial concentrations of aldehydes varying from zero to 0.15 ppm. The results of these simulations are shown in Figure 18. The simulations with initial aldehyde concentrations show high amounts of ozone during the early

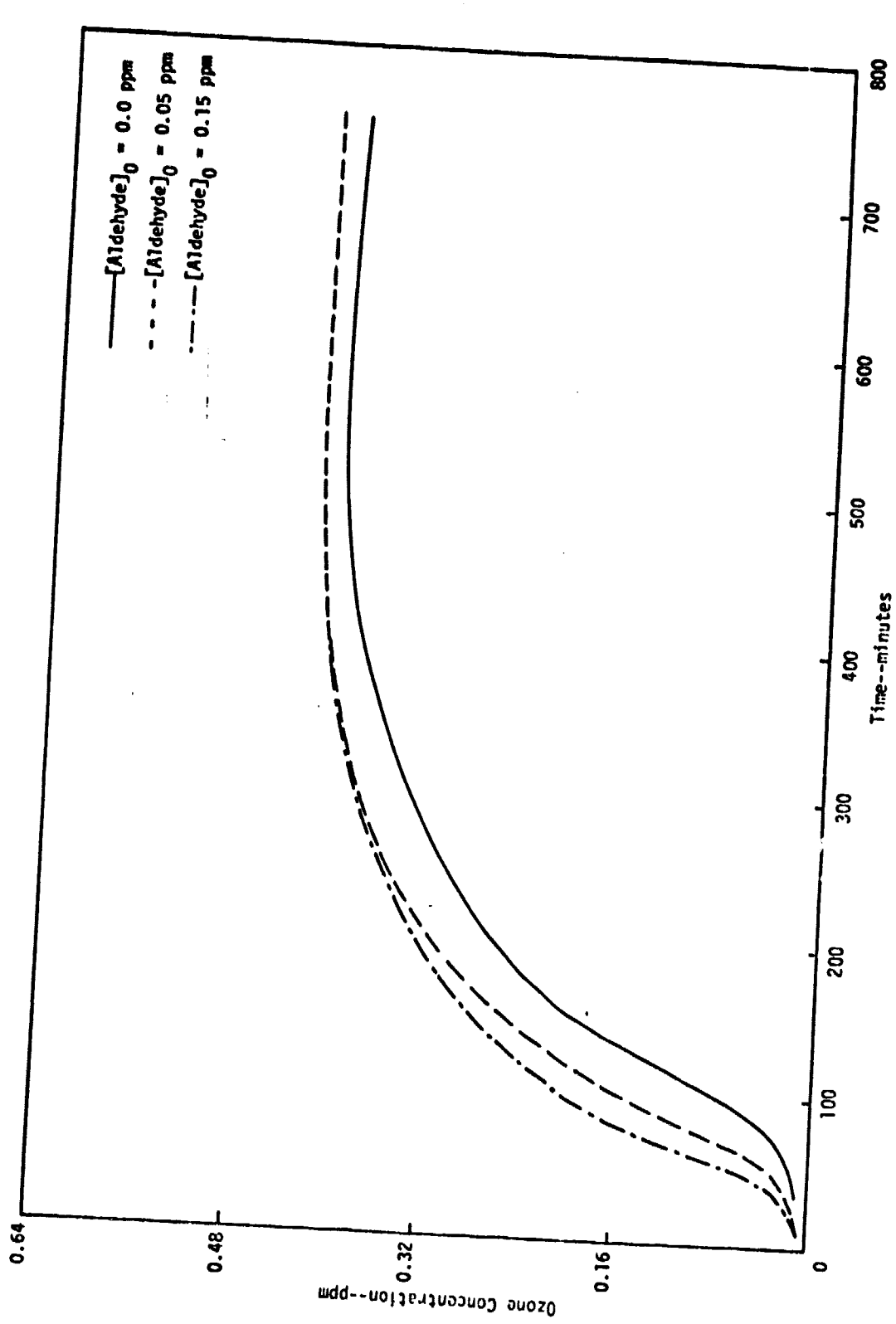

FIGURE 18. EFFECTS OF VARYING INITIAL ALDEHYDE CONCENTRATIONS ON THE OZONE BEHAVIOR FOR MIXTURE 3, $[NO_x]_0$ = 0.3 ppm, $[Hydrocarbon]_0$ = 6 ppm C

hours of the simulations. The simulation with initial aldehyde concentration equal to 0.15 ppm shows a more rapid ozone formation in the early hours than the simulation with initial aldehyde concentration at 0.05 ppm. But by the end of the simulations the ozone concentrations for the different initial aldehyde concentrations are essentially the same. Therefore, increasing the initial aldehyde concentration has an effect on the induction period, but little effect on the concentration of ozone near the end of the simulation for the initial hydrocarbon and NO_x concentrations used in these simulations.

As in the case of aldehydes, unless some HNO_2 is assumed to be present initially, photolysis of HNO_2 cannot occur until it is formed in the heterogeneous surface reaction:

$$NO + NO_2 + H_2O \rightarrow 2HNO_2 \quad .$$

Surface reactions involving NO_x and water are strongly dependent on the characteristics of the smog chamber. Durbin et al. (1975) performed sensitivity runs in which they varied the rate constants of the first two reactions listed as surface reactions in Table 23. They also varied the initial HNO_2 concentrations. The results of their simulations are presented in Figures 19 and 20. Increasing the rate constant for the formation of HNO_2 causes a rapid buildup of ozone in the first few hours of simulation. Yet, the concentrations for the different runs are the same at the end of the simulations.* The same effects were observed when the simulations were run with increased initial concentrations. The result of a simulation using the generalized kinetic mechanism without the heterogeneous HNO_2 chemistry is shown in Figure 21. There is a decrease in ozone concentration in the early hours, but the final ozone concentration is the same as in the simulation with the heterogeneous HNO_2 chemistry. A second simulation was performed with an initial aldehyde concentration equal to 0.05 ppm and without the HNO_2 chemistry. The results (Figure 21) show an increase in ozone formation in the early hours and a final concentration similar to that in the simulation with no initial aldehyde concentration, but with the HNO_2 chemistry.

---

*Note that these simulations were carried out for only a six-hour period.

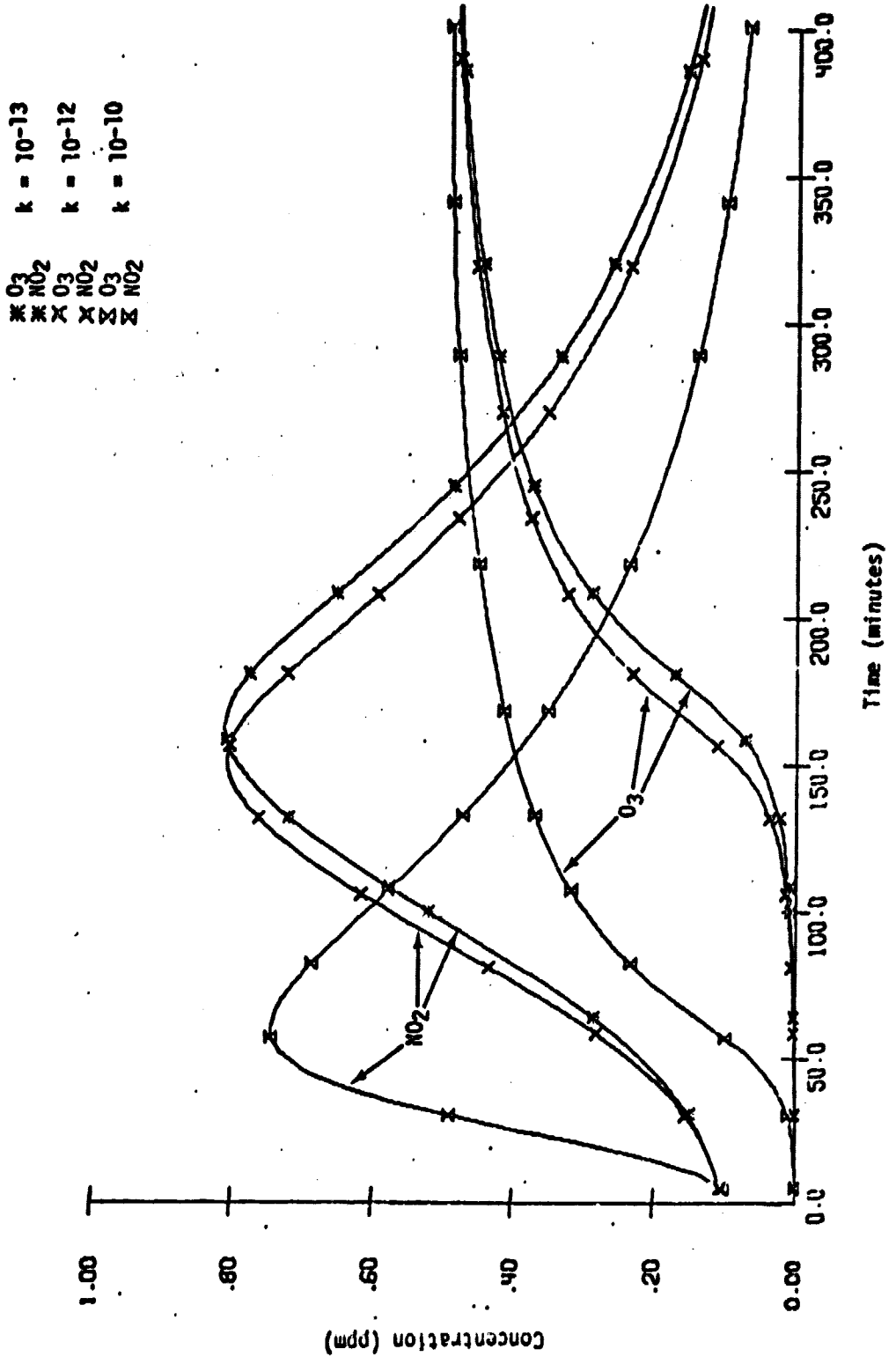

FIGURE 19. SMOG PROFILES FOR DIFFERENT VALUES OF THE RATE CONSTANT FOR THE REACTION $2H_2O + NO + NO_2 \rightarrow 2HNO_2 + H_2O$

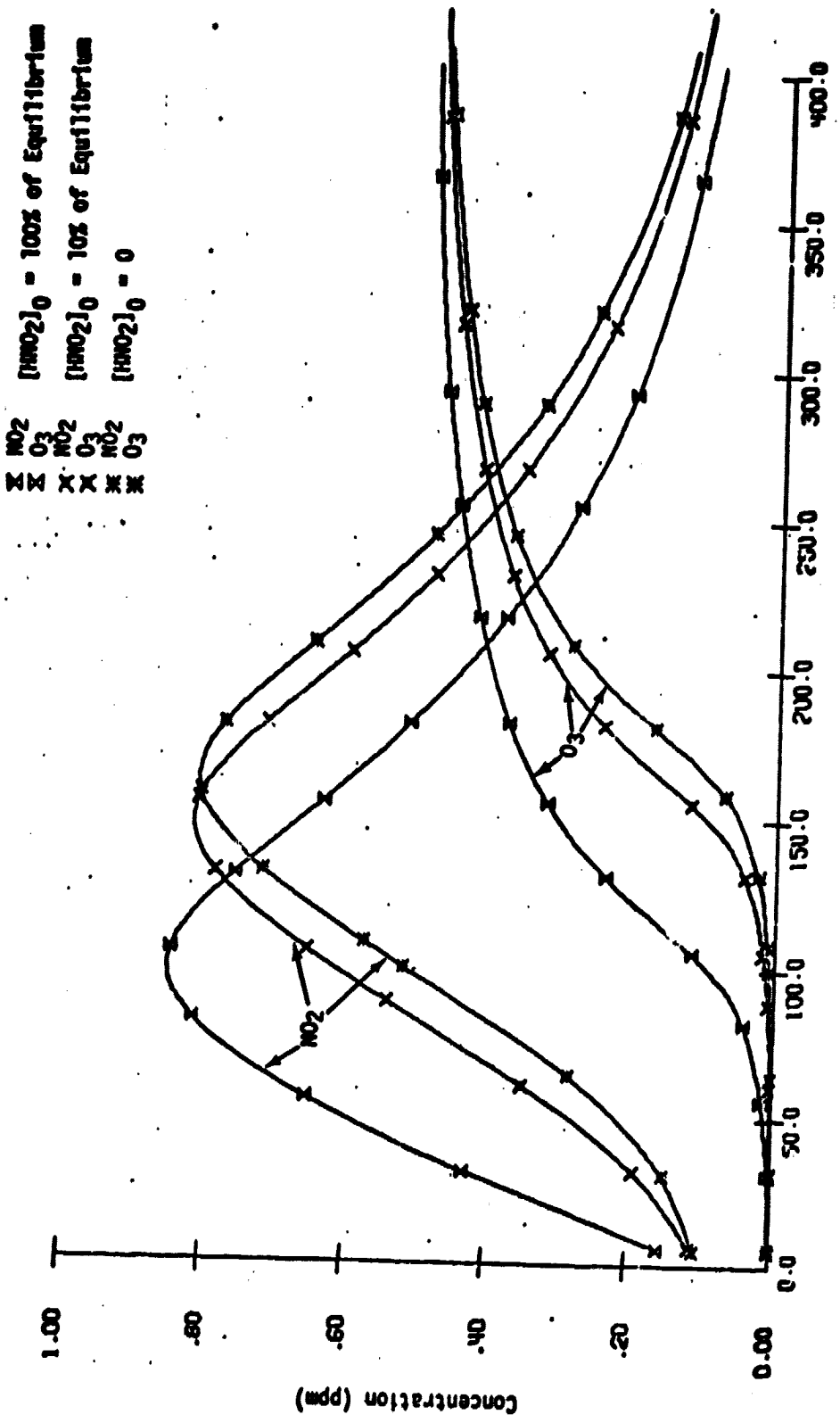

FIGURE 20. SMOG PROFILES FOR DIFFERENT INITIAL CONCENTRATIONS OF HNO_2

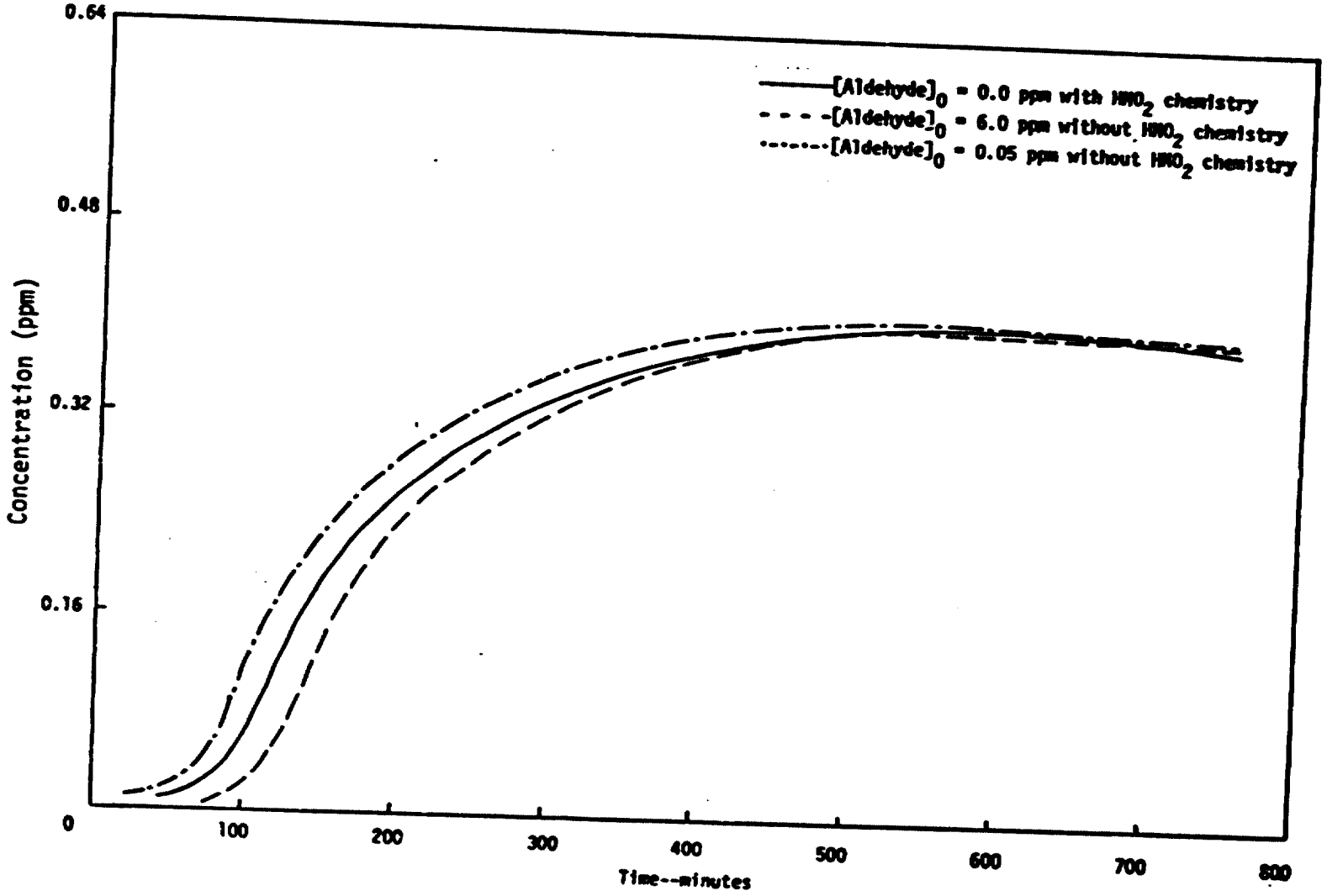

FIGURE 21. EFFECTS OF HETEROGENEOUS HNO_2 CHEMISTRY ON OZONE BEHAVIOR FOR MIXTURE 3
$[NO_x]_0$ = 0.3 ppm, $[Hydrocarbon]_0$ = 6.0 ppm C

The rate of the NO_2 photolysis reaction is dependent upon the initial concentration of NO_2. Due to the wide range of values for the ratio of NO to NO_2 in aircraft emissions, sensitivity runs were performed on the generalized kinetic mechanism with varying initial NO and NO_2 concentrations. Runs were made with NO to NO_2 ratios of 2:1 and 20:1. The results of these simulations are shown in Figure 22 along with those of a simulation using the standard NO/NO_2 ratio of 9:1. These simulations show more rapid initial ozone formation with decreasing NO/NO_2 ratios, but changes in the ratio do not affect the ozone behavior near the end of the simulations. Therefore, for the range of NO/NO_2 ratios that typify aircraft emissions data, the value of the ratio chosen (9 in this case) will affect the ozone behavior only in the early hours of the simulation.

A. SENSITIVITY OF REACTIONS IN THE KINETIC MECHANISM

Sensitivity analyses for each reaction in the kinetic mechanism have been performed by Hecht et al. (1974a). Because only small changes have been made in the kinetic mechanism (additions or deletions of certain reactions and some revision of rate constants), a brief sensitivity study was performed on only the previously determined nine most uncertain reactions in the kinetic mechanism The reactions considered in this study are shown in Table 26.

The procedure for the sensitivity study was essentially the same as that used by Hecht et al. (1974a). The standard concentration-time profile of ozone was obtained by computer simulation of Mixture 3 from Table 24, with all rate constants at their standard values (Table 23). Then simulations were performed in which the rate constant of one of the nine reactions mentioned above was doubled while all other rate constants were unchanged. The concentration-time profiles of ozone obtained from these computer simulations are based on the same initial conditions as the "standard" simulation, with the exception of a single rate constant change. These profiles were then compared with the "standard" profile. The areas of the absolute differences between these profiles and the standard were calculated. Then the procedure was repeated with each rate constant in turn decreased by a factor of 2.

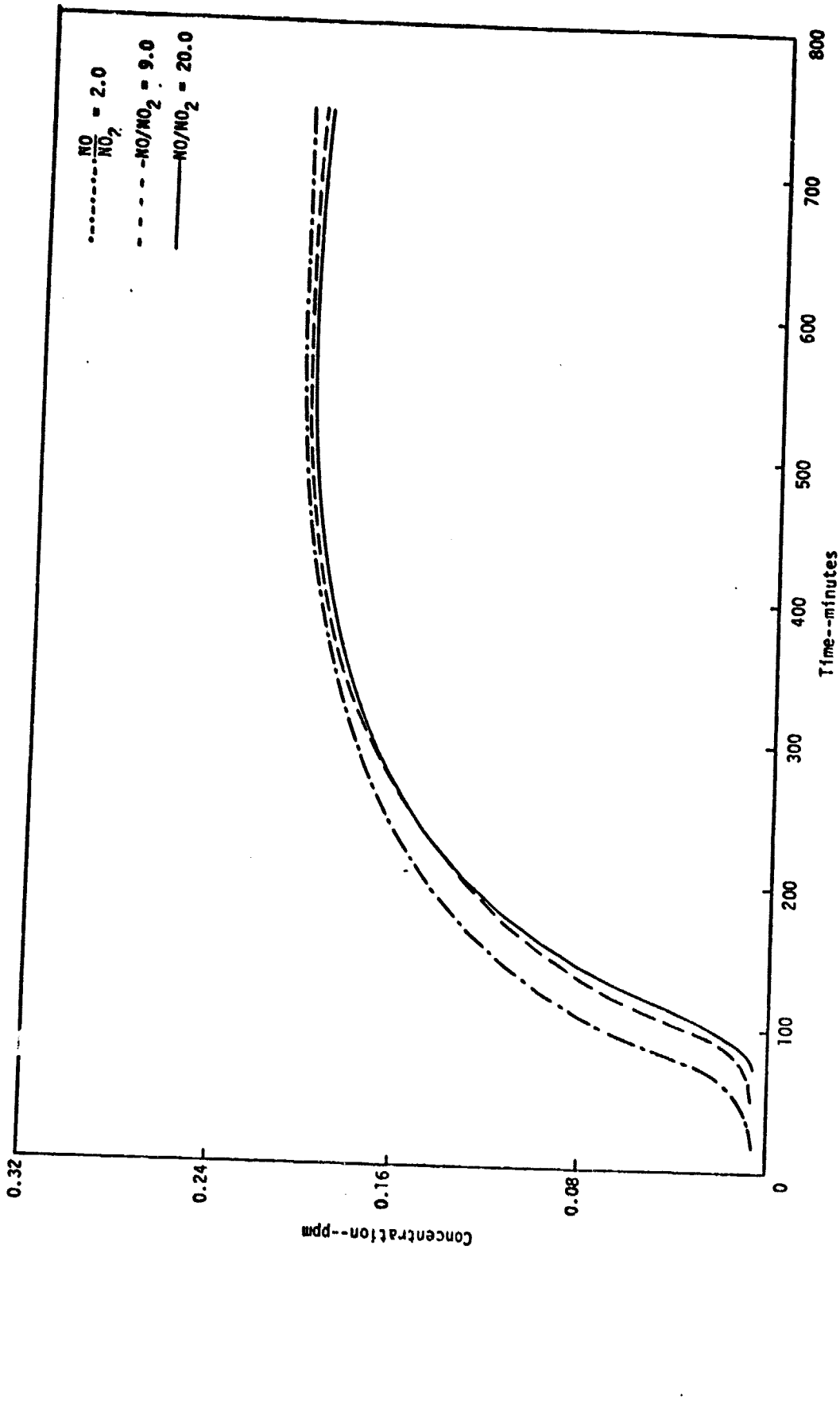

FIGURE 22. EFFECTS OF VARYING THE NO/NO2 RATIO ON OZONE BEHAVIOR FOR MIXTURE 3
$[NO_x]_0$ = 0.3 ppm, $[Hydrocarbon]_0$ = 6 ppm C

Table 26

REACTIONS CONSIDERED IN THE SENSITIVITY STUDY

Reaction	Rate Constant
$NO_2 + h\nu \rightarrow NO + O\cdot$	0.25 min^{-1}
$O_3 + NO \rightarrow NO_2 + O_2$	25.2 $ppm^{-1}\ min^{-1}$
$HO_2 + NO \rightarrow NO_2 + OH\cdot$	800 $ppm^{-1}\ min^{-1}$
$OH\cdot + NO_2 \rightarrow HNO_3$	1×10^4 $ppm^{-1}\ min^{-1}$
$HNO_2 + h\nu \rightarrow NO + OH\cdot$	1.75×10^{-1} min^{-1}
Aldehyde + $h\nu \rightarrow$ Products	1.13×10^{-3} min^{-1}
Aldehyde + $h\nu \rightarrow (1+\delta)HO_2 + (1-\delta)RO_2 + CO$	1.13×10^{-3} min^{-1}
Alkene + $OH\cdot \rightarrow$ Aldehyde + $\alpha HO_2 + (1-\alpha)RO_2$	2.5×10^4 $ppm^{-1}\ min^{-1}$
$NO + NO_2 + H_2O \rightarrow 2HNO_2$	2.6×10^{-7} $ppm^{-2}\ min^{-1}$

The areas of absolute differences for each rate constant were averaged. These averages were normalized to the area under the curve of the "standard" profile and multiplied by 100 to give the sensitivity due to a change by a factor of 2 in the rate constants. The results of this sensitivity study are shown in Table 27. Note that the two aldehyde reactions have been combined into one reaction in the sensitivity study.

In addition to the sensitivity, the uncertainty of each rate constant has an effect on predictions made with the kinetic mechanism. If a rate constant is well established, little uncertainty is introduced into the predictions by its use, even though the results may be highly sensitive to that rate constant. On the other hand, a rate constant with a high degree of uncertainty may have little effect on predictions if the mechanism is relatively insensitive to that constant. Table 28 lists the uncertainty factors of the eight reactions. Hecht et al. (1974a) postulated an ad hoc index called the S*U index to tabulate the major sources of uncertainty in the kinetic mechanism. S*U index is defined as:

S*U = Sensitivity x Uncertainty Factor

Table 27

SENSITIVITY OF THE REACTIONS

Rank	Reaction	Sensitivity
1	$O_3 + NO \rightarrow NO_2 + O_2$	34
2	$NO_2 + h\nu \rightarrow NO + O\cdot$	29
3	$NO + HO_2 \rightarrow NO_2 + OH\cdot$	16
4	$NO_2 + OH\cdot \rightarrow HNO_3$	14
5	Aldehyde + $h\nu$ → Products	11
6	Alkene + $OH\cdot \rightarrow$ Aldehyde + $\alpha HO_2 + (1-\alpha)RO_2$	6
7	$HNO_2 + h\nu \rightarrow NO + OH\cdot$	3
8	$NO + NO_2 + H_2O \rightarrow 2HNO_2$	2

Table 28

UNCERTAINTY FACTORS OF THE REACTIONS

Reaction	Uncertainty Factor*
$O_3 + NO \rightarrow NO_2 + O_2$	1.3†
$NO_2 + h\nu \rightarrow NO + O\cdot$	1.4
$NO + HO_2 \rightarrow NO_2 + OH\cdot$	3.2†
$NO_2 + OH\cdot \rightarrow HNO_3$	2.0†
Aldehyde + $h\nu$ → Products	3
Alkene + $OH\cdot \rightarrow$ Aldehyde + $\alpha HO_2 + (1-\alpha)RO_2$	1.2
$HNO_2 + h\nu \rightarrow NO + OH\cdot$	3.0
$NO + NO_2 + H_2O \rightarrow 2HNO_2$	10.0

*Subjective estimates.

†Hampson and Garvin (1975).

Table 29 lists the reactions studied in order of decreasing S*U index. The reaction of NO with $HO_2^{\cdot}$ radicals shows the highest S*U index, while the reaction of alkenes with OH· radicals shows the least S*U index of this group. The uncertainties in the predictions of the kinetic mechanism may be reduced if more reliable rate constants are found for the reactions investigated in this study.

B. EXTENSION OF THE KINETIC MECHANISM TO INCLUDE LONGER CHAIN HYDROCARBONS

The kinetic mechanism has been validated only for butane and propylene. Therefore, extending the mechanism to include longer chain hydrocarbons involves, at a minimum, performing sensitivity studies of the parameters that are intended to account for the longer chain hydrocarbons. Conkle et al.

Table 29

COMBINED SENSITIVITY AND UNCERTAINTY OF THE REACTIONS

Rank	Reaction	S*U Index
1	$NO + HO_2^{\cdot} \rightarrow NO_2 + OH\cdot$	51.2
2	$O_3 + NO \rightarrow NO_2 + O_2$	44.2
3	$NO_2 + h\nu \rightarrow NO + O$	40.6
4	Aldehyde + $h\nu$ → Products	33.0
5	$NO_2 + OH\cdot \rightarrow HNO_3$	28.0
6	$NO + NO_2 + H_2O \rightarrow 2HNO_2$	20.0
7	$HNO_2 + h\nu \rightarrow NO + OH\cdot$	9.0
8	Alkene + $OH\cdot \rightarrow$ Aldehyde + $\alpha HO_2^{\cdot} + (1-\alpha)RO_2^{\cdot}$	7.8

(1975) observed that n-octane, propylene, 1-butene, and p-xylene are the most abundant molecules emitted from a T-56 combustor. We performed sensitivity runs on different combinations of these molecules with aircraft exhaust emissions consisting of 55 percent alkanes, 25 percent alkenes, and 20 percent aromatics (Mixture 3). Three points on the hydrocarbon/NO_x block (Figure 1) were used as starting conditions. The first two simulations represent situations where exhaust having high hydrocarbon and low NO_x concentrations is emitted into the atmosphere (the hydrocarbon/NO_x ratio is high). The first simulation was performed with a hydrocarbon/NO_x ratio of 30:1 (ppm as carbon/ppm as NO_x). The starting conditions were 3.0 ppm C of hydrocarbon and 0.1 ppm of NO_x. The second simulation was performed with a hydrocarbon/NO_x ratio of 20:1. The starting concentrations were 6.0 ppm C for the hydrocarbons and 0.3 ppm of NO_x. The third simulation, starting with hydrocarbon and NO_x concentrations equal to 3.0 ppm C and 1.2 ppm, respectively, is representative of systems with low hydrocarbon emissions and high NO_x emissions. The new rate constants for these simulations are shown in Table 30.

Table 30

RATE CONSTANTS FOR LONGER CHAIN HYDROCARBONS

Reaction	Rate Constants (ppm^{-1} min^{-1})
Alkane (n-octane) + O· → RO_2 + OH·	500
Alkane (n-octane) + OH· → $RO_2^{\cdot}$ + H_2O	1×10^4
Aromatic (p-xylene) + O· → $RO_2^{\cdot}$ + OH·	290
Aromatic (p-xylene) + OH· → $RO_2^{\cdot}$ + H_2O	2.7×10^4
Alkene (1-butene) + OH· → Aldehyde + $\alpha HO_2^{\cdot}$ + $(1 - \alpha)RO_2^{\cdot}$	6×10^4

Sources: Doyle et al. (1975), Hampson and Garvin (1975), Project Clean Air (1970).

Again, the computer simulations were performed under conditions similar to those of smog chamber experiments (i.e., constant irradiation during the simulation period and inclusion of surface reactions). The results of the three simulations are shown in Figures 23, 24, and 25. For the two simulations representing systems with high HC/NO_x ratios (Figures 23 and 24), changing to the longer chain hydrocarbons does not have a large effect on the ozone concentration compared to the simulation with a lower HC/NO_x ratio (Figure 25). In Figures 23 and 24, the longer chain molecule combinations increase the ozone concentration much faster in the early hours. At any given time there is a greater concentration of ozone than in the shorter chain system. The two different longer chain systems give similar ozone concentrations, which is to be expected, because propylene and 1-butene differ by only one carbon atom. Since the longer chain hydrocarbon system is more representative of typical hydrocarbons emitted from aircraft engines, the ozone isopleths for longer chain systems as a function of time would show a faster buildup of ozone in the early hours for the lower hydrocarbon and NO_x concentrations. In Figure 25, changing to the longer chain hydrocarbons has a big effect on the ozone behavior for the low HC/NO_x system. The final ozone concentration is more than a factor of two higher in the longer chain systems than in the shorter chain system.

Besides varying the species in the sensitivity runs, we also varied the closure parameters, δ and ϵ. As discussed previously, these closure parameters are dependent on the specific alkane and alkene molecules used in the kinetic mechanism. For the mixture consisting of n-octane, 1-butene, and p-xylene, the closure parameters were varied from their original values of 0.5 to the new values of 0.25. The closure parameters, δ and ϵ, are functions of the length of the hydrocarbon chain. These parameters limit the number of $RO_2^{\cdot}$ and $HO_2^{\cdot}$ radicals formed in the following reactions:

$$\text{Aldehyde} + h\nu \rightarrow (1 + \delta)HO_2^{\cdot} + (1 - \delta)RO_2^{\cdot} + CO$$

$$\text{Aldehyde} + OH\cdot \rightarrow \delta HO_2^{\cdot} + (1 - \delta)RO_2^{\cdot}$$

$$RO_2^{\cdot} + NO \rightarrow \text{Aldehyde} + 0.5(1 + \epsilon)HO_2^{\cdot} + 0.5(1 + \epsilon)CO + 0.5(1 - \epsilon)RO_2^{\cdot} + NO_2$$

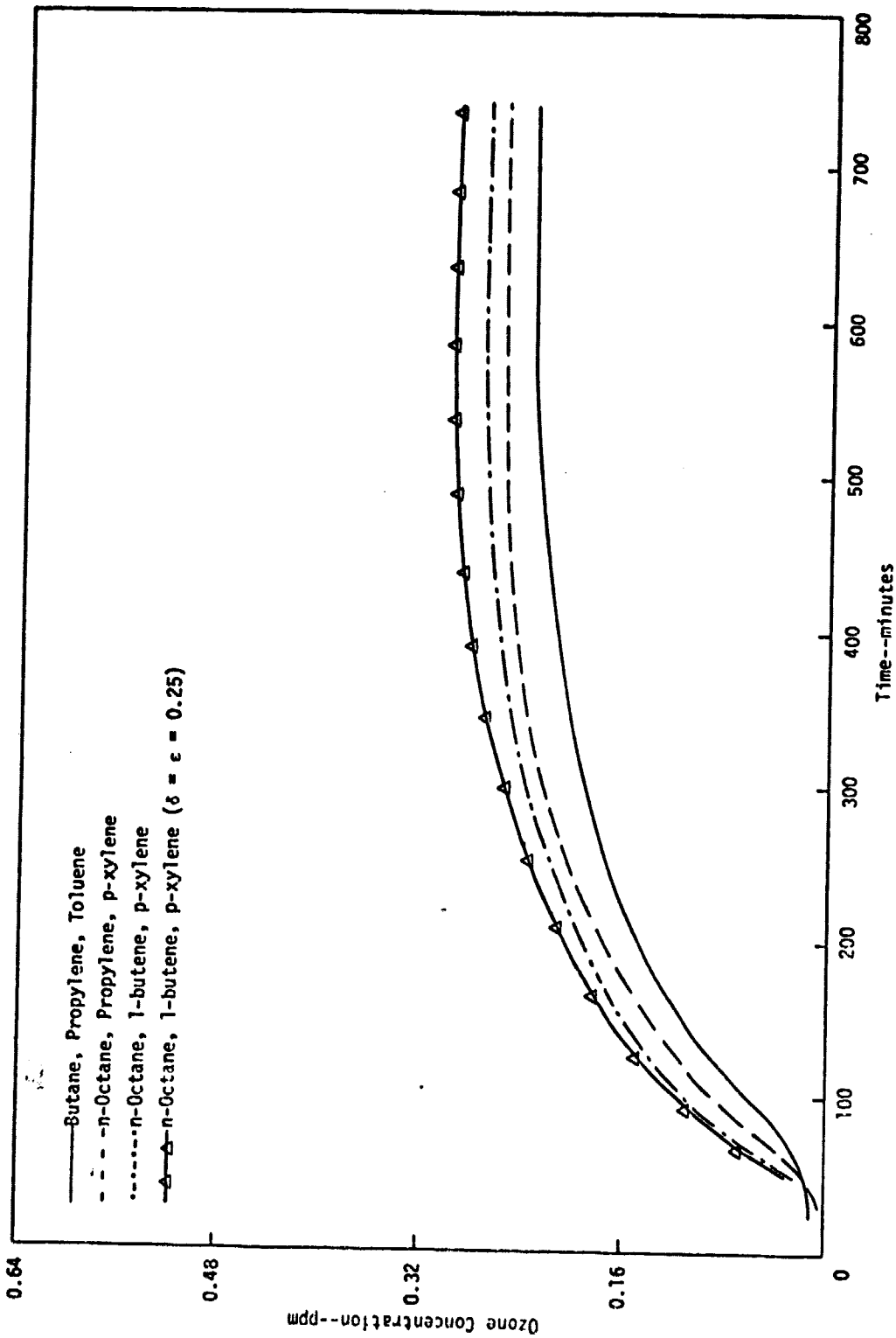

FIGURE 23. EFFECTS OF DIFFERENT COMBINATIONS OF HYDROCARBONS ON OZONE BEHAVIOR FOR MIXTURE 3 $[NO_x]_0$ = 0.1 ppm, [Hydrocarbon]$_0$ = 3 ppm C and [Aldehyde]$_0$ = 0.0 ppm

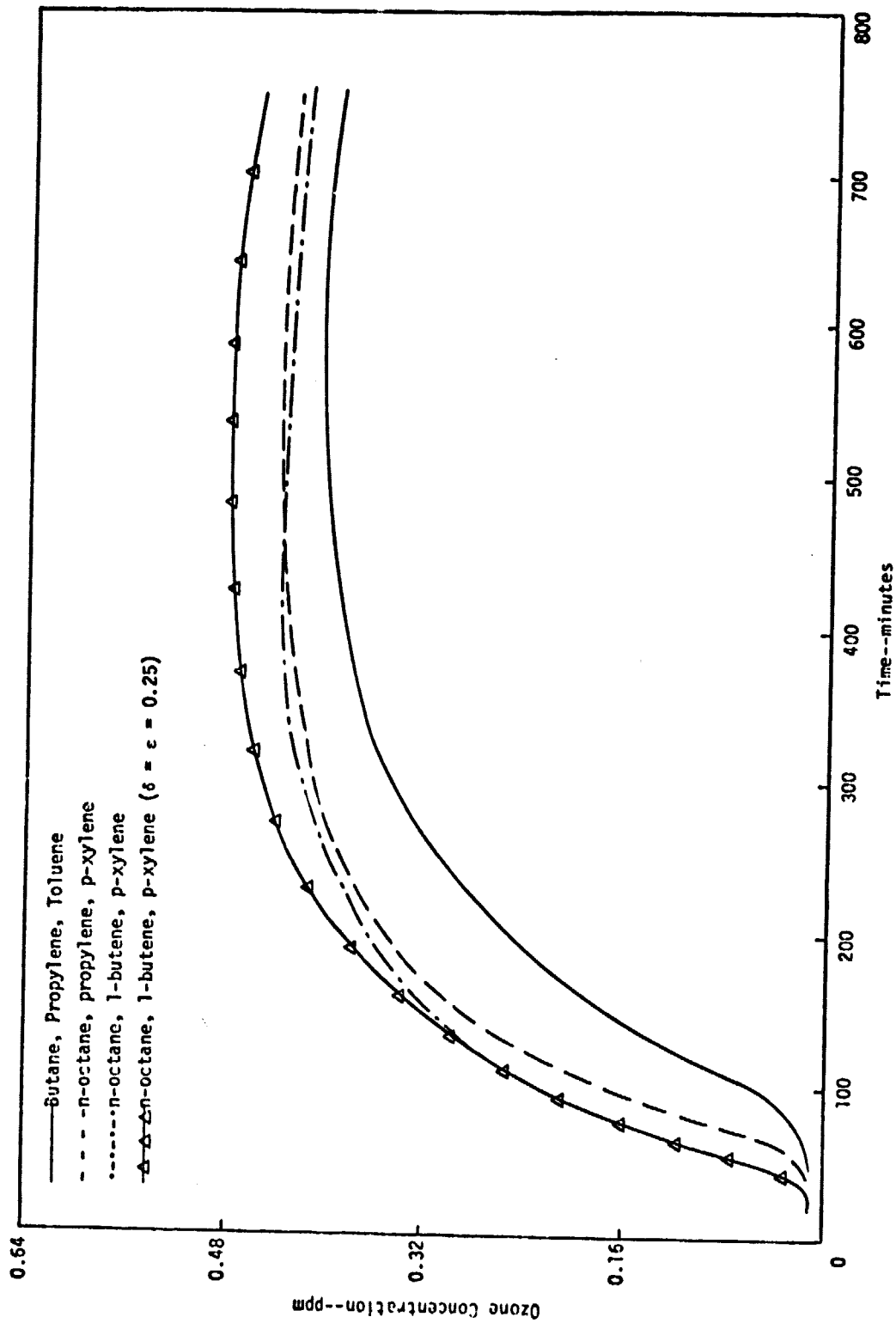

FIGURE 24. EFFECTS OF DIFFERENT COMBINATIONS OF HYDROCARBONS ON OZONE BEHAVIOR FOR MIXTURE 3 $[NO_x]_0$ = 0.3 ppm, $[Hydrocarbon]_0$ = 6 ppm C and $[Aldehyde]_0$ = 0.0 ppm

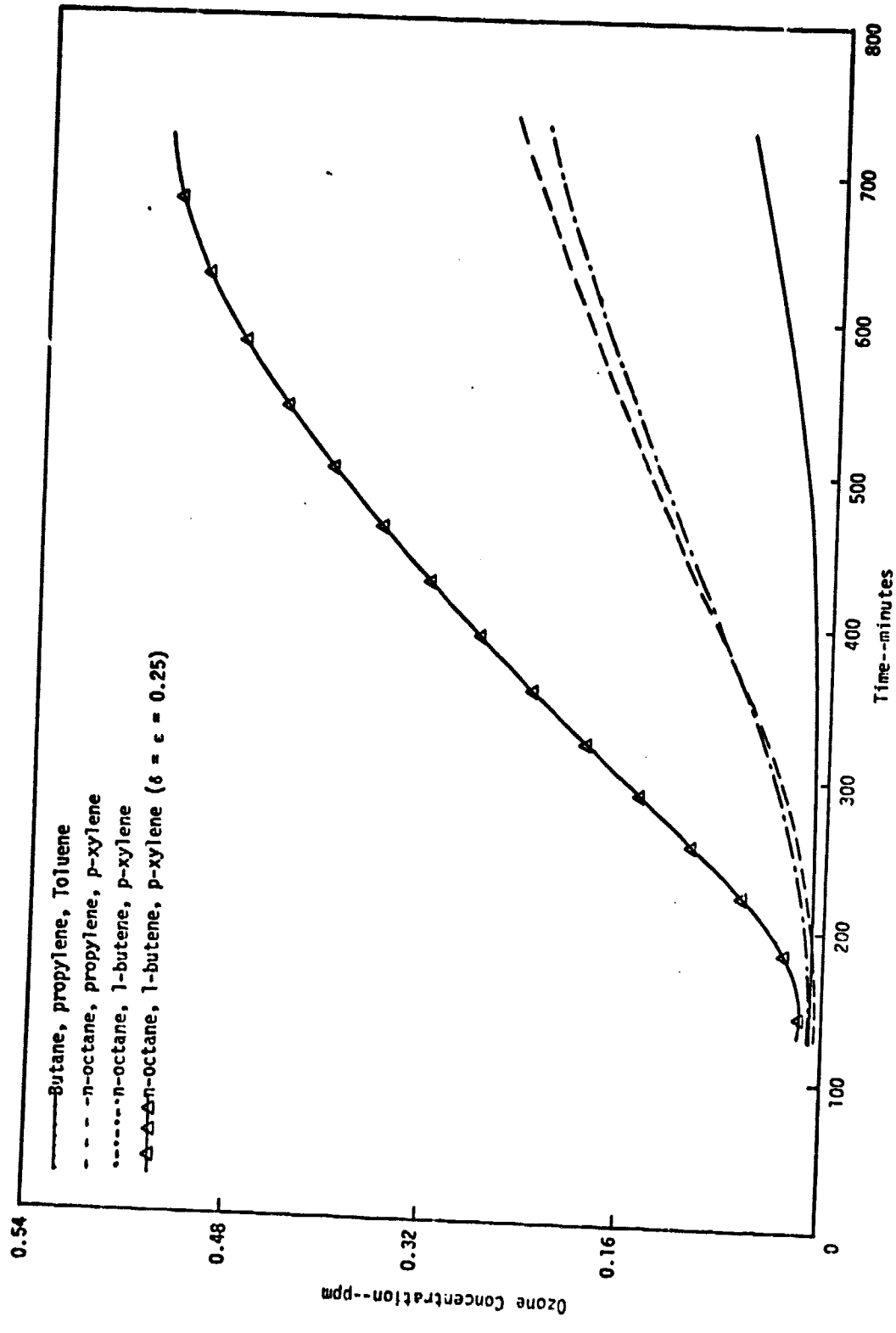

FIGURE 25. EFFECT OF DIFFERENT COMBINATIONS OF HYDROCARBONS ON OZONE BEHAVIOR FOR MIXTURE 3 $[NO_x]_0$ = 1.2 ppm, $[Hydrocarbon]_0$ = 3 ppm C and $[Aldehyde]_0$ = 0.0 ppm

Consequently, the closure parameters limit the amount of ozone formed. If the amount of formaldehyde is a substantial fraction of the total aldehydes, the first two reactions will be less important. Also, if a substantial amount of $RO_2^{\cdot}$ is in the form of peroxymethyl ($CH_3O_2^{\cdot}$) radicals, then the third reaction will also be less important. With longer chain molecules, the fractions of formaldehydes and $CH_3O_2^{\cdot}$ are expected to be lower than for shorter chain molecules. Therefore, for the longer chain molecule systems lower values of δ and ϵ are expected. The value of 0.25 for δ and ϵ may be a lower limit because the rate at which the longer hydrocarbons break down to smaller hydrocarbons (shorter lengths) as a function of chain length is presently unknown. For example, if the rate of breakdown of the chain is fast, then the amounts of $CH_3O_2^{\cdot}$ and formaldehyde may be larger than the amounts determined by the fractions given by δ and ϵ. Therefore, δ and ϵ are estimated to have a lower limit of 0.25 for the longer chain hydrocarbon systems in this study.

Figures 23, 24, and 25 show the results of the closure parameter changes at the three different starting conditions. Again, for the simulations with high HC/NO_x ratios (Figures 23 and 24), varying the closure parameters has little effect on the ozone concentration when predictions are compared with those of the simulation of the system with the low HC/NO_x ratio (Figure 25). Varying the closure parameters for the low HC/NO_x system resulted in twice as much ozone at the end of the simulation.

The overall effect of the presence of longer chain hydrocarbons (including changes in the closure parameters) is an increase in ozone concentration of approximately 20 to 30 percent at the end of the simulation period for the systems having high HC/NO_x ratios (Figures 23 and 24) and an increase in ozone concentration of approximately a factor of 6 at the end of the simulation period for the shorter chain system for the low HC/NO_x system (Figure 25). The unreactive low hydrocarbon and high NO_x system was affected more by the longer chain hydrocarbons than was the more reactive system (high hydrocarbon and low NO_x).

V SIMULATIONS OF MIXED AUTOMOBILE AND AIRCRAFT EMISSIONS

In the previous chapters, we presented emissions data for jet aircraft and for automobiles. Each of these sources emits pollutants that can lead to ozone production in the presence of ultraviolet radiation. In this chapter we discuss simulations of systems containing both jet emissions and automotive emissions. Such systems might occur in the real world where an airport is located in or near a region of significant automotive emissions, such as an urban area or a freeway. We are interested in these systems because of the possibility of enhanced ozone production--that is, the possibility that a system with mixed emissions will produce more ozone than a system wherein jet and automotive emissions are kept segregated.

The creation and validation of a complete numerical model of a mixed system at any particular airport would have to include the effects of such factors as:

- Transport and dispersion of pollutants in the atmosphere as a function of space and time.
- The spatial and temporal character of emissions.
- The dilution of pollutants with clean air.
- The extent of mixing of jet and automotive emissions.
- Variations in the duration and intensity of sunlight.
- The reactions of pollutants before and during mixing.
- Differences in the types of hydrocarbons emitted from different sources.
- The relative concentrations of pollutants.
- Induction effects.

A model of this complexity is beyond the scope of this study. Consequently, instead of real physical situations, we discuss several idealized physicochemical models of the reaction and mixing processes, with the intent to illustrate rather than document the phenomena that may occur when jet and

automotive emissions mix. These models were constructed to meet three objectives: ease of calculation, ease of interpretation, and physical significance. The effects of dilution and other variations in pollutant concentrations were not included in the models. Although inclusion of these effects causes only slight changes in the total amount of ozone formed from a given quantity of pollutants, it can cause large spatial variations in ozone concentrations, which would obscure enhancement effects.

Before discussing the models and simulations of idealized mixed systems, we present a simple example that, although not explicitly related to a physical situation, will provide insight into the causes of enhanced ozone production.

A. THE POSSIBILITY OF ENHANCED OZONE PRODUCTION FROM MIXING-- A SIMPLE EXAMPLE USING INITIAL CONDITIONS

To illustrate the possibility of enhanced ozone production, we plotted isopleths of the maximum 1-hour average ozone concentrations for Mixture 3 (Figure 26). (Plots of maximum 1-hour average isopleths, are more convenient for the present discussion because they do not depend on time.) In Figure 26, Line A, at an HC/NO_x ratio of 12.0 (ppm as C/ppm as NO_x), represents typical aircraft emissions, which have high hydrocarbon concentrations and low NO_x concentrations. Line B, at an HC/NO_x ratio of 3.0 is representative of automobile emissions. The isopleth plot shows that the initial concentrations of Point 1 on Line A (12 ppmC hydrocarbons and 0.1 ppm NO_x) produce a maximum 1-hour average ozone concentration of approximately 0.25 ppm. The initial concentrations of Point 2 (3 ppmC hydrocarbons and 1.0 ppm NO_x) produce a maximum 1-hour-average ozone concentration of approximately 0.35 ppm. Now, consider the averaging of the initial concentrations of Points 1 and 2. This may be visualized as the combination and mixing of two air parcels of equal volume, each parcel containing one set of initial concentrations of HC and NO_x. The average of the initial concentrations of Points 1 and 2 is 7.5 ppmC hydrocarbons and 0.55 ppm NO_x, which is shown as Point 3 on Line C in Figure 26. One might expect that the maximum 1-hour-average

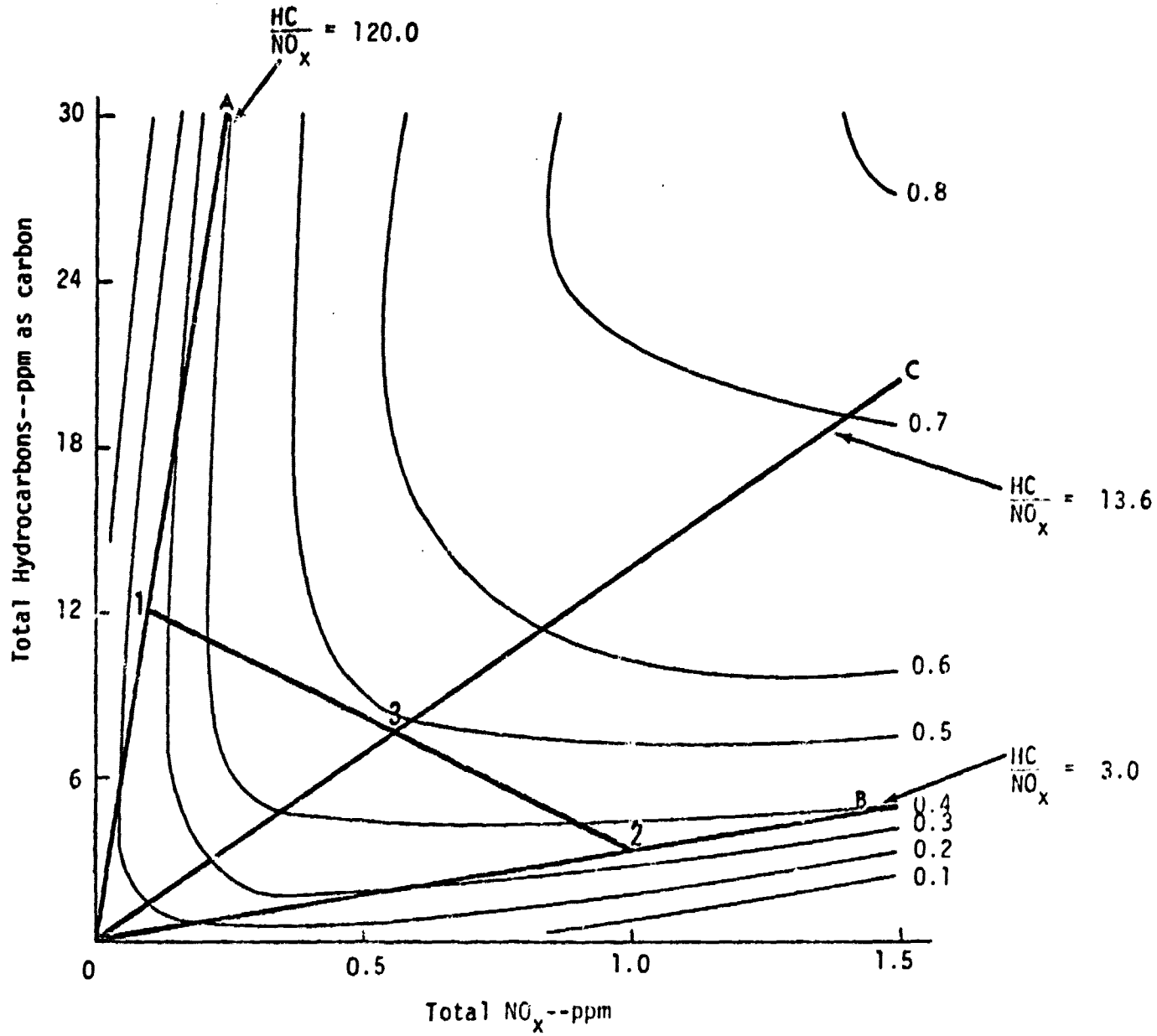

FIGURE 26. ISOPLETHS OF MAXIMUM 1-HOUR-AVERAGE OZONE CONCENTRATIONS FOR MIXTURE 3

ozone concentration produced from the average initial concentrations of HC and NO_x (Point 3), would equal the average of the ozone concentrations at Points 1 and 2, which is 0.3 ppm. But this is not the case; the ozone concentration at Point 3 is about 0.47 ppm. The difference of 0.17 ppm ozone is the "enhanced" ozone production.

The cause of the enhanced ozone production may be explained in terms of the HC/NO_x ratios of the emissions. The isopleth diagram shows that for a given concentration of HC, there is an HC/NO_x ratio for which ozone production is a maximum. The same is true for a given concentration of NO_x, although the HC/NO_x ratio is different. The HC/NO_x ratios that maximize ozone production with respect to HC and with respect to NO_x both have numerical values between the HC/NO_x ratio of jet emissions on the one hand and automotive emissions on the other. Thus, we expect that enhanced ozone production will often occur when jet and automotive emissions mix.

The simple example described above omits many possibly important influences on ozone production such as mixing, dilution, and variations in sunlight. It also assumes that the reactivities of the hydrocarbons in jet and automotive emissions are equal. As noted above, accounting for these influences in a complete numerical model is beyond the scope of this study. It is possible, however, to examine ozone enhancement more carefully by using models more complex than the simple example just described. The following sections describe three such models, and the results of simulations using these models.

B. DESCRIPTION AND PHYSICAL SIGNIFICANCE OF THE MODELS

1. Model 1--Emissions Mixed Initially

The first model is that in which jet and automotive emissions mix before any chemical reactions occur. This model includes two cases (see Figure 27). In the first case, the initial concentrations of pollutants are simply added; this represents injection of jet and automotive emissions

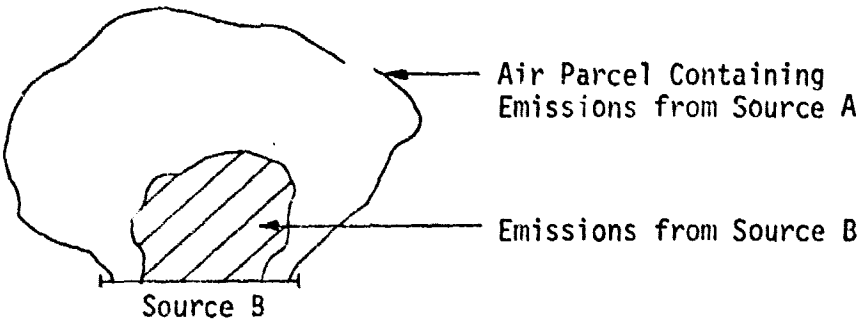

a) Case 1--Addition of emissions from Source B to an air parcel containing emissions from Source A. It is assumed that no chemical reaction occurs until emissions from both sources are mixed homogeneously within the parcel.

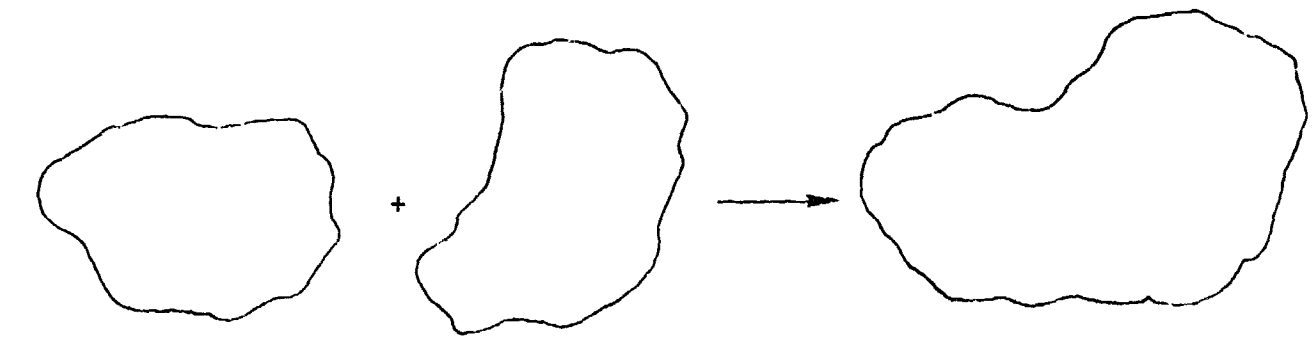

b) Case 2--Mixing of emissions without reduction in volume, or "averaging" of emissions over two parcels. Again, it is assumed that no chemical reaction occurs until emissions from both sources are mixed homogeneously within the parcel.

FIGURE 27. MODEL 1, CASES 1 AND 2--EMISSIONS MIXED INITIALLY

into the same air parcel. In the second case, the concentrations of pollutants are averaged; this represents the mixing, at some distance from the sources of emissions, of two separate air parcels carrying different emissions. The two cases of Model 1 approximate physical situations in which, during the daytime, mixing is very rapid compared with the rate of chemical reaction, such as when air containing jet emissions mixes with air from a nearby freeway. Model 1 also represents the physical situation during nighttime, when no photochemical reactions are occurring, and air parcels containing different types of emissions have a long time (and, depending on meteorological conditions, a large volume) in which to mix. In terms of the concentrations of pollutants after mixing, most physical situations probably lie between the two cases of Model 1.

2. Model 2--Emissions Injected into an Air Parcel Containing Reacting Emissions

Model 1 and the base case (unmixed emissions in separate air parcels) represent the extremes of transport limited and reaction limited situations. If the production of photochemical smog were a linear process, those extremes would provide us with all the information necessary to predict ozone/precursor relationships for combined automotive and aircraft emission systems. However, because of the nonlinearities of photochemical smog production, mixing in a partly reacted system may show phenomena not seen in fully mixed reacting systems.

In the second idealized model, emissions are injected into an air parcel containing other emissions that are already undergoing chemical reaction (see Figure 28). As one example, this model represents an air parcel passing over an airport and then a freeway, if, during the travel time between the airport and the freeway, the jet emissions in the air parcel undergo significant chemical reaction. In using Model 2, we considered both jet emissions injected into automotive emissions and vice-versa. Although Model 2 is physically similar to Case 1 of Model 1, it differs chemically because of the assumption of continuous chemical reaction.

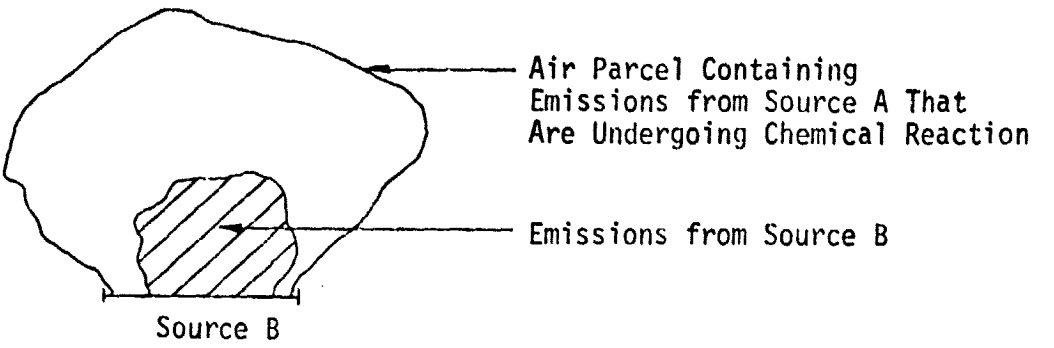

FIGURE 28. MODEL 2--EMISSIONS INJECTED INTO AN AIR PARCEL CONTAINING REACTING EMISSIONS

3. Model 3--Mixing of Two Air Parcels Containing Reacting Emissions

In the third idealized model, an air parcel containing, say, reacting jet emissions mixes slowly with an air parcel containing reacting automotive emissions (Figure 29). It is assumed that no new emissions are added during the mixing. Model 3 is physically similar to Case 2 of Model 1, but differs chemically because of the continuous chemical reaction before and during mixing.

In addition to these three models, we also performed simulations with varying UV irradiation during the simulations, and with averaged rate constants and closure parameters for jet and automotive emissions. The effects of these changes are presented in a later section.

C. INITIAL CONDITIONS FOR SIMULATIONS OF MIXED SYSTEMS

The computer simulations discussed in the remainder of this chapter are based on mixtures of hydrocarbons and oxides of nitrogen chosen to represent airport and freeway emissions. This section presents details of the selection of the following items:

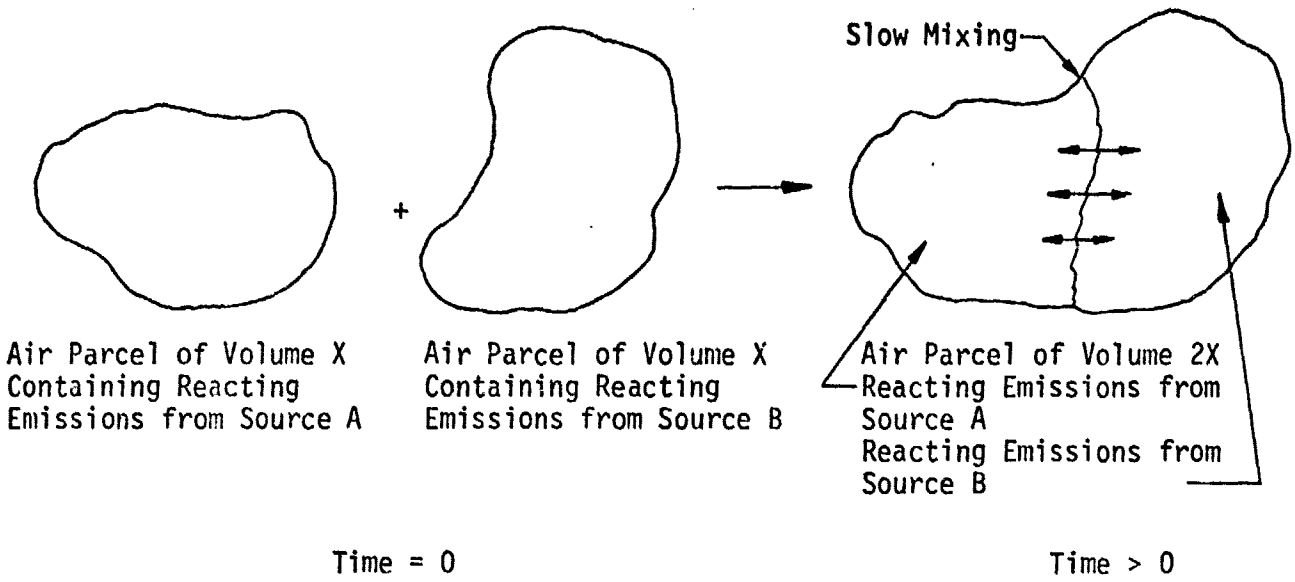

FIGURE 29. MODEL 3--MIXING OF AIR PARCELS CONTAINING REACTING EMISSIONS

- Hydrocarbon/NO_x ratios representative of airport and freeway emissions.
- Hydrocarbon compositions representative of airport and freeway emissions.
- A ratio of airport emissions to freeway emissions.
- An initial concentration of hydrocarbons appropriate for use in the simulations.
- Variation of intensity of sunlight during the simulations.

In these simulations we used an HC/NO_x ratio of 31.0 (ppm as carbon/ppm as NO_x) to represent the total airport emissions, in contrast to the average ratio of approximately 50 that was presented in Section II-D for jet emissions alone. The lower ratio takes into account the emissions of access and service vehicles, which operate at slower speeds and produce

emissions having higher HC/NO_x ratios than automobiles driven at highway speeds (as shown by the EPA data in Table 22). A $hydrocarbon/NO_x$ ratio of 3.0 (ppm as C/ppm as NO_x) was used for the freeway emissions.

A hydrocarbon composition representative of airport emissions was derived primarily from the data of Conkle et al. (1975). The composition used was 57 percent alkanes, 18 percent alkenes, and 25 percent aromatics. Actually, Conkle et al. reported 7 percent aromatics and 17 percent aldehydes. The aldehyde value may be high; Lozano et al. (1968) and Groth and Robertson (1974) reported low values (Section II-B). Also, Lozano et al. (1968) and Groth and Robertson (1974) reported that aromatics were approximately 25 to 30 percent of the total hydrocarbons. Therefore, a hydrocarbon composition consisting of 25 percent aromatics was used for the simulations. Initial aldehyde concentrations were not included in view of the insensitivity of the ozone behavior to variations in these concentrations after the induction period (Section IV-A). We calculated an "averaged" hydrocarbon from data reported by Conkle et al. (1975) in order to convert hydrocarbon emissions into units of moles; similarly, an "averaged" molecule was used to convert ppm NO_2 into moles of NO_x. The "averaged" hydrocarbon was a C_6 molecule (hexane). Therefore, the molecular $hydrocarbon/NO_x$ ratio used in the simulations was 3.0 (see Appendix).

A similar procedure was used to find the hydrocarbon composition for freeway emissions. The Bureau of Mines (1973) reported a detailed breakdown of hydrocarbon compositions from automotive emissions (Table 25). Based on these data, it was determined that a hydrocarbon composition consisting of 20 percent alkanes, 45 percent alkenes, and 35 percent aromatics would be suitable for use. The representative molecules for each hydrocarbon group are butane for alkanes, propylene for alkenes, and p-xylene for aromatics. The "averaged" hydrocarbon calculated from Table 25 was a C_4 molecule. This gives a value of approximately 0.4 for the molecular $hydrocarbon/NO_x$ ratio in units of ppm as an "averaged" molecule per ppm as NO_x (see Appendix).

In most of the simulations we assumed that the concentrations of hydrocarbons in air parcels containing airport and freeway emissions are approximately equal. To compare this assumption with "real world" conditions, we estimated the emissions from San Francisco Airport and from the Bayshore Freeway, which is adjacent to that airport. From traffic count data for automobiles on the freeway, data on the number of flights to and from the airport, and the emissions data reviewed in Chapter II, we found that the hydrocarbons emitted from the airport equal the hydrocarbons emitted from 30 miles of the freeway. Because jet emissions have a higher HC/NO_x ratio than automotive emissions, the emissions of nitrogen oxides from the airport are only about 10 percent of the NO_x emissions from the 30 miles of freeway. Airport emissions are generally more concentrated at first than are freeway emissions. But an airport is similar to a point source of pollutants, and consequently its emissions often undergo more rapid dilution than freeway emissions, which come from a line source. It may be expected that at some time during the dilution of jet emissions and entrainment of freeway emissions, the conditions in an air parcel approximate our assumed conditions.

The total initial concentration of hydrocarbons used in each simulation was chosen so that the resulting ozone concentration would lie in a range between the federal standard of 0.08 ppm and 0.5 ppm, which is typical of a very smoggy day in the Los Angeles Basin. Another reason for our choice of initial concentrations was to study airport emissions and freeway emissions that have similar potential for ozone production. If the ozone concentrations produced separately by the airport emissions and by the freeway emissions were widely different, the simulation results would be highly influenced by dilution. As noted above, this dilution might obscure enhancement effects.

In all the computer simulations presented in the following sections, we attempted to simulate physical systems more realistically by using a varying NO_2 photolysis rate constant that corresponds to the variation in intensity of sunlight on an equinox day near 36° latitude (Jeffries et al., 1974). The maximum NO_2 photolysis rate, and in most cases the maximum ozone concentration,

Table 31

INITIAL CONDITIONS FOR SIMULATIONS

Initial Condition	Airport Emissions	Freeway Emissions
Hydrocarbon Concentration (ppm as C)		
Alkanes*	0.0855	0.05
Alkenes*	0.027	0.1125
Aromatics*	0.0375	0.0875
Total HC	0.15	0.25
NO_x Concentration (ppm as NO_x)		
NO	0.045	0.54
NO_2	0.005	0.06
Total	0.05	0.60
HC/NO_x Ratio (ppm as "averaged" molecule/ppm as NO_x)	3.0	0.42

*In simulations in which hydrocarbons were handled explicitly, rather than as generalized or "lumped" species, alkenes were represented by propylene, aromatics by p-xylene, and alkanes by n-octane in the airport emissions and by butane in the freeway emissions.

occurred at six hours (or noontime) in the computer simulations. The variation in sunlight, and hence in UV irradiation, affects the following reactions in the chemical kinetic mechanism:

Reaction	Rate Constant
$NO_2 + h\nu \rightarrow NO + O\cdot$	k_1
$H_2O_2 + h\nu \rightarrow 2OH\cdot$	$0.0036\ k_1$
Aldehyde + $h\nu \rightarrow$ Products	$0.0045\ k_1$
Aldehyde + $h\nu \rightarrow (1 + \delta)HO_2^{\cdot} + (1 - \delta)RO_2^{\cdot} + CO$	$0.0045\ k_1$
$HNO_2 + h\nu \rightarrow NO + OH\cdot$	$0.07\ k_1$

Table 31 lists the initial conditions for the computer simulations. A simulation was performed with each HC/NO_x ratio to determine the amount of oxidant (ozone) produced. Then, a combination of the freeway ratio with the aircraft ratio was used in a set of simulations. In all simulations, the initial ratio of NO to NO_2 in both airport and freeway emissions was assumed to be 9. This assumed value is close to measured values for aircraft emissions (Table 7). Measurements of ambient NO_x concentrations show that between 6 a.m. and 9 a.m. on weekdays, the NO/NO_2 ratio in the Los Angeles Basin ranges from approximately 2.0 to 10.0 (Roberts and Roth, 1971). Thus the ratio of NO to NO_2 for automotive emissions was chosen to be 9.0.

D. SIMULATION RESULTS FOR INITIALLY MIXED SYSTEMS

The initial conditions developed in the previous section were used in simulations of photochemical smog formation. This section presents the results of simulations for systems in which airport and freeway emissions are well mixed before chemical reactions begin. Also presented are the results of tests performed to determine whether our parameter estimation methods influenced the ozone enhancement effects seen in the simulations.

In all simulations a modified version of the Hecht, Seinfeld, and Dodge (1974) kinetic mechanism was used, and the physical processes of transport and dispersion were not taken into account. Instead, we used the models presented in Section B. We wish to emphasize these limitations because turbulent mixing generally has a significant effect on photochemical smog formation in the atmosphere.

1. Model 1 Case 1--Simulation Results

As described above, in Model 1 Case 1 airport and freeway emissions are added to a single air parcel. Thus the initial hydrocarbon concentration is the sum of the initial hydrocarbon concentrations presented in Table 31 for airport emissions (0.15 ppm C) and for the freeway emissions (0.25 ppm C), or 0.40 ppm C. In the simulation of Model 1 Case 1 the alkanes were treated explicitly in the chemical kinetic mechanism as described in Chapter IV. For this case, one might expect that the ozone concentration in the absence of enhancement would be the average of the ozone concentrations generated by twice the airport emissions in a single air parcel unmixed with freeway emissions and by twice the freeway emissions unmixed with airport emissions. But Figure 30 shows that the addition of airport and freeway emissions generates much more ozone than either twice the airport emissions taken alone or twice the freeway emissions taken alone. The difference between the ozone concentration predicted for Model 1 Case 1 and the average of the other two ozone concentrations in Figure 30 is the enhanced ozone production.

The ozone concentrations shown in Figure 30 decrease after about 600 minutes of simulation because of the decreasing NO_2 photolysis rate, which, in turn, is caused by the decreasing intensity of sunlight. This process can be clarified by examination of the following reactions.

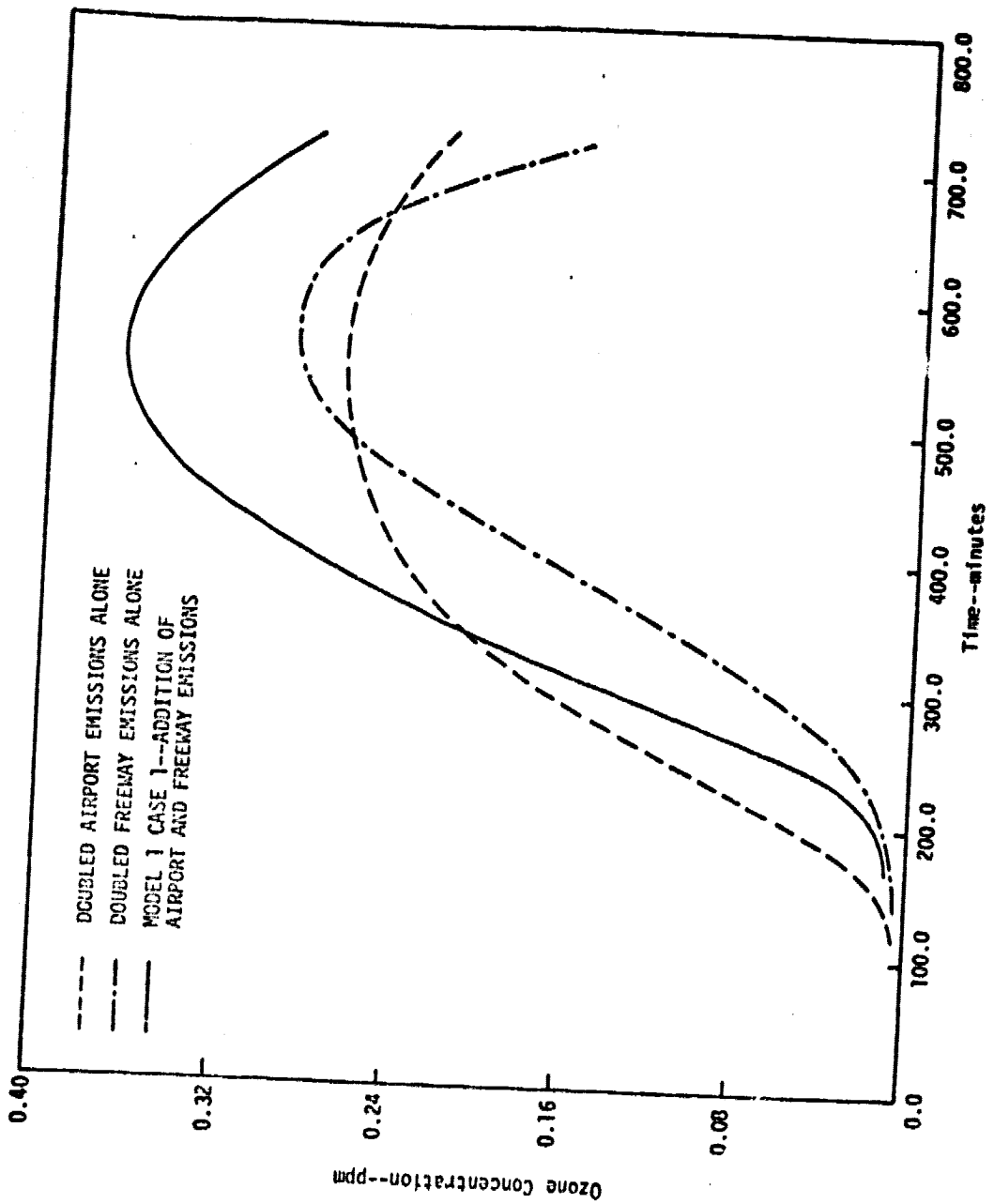

FIGURE 30. SIMULATION RESULTS FOR MODEL 1 CASE 1 AND FOR DOUBLED AIRPORT EMISSIONS ALONE AND DOUBLED FREEWAY EMISSIONS ALONE

$$NO_2 + h\nu \xrightarrow{k_1} NO + O\cdot \qquad (1)$$

$$O + O_2 + M \xrightarrow{k_2} O_3 + M \qquad (2)$$

$$O_3 + NO \xrightarrow{k_3} NO_2 + O_2 \qquad (3)$$

$$O_3 + NO_2 \xrightarrow{k_4} NO_3 + O_2 \qquad (4)$$

These are the main reactions for formation and destruction of ozone. The rate of formation of "odd" oxygen can be written as follows:

$$\frac{d[O]}{dt} = k_1[NO_2] - k_2[O][O_2][M]$$

$$\frac{d[O_3]}{dt} = k_2[O][O_2][M] - k_3[NO][O_3] - k_4[NO_2][O_3]$$

$$\frac{d[O_x]}{dt} = \frac{d\left([O] + [O_3]\right)}{dt} = k_1[NO_2] - \left(k_3[NO] + k_4[NO_2]\right)[O_3]$$

Making the steady-state assumption for the oxygen atoms (i.e., $d[O]/dt = 0$), we obtain

$$\frac{d[O_3]}{dt} = k_1[NO_2] - \left(k_3[NO] + k_4[NO_2]\ [O_3]\right)$$

Making a second steady-state assumption for ozone (i.e., $d[O_3]/dt = 0$), the ozone concentration as a function of NO_x is found:

$$[O_3] = \frac{k_1[NO_2]}{k_3[NO] + k_4[NO_2]}$$

For a situation in which the value of k_1 (the NO_2 photolysis rate constant) is kept constant, the ozone concentration can always build up as the concentration of NO decreases. When k_1 varies with the sunlight intensity, k_1 is small in the early hours of the day and the NO concentration is high. Therefore, ozone formation is delayed. Near the end of the day k_1 goes to zero.

As k_1 decreases, the numerator of the steady-state expression for ozone (i.e., the rate of NO_2 photolysis) decreases. The ozone in the system reacts with the remaining NO, which lowers the rate $k_3[NO]$ until it nearly equals $k_4[NO_2]$. The time at which $k_3[NO] \approx k_4[NO_2]$ depends on the ratio of NO_x to ozone in the system. If the amount of NO_x is small compared to the amount of ozone, the ozone destruction reactions are slow. Normally when k_1 is large the reaction of ozone with NO is very much faster than ozone destruction by $NO_2\left(k_4[NO_2]\right)$. Then the steady state expression is approximately

$$[O_3] = \frac{k_1[NO_2]}{k_3[NO]} \quad .$$

In this case the amount of ozone produced is independent of the absolute amount of NO_x; it depends primarily on the ratio of NO_2 to NO. Hence, when irradiation intensity is invariant with time, the ratio of NO_2 to NO controls the amount of ozone at all times. However, the ratio of total NO_x to ozone becomes important when solar radiation is varied in the simulations. For automative emissions the NO_x/ozone ratio is high, therefore the ozone concentration decreases as the sunlight decreases. Thus, the steady-state relationship is followed more closely in systems with a high ratio of NO_x to ozone. As k_1 decreases rapidly the low NO_x (airport) system "lags" behind the steady-state value and ozone may even remain at appreciable concentrations after the steady-state value goes to zero (after the sun sets), provided there is insufficient NO_x remaining in the system to consume it.

2. Model 1 Case 2--Simulation Results

a. Alkane Reaction Rate Constants Averaged

In Model 1 Case 2, an air parcel of volume X containing airport emissions mixes with an air parcel of volume X containing freeway emissions. It is assumed that both emissions are mixed homogeneously throughout a volume of 2X before any chemical reaction occurs. The initial simulation of Model 1 Case 2 was performed using averaged alkane reaction rate constants in the chemical kinetic mechanism, rather than handling butane and n-octane reactions explicitly. The results of this simulation and of simulations of airport emissions alone and freeway emissions alone are shown in Figure 31. Ozone enhancement is observed; the predicted ozone concentrations for Model 1 Case 2 are significantly higher than the predicted concentrations for the unmixed emissions.

b. Alkane Reaction Rate Constants Treated Explicitly

The simulation results of Model 1 Case 2 presented in Figure 31 were obtained assuming an averaged alkane reaction rate constant, and assuming that all alkanes produce the same radical ($RO_2^{\cdot}$) in the kinetic mechanism. We performed other simulations of Model 1 Case 2 to determine whether the ozone enhancement effect shown in Figure 31 was influenced by these assumptions. The initial conditions for these simulations are similar to those used in the original simulation of Model 1 Case 2, (Figure 31), with the exceptions noted:

(1) Model 1 Case 2 simulation using "explicit" alkanes (butane and n-octane) and their rate constants, and assuming that these alkanes produce the same radical ($RO_2^{\cdot}$). (The results of this simulation are shown as Curve 1 in Figure 32.)

(2) Repeat of simulation (1) with butane and n-octane producing different radicals and aldehydes. (Curve 2 in Figure 32.)

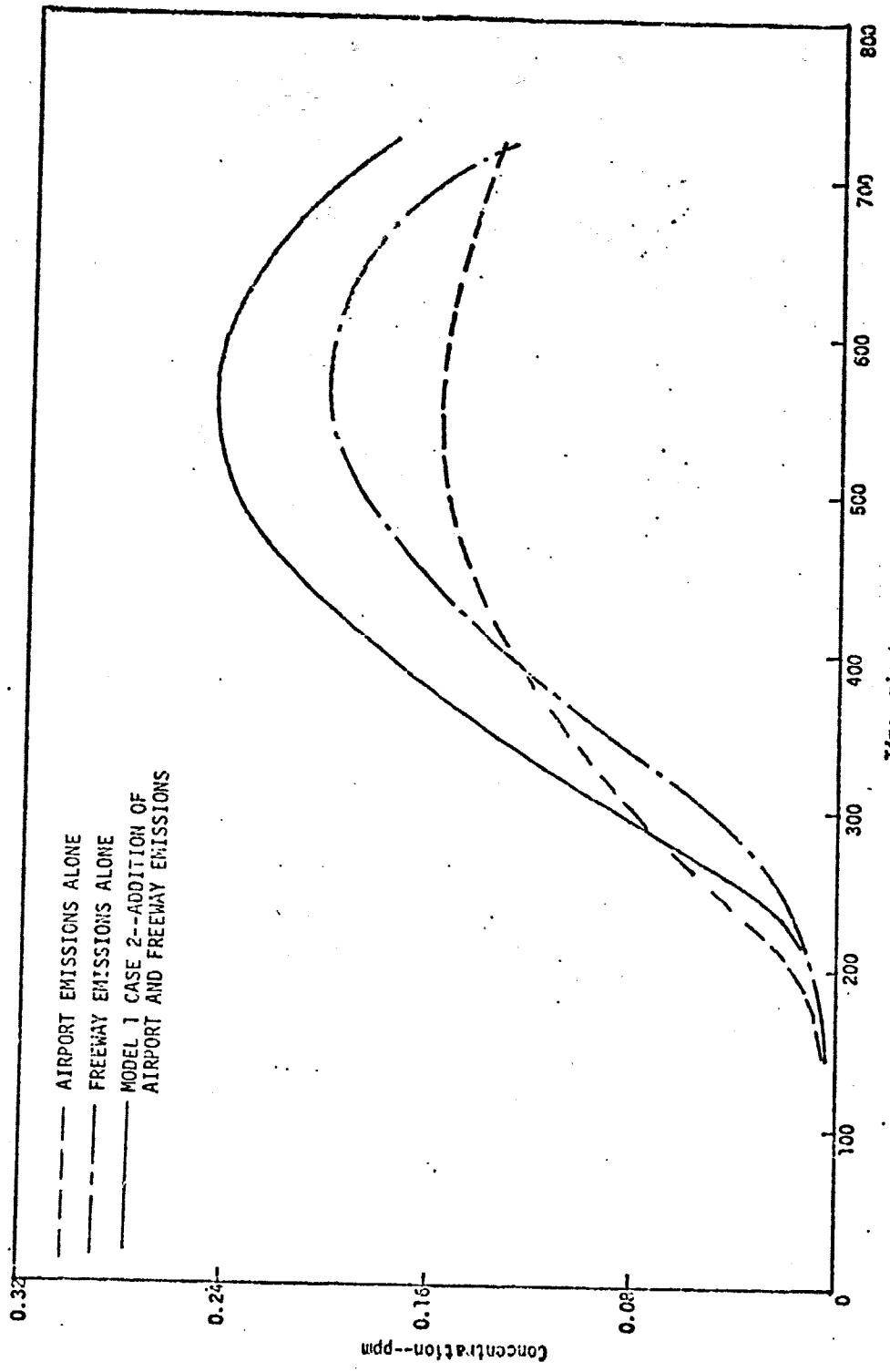

FIGURE 31. SIMULATION RESULTS FOR MODEL 1 CASE 2 AND FOR AIRPORT EMISSIONS ALONE AND FREEWAY EMISSIONS ALONE

C-2

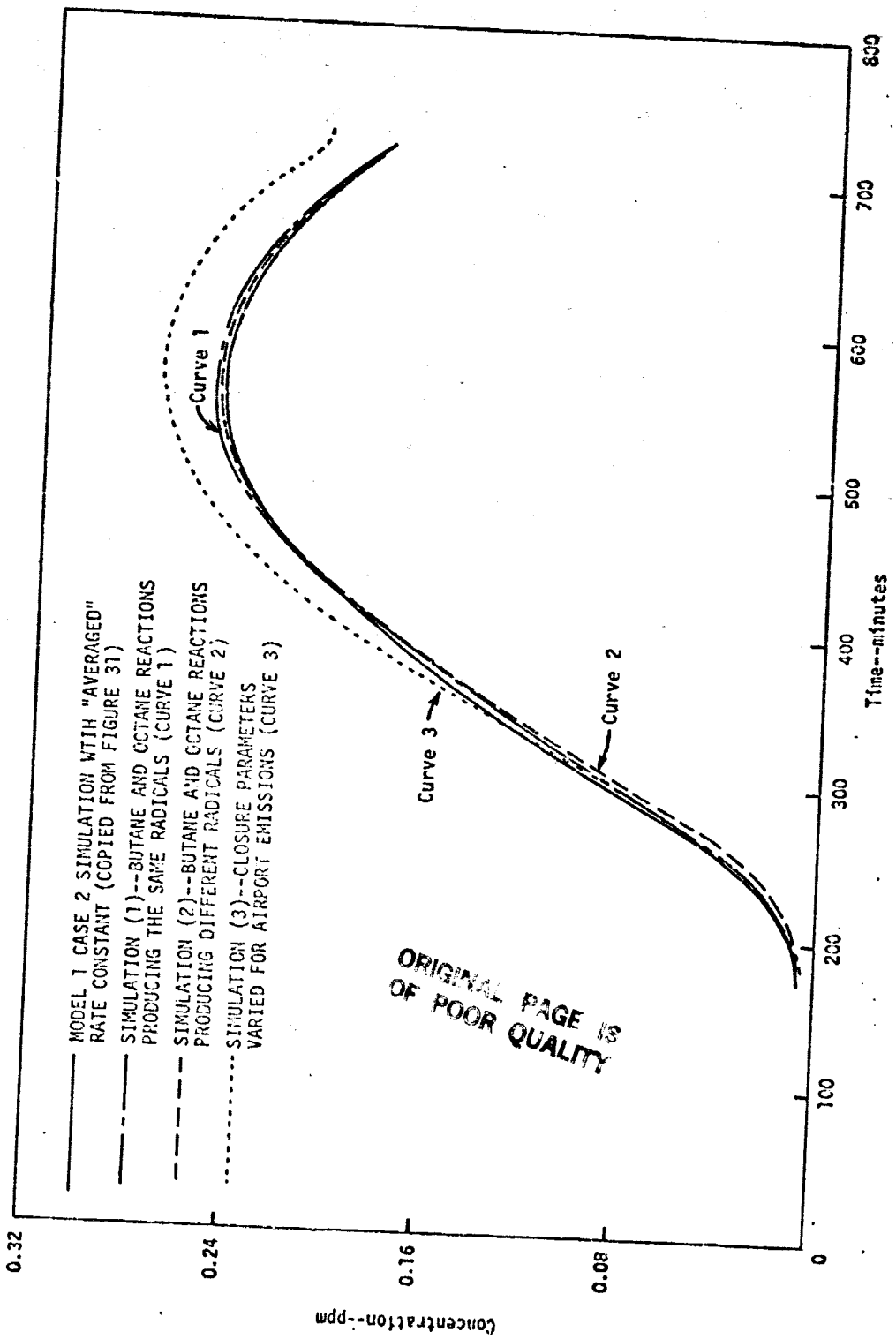

FIGURE 32. EFFECT OF DIFFERENT METHODS OF TREATING COMBINED AIRCRAFT AND AUTOMOBILE EMISSIONS

(3) Repeat of simulation (2) with closure parameters in the kinetic mechanism changed to 0.25 (from 0.5) for reactions involving airport emissions. (Curve 3 in Figure 32.)

The original simulation results for Model 1 Case 2 from Figure 31 are reproduced in Figure 32 to facilitate comparison. The similarity of the curves in Figure 32 demonstrates that the assumptions used in the initial simulation have very little effect on the observed enhancement of ozone production.

3. Model 2--Simulation Results

Model 2 is an idealization of a common physical situation: An air parcel passes over one emissions source, and then the same air parcel passes over another emissions source. Model 2 simulations require specification of a number of variables, such as which source emits into the air parcel first, how much time elapses before the air parcel passes over the second emissions source, and how rapidly the second source injects emissions into the air parcel. Each simulation in this section represents an air parcel containing either airport or freeway emissions at the concentrations listed in Table 31. Other emissions are injected into this parcel at a constant rate, beginning at the start of the simulation and continuing until the injected emissions total 0.15 ppm C for airport emissions or 0.25 ppm C for freeway emissions. All the simulations were performed with explicit alkanes, i.e. butane in freeway emissions and n-octane in airport emissions, but the products and closure parameters were not separated. Table 32 lists the Model 2 simulations performed and the maximum ozone concentrations in the simulations. The results of these simulations are shown in Figures 33 and 34. The results of the Model 1 Case 1 simulation are reproduced in both figures for comparison purposes.

Table 32

MODEL 2 SIMULATIONS

Simulation	Emissions Present Initially (in Concentrations Listed in Table 31)	Injected Emissions	Injection Time* (hours)	Maximum Ozone Concentration (ppm)
1	Freeway	Airport	6	0.23
2	Freeway	Airport	9	0.20
3	Airport	Airport	6	0.12
4	Airport	Airport	9	0.11
5	Airport	Freeway	4	0.22
6	Airport	Freeway	10	0.14
7	Freeway	Freeway	4	0.19
8	Freeway	Freeway	10	0.11

*In each simulation the rate of injection was adjusted so that the total amount of emissions shown in Table 31 was injected at a constant rate in the number of hours listed here, after which injection ceased.

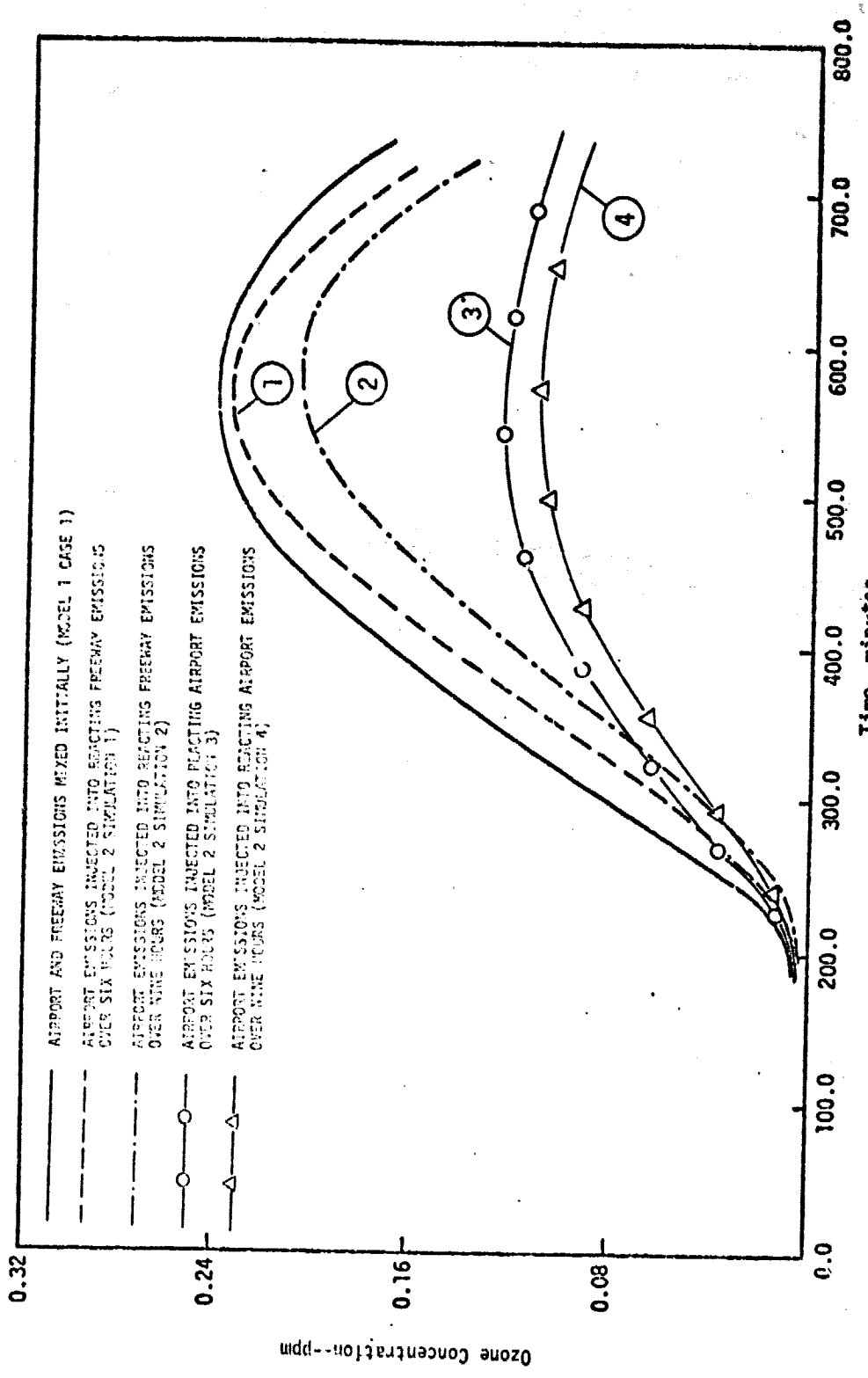

FIGURE 33. RESULTS OF MODEL 2 SIMULATIONS 1 THROUGH 4

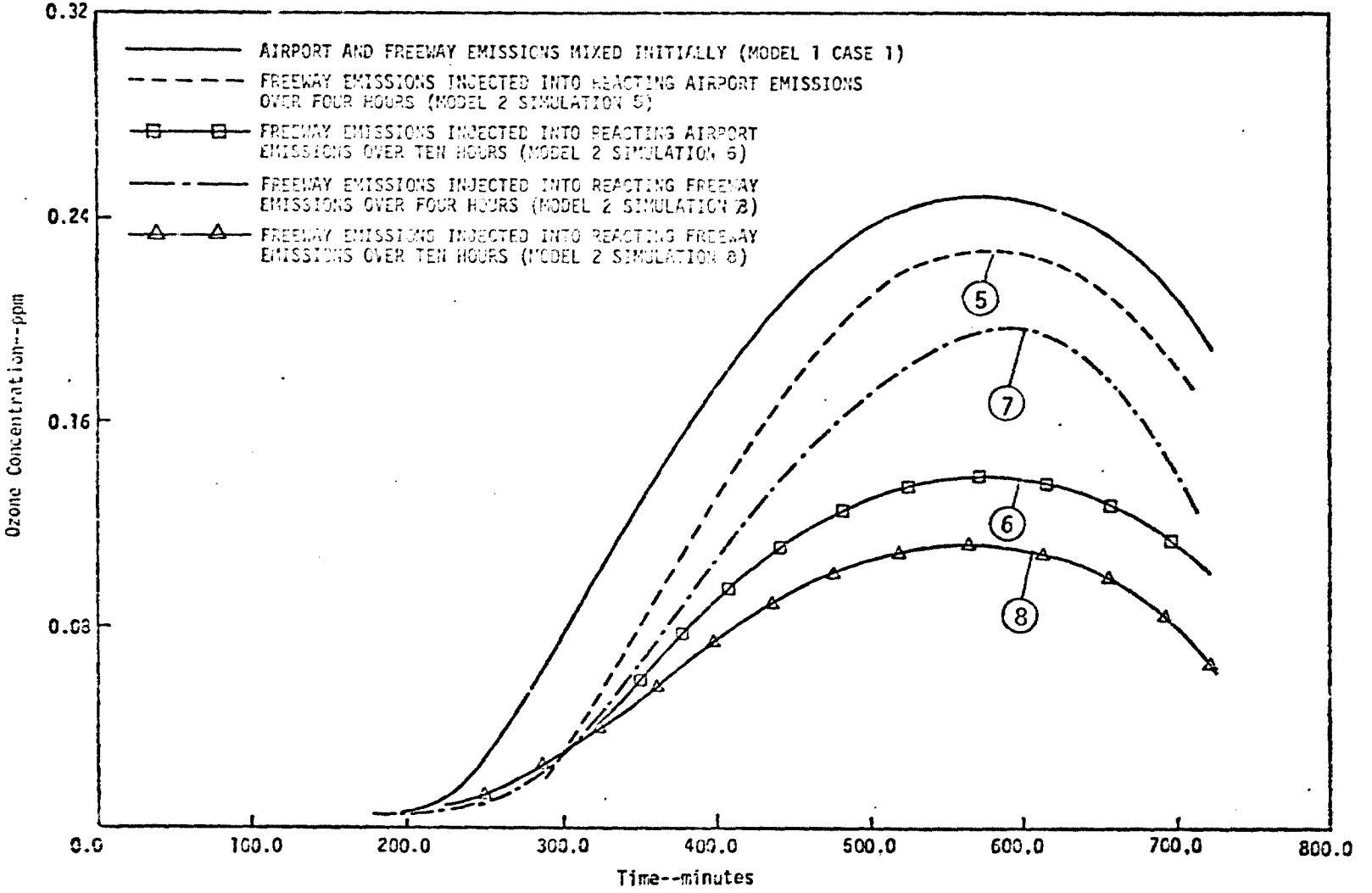

FIGURE 34. RESULTS OF MODEL 2 SIMULATIONS 5 THROUGH 8

It is difficult to define or demonstrate ozone enhancement in simulations with continuous injection of emissions. In such simulations, the total mass of pollutants increases with time, unlike all of the simulations (including the base cases) discussed in the previous sections. In addition, the injection of NO inhibits ozone formation. It is still possible to observe enhancement, however, by comparing continuous injection simulations with one another. For example, in Simulations 1 and 3, airport emissions are injected into reacting freeway and airport emissions, respectively (Figure 33). The mixing of the two types of emissions in Simulation 1 produces a maximum ozone concentration of 0.23 ppm; Simulation 3, with only airport emissions, produces 0.12 ppm ozone. It may be objected that this difference is not due to enhancement, but rather to the greater mass of pollutants in Simulation 1 than in Simulation 3 at any given time. (The initial conditions are 0.25 ppmC in Simulation 1 and 0.15 ppmC in Simulation 3.) This objection cannot be raised against the enhancement observed by comparing Simulations 5 and 7, with freeway emissions injected into reactive airport and freeway emissions, respectively (Figure 34). Although the amounts and rates of injection of freeway emissions are the same for Simulations 5 and 7, the pollutant mass (ppmC) in Simulation 7 always is greater than in Simulation 5 because of the difference in initial conditions: Simulation 7 initially has 0.25 ppmC freeway emissions, and Simulation 5 has 0.15 ppmC airport emissions. Despite this difference, the maximum ozone concentration in Simulation 5 is 0.22 ppm, compared to 0.19 ppm for Simulation 7. A Similar enhancement effect may be noted by comparing Simulations 6 and 8.

The inhibition of ozone formation by NO can also be demonstrated through simulations with continuous injection of freeway emissions. (As shown in Table 31, it is assumed that freeway emissions contain much more NO than airport emissions.) The inhibition by NO may be seen by comparing Simulations 7 and 8 with the results of freeway emissions alone (Figure 31). In Simulations 7 and 8, freeway emissions are being injected into reacting freeway emissions over four hours and ten hours, respectively. By the end

of the injections Simulations 7 and 8 both contain twice as much total pollutant (in ppmC) as the simulation of freeway emissions alone. But the maximum ozone concentrations for Simulations 7 and 8 are 0.19 and 0.11 ppm, respectively, compared with 0.19 ppm for freeway emissions alone. Note also that, although the maximum ozone concentrations reached in Simulation 7 and in the simulation of freeway emissions alone are the same, the rate of ozone formation is different. In the latter simulation ozone begins to accumulate after about 200 minutes of simulation time, but in Simulation 7 ozone does not accumulate until after injection stops at 240 minutes. In Simulation 8, the injection of NO over a ten-hour period inhibits ozone formation through most of the simulation, resulting in the low maximum ozone concentration.

4. Model 3--Simulation Results

Model 3 is an idealization of a physical situation in which two air parcels, each containing reacting emissions, slowly merge with one another. In the Model 3 simulation, one air parcel contained freeway emissions and the other airport emissions, and the two air parcels were assumed to mix at a rate of 5 percent per hour. The ozone maximum in each parcel was slightly greater than 0.22 ppm and occurred near 600 minutes (Figure 35). At that time diffusion was only about 40 percent complete, yet the enhancement phenomenon is apparent from comparison with the ozone maxima produced by freeway emissions alone and airport emissions alone (0.20 and 0.15 ppm ozone respectively, from Figure 31).

The predicted ozone concentrations in the two parcels of Model 3 are generally not as great as those in the initially mixed system of Model 1 Case 2. There is one exception: For a brief time in the morning, airport emissions produce a faster ozone formation rate than does the initially mixed system. This faster rate early in the simulation occurs because the low concentration of NO in airport emissions is oxidized to NO_2 in a short time, so ozone formation begins early.

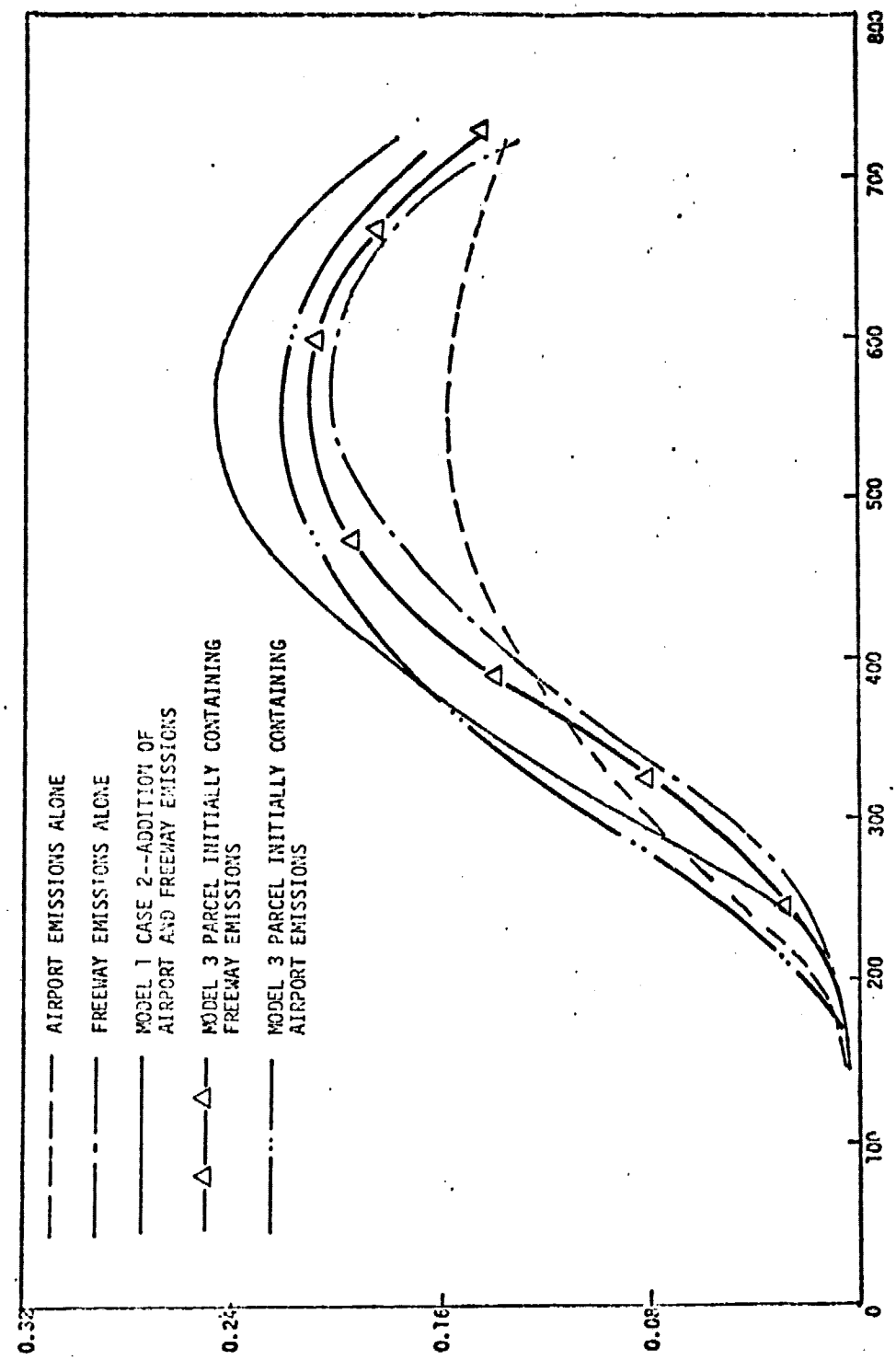

FIGURE 35. SIMULATION RESULTS FOR MODEL 3

E. CONCLUSIONS

We have emphasized the nonlinear nature of ozone formation kinetics and the requirements for caution in generalizing about such a process. However, the idealized models recounted in this chapter do have some claim to physical significance, and in each of them we observe some degree of enhancement of ozone formation caused by a mixing of airport and freeway emissions. Thus, our analysis leads us to conclude that such enhancement occurs regularly in the atmosphere. The simulations presented in this chapter were formulated to demonstrate enhancement effects; enhancement in the atmosphere will be insignificant in many cases due to the mixing of air parcels having very different concentrations of pollutants or other forms of dilution.

VI CONCLUSIONS

The purpose of this research is to provide a basis for estimating the contribution of jet exhaust to smog. We began by searching the available literature on jet exhaust emissions in an attempt to determine both their composition and quantity. Virtually all the hydrocarbon emissions were found to come from the taxi-idle mode. Various engines, fuels, and operating conditions were found to give a range of hydrocarbon mixes. By computer simulation, these mixes were shown to be capable of generating high concentrations of ozone in the presence of nitrogen oxides and sunlight. The computer simulations used hydrocarbon emissions data and various amounts of nitrogen oxides as starting conditions, as in a smog chamber experiment. The results of the simulations were qualitatively similar: each mixture of hydrocarbons showed two regions of roughly equal potential for ozone formation, one at high HC/NO_x ratios and the other at low ratios. The maximum potential for ozone formation occurred at an intermediate HC/NO_x ratio.

The sensitivity of these simulations to various parameters was studied and the relevance of these computer simulations to the actual atmosphere was discussed. In general, a change in an input parameter caused one of two effects: either the induction time to the ozone peak changed or the maximum amount of ozone formed was affected. The length of the induction period was most sensitive to the presence of photochemical radical precursors (such as nitrous acid and aldehydes), uncertainties associated with sensitive reactions in the kinetic mechanism, and the NO/NO_2 ratio. The parameters that had the greatest effect on the amount of ozone formed were the closure parameters (which have not yet been established using data from smog chamber experiments) and the rate constants that are intended to make the kinetic mechanism applicable to longer chain hydrocarbons. Surprisingly, the amount of ozone formed was sensitive to the values of the closure parameters and rate constants only at low HC/NO_x ratios. Published jet emissions data show that

these emissions have high HC/NO_x ratios. Automobile emissions, on the other hand, have low HC/NO_x ratios, but the original closure parameters and rate constants were validated for these emissions at low HC/NO_x ratios.

Our results indicate that atmospheric blending of jet emissions (high HC/NO_x ratio) with automobile emissions (low HC/NO_x ratio) may produce a mixture having an intermediate HC/NO_x ratio associated with increased ozone production. Control strategies for ozone are usually most effective when they shift the HC/NO_x emissions ratio away from this intermediate ratio. For the case of jet emissions, however, the possibility of their mixing with automobile exhaust must be considered. The ozone isopleths from our simulations indicate that reductions in nitrogen oxide emissions alone would produce the largest reductions in ozone for the jet emissions by themselves. But this strategy would be effective only for airports located in areas with no sources of NO_x*; it would not control the enhancement of ozone formation that might arise from the mixing of jet emissions with nitrogen oxides from other sources (such as automobiles or fossil-fueled power plants).

According to Bahr and Gleason (1974), the application of existing technology could reduce hydrocarbons emitted by jets during the taxi-idle mode by a factor of ten. Such a reduction in aircraft hydrocarbon emissions would have a number of effects. The overall emissions (and likewise the overall potential for oxidant formation) would be reduced. The HC/NO_x ratio of jet emissions would more closely match typical urban ratios, which are due mostly to automobile emissions. A sufficient change in the HC/NO_x ratio of jet emissions would eliminate the possibility of an enhancement effect from the mixing of automobile and aircraft emissions. If the HC/NO_x emissions ratio for jet aircraft was reduced to that of automobiles, future studies like the present one would require experimental validation of the closure parameters for long chain molecules as previously mentioned. The hydrocarbon mixtures used in the simulations might also require revision, since reducing the HC/NO_x ratio of an engine's emissions might change the composition of its

*Rasmussen (1972) has shown that rural areas have high HC/NO_x ratios.

exhaust hydrocarbons. And lastly, such a reduction might reduce the relative importance of the taxi-idle mode as a source of emissions.

It is important to keep in mind that the conclusions drawn from this study are based on results derived for a well mixed system; chemistry was examined in depth but transport and mixing were not. If future planning needs warrant more careful and accurate examination of the impact of jet emissions, it will be necessary from an analytic standpoint to incorporate the kinetic mechanism in a mesoscale air pollution simulation model that describes the relevant atmospheric processes. Results derived from exercising a model of this type would lead to less restrictive, more general conclusions.

APPENDIX
CONVERSION FACTORS

Due to the different methods of reporting emissions data (e.g., lbs., lbs./hour, lbs./1000 lbs. fuel, ppm as carbon, etc.), a more uniform system of units was used in this report: All data taken from studies by different investigators were reported in the units they used, but all hydrocarbon/NO_x ratios were reported as moles of carbon/moles of NO_2. All data of hydrocarbon emissions were converted to moles of carbon from pounds by multiplying by 37.88 moles as carbon/lb. All data of oxides of nitrogen emissions (unless specified otherwise) were converted from units of lbs. to moles of NO_2 by multiplying by 9.85 moles as NO_2/lb.

The sections on synergistic effects required emissions per total LTO cycle. Therefore, where emission rates were reported for individual modes (in units of lbs./hour or kg/hour), the rates were multiplied by the fraction of time spent in each mode. The time factors are taken from Table 3.

The input data for the computer simulations require concentrations in units of ppm as "some" molecule. Therefore, a converting factor is needed to convert ppm as carbon to ppm as a molecule. For aircraft systems, the study by Conkle et al. (1975) of the T-56 combustor was the most detailed. Even though the T-56 engines constitute only 11.2 percent of the major engines in the U.S. Air Force (Table 32), they are used in 15.8 percent of the flying hours. Conkle et al. reported the following compositions for hydrocarbons emitted at 15 psig combustor pressure: 57 percent alkanes, 18 percent alkenes, 7 percent aromatics, and 17 percent aldehydes. Multiplying these percentages by the molecular weight reported by Conkle et al. for each group, an average molecular weight of 86 g/mole is found. The hydrocarbon C_6H_{14} has the same molecular weight. Therefore, this molecule is used to convert from moles of carbon to moles as an "average" molecule. The converting factor is 0.14 moles as C_6H_{14}/moles as carbon. For the

Table 32

USAF AIRCRAFT ENGINE USAGE*

Engine	Percentage of Major Engines	Percentage of Flying Hours
J-57	30.1	26.3
TF-33	9.3	17.8
T-56	11.2	15.8
J-85	10.5	10.5
J-79	15.6	9.5
J-69	6.6	7.2
J-60	1.4	2.5
T-76	.9	1.6
TF-30	2.8	1.5
J-33	2.2	1.5
TF-39	.9	1.1
J-75	2.0	1.0
T-58	1.4	1.0
TF-41	1.7	.8
J-65	1.1	.5
T-64	.5	.4
T-53	.6	.3
T-400	.5	.3
J-71	.4	.3
J-47	.3	.1

*Based on data from AFLC/WPAFB for 19,036 installed active engines for the first quarter of 1972.

Source: Naugle (1974).

automobile system, the Bureau of Mines (1973) reported that most of the alkanes emitted were C_3-C_5 molecules, most of the alkenes were C_3-C_5 molecules, and the aromatics were C_7+ molecules. They also reported that hydrocarbon emissions were 20 percent alkanes, 45 percent alkenes, and 35 percent aromatics. This gave an average molecular weight around 68 g/mole. A C_4 molecule was assumed to be the average molecule for the automobile system. The converting factor is 0.18 moles as C_4/moles as carbon.

NO_x concentrations were calculated by multiplying by 1.44 moles as NO_x/mole as NO_2. The average molecular weight of NO_x was found by assuming the ratio of NO/NO_2 to be equal to 9.

REFERENCES

Atkinson, R., and J. N. Pitts, Jr. (1975), J. Phys. Chem., Vol. 79, pp. 295-298.

Bahr, D. W., and C. C. Gleason (1974), "Technology for the Reduction of Aircraft Turbine Engine Pollutant Emissions," presented at 9th Congress of the International Council of the Aeronautical Sciences, Haifa, Israel (August 25-30).

Bogdan, L., and H. T. McAdams (1971), "Analysis of Aircraft Exhaust Emission Measurements," Cornell Aeronautical Laboratory, Incorporated, Buffalo, New York, CAL Report No. NA-5007-K-1.

Broderick, A. J., W. E. Harriott, and R. A. Walter (1971), "Aircraft Emissions Survey," Report No. DOT-TSC-OST-71-5, U. S. Department of Transportation, Cambridge, Massachusetts.

Bureau of Mines (1973), "Aldehyde and Reactive Organic Emissions from Motor Vehicles," Parts I and II, Publications EPA-IAG-0188, MSPCP-IAG-001, Fuels Combustion Research Group, Bureau of Mines, Bartlesville, Oklahoma.

Cirillo, R. R. J. F. Tschanz, and J. E. Camaioni (1975), "An Evaluation of Strategies for Airport Air Pollution Control," Publication EPA-IAG-095(D), Argonne National Laboratory, Argonne, Illinois.

Conkle, J. P., W. W. Lackey, and R. L. Miller (1975), "Hydrocarbon Constituents of T-56 Combustor Exhaust," Report No. SAM-TR-75-8, USAF School of Aerospace Medicine, Brooks Air Force Base, Texas.

Davis, D. D. (1974), "Absolute Rate Constants for Elementary Reactions of Atmospheric Importance: Results from the University of Maryland's Gas Kinetics Laboratory," Chemistry Department, University of Maryland, College Park, Maryland.

Doyle, G. J., A. C. Lloyd, K. R. Darnall, A. M. Winer, and J. N. Pitts, Jr. (1975), Environ. Sci. Techno., Vol. 9, p. 237.

Durbin, P. A., T. A. Hecht, and G. Z. Whitten (1975), "Mathematical Modeling of Simulated Photochemical Smog," Publication EPA-650/4-75-026, Environmental Protection Agency, Research Triangle Park, North Carolina.

EPA (1973), "Compilation of Air Pollutant Emission Factors," AP-42, Environmental Protection Agency, Research Triangle Park, North Carolina, pp. 3.2.1-1 to 3.2.1-5 (April, 1973).

EPA (1973), "Supplement No. 2 for Compilation of Air Pollutant Emission Factors," 2nd Ed. Publication AP-42, Environmental Protection Agency, Research Triangle Park, North Carolina.

_____, (1971), "National Primary and Secondary Ambient Air Quality Standards, Appendix D--Reference Method for the Measurement of Photochemical Oxidants Corrected for Interferences due to Nitrogen Oxide and Sulfur Dioxide," Federal Register, Vol. 36 and 84, p. 8195 (April 30).

_____, (1975), "Supplement No. 5 for Compilation of Air Pollutant Emission Factors," 2nd Ed., Environmental Protection Agnecy, Research Triangle Park, North Carolina.

Fox, D. L., R. Kamens, and H. E. Jeffries (1975), "Photochemical Smog Systems: Effect of Dilution on Ozone Formation," Science, Vol. 188, p. 1113.

Groth, R. H., and D. J. Robertson (1974), "Reactive and Unreactive Hydrocarbon Emissions from Gas Turbine Engines," 67th Annual Meeting of the Air Pollution Control Association (June 9-13), Denver, Colorado.

Hampson, R. F., and D. Garvin (1975), "Chemical Kinetic and Photochemical Data for Modelling Atmospheric Chemistry," NBSTN 866, National Bureau of Standards, Washington, D. C.

Hecht, T. A., M. K. Liu, and D. C. Whitney (1974a), "Mathematical Simulation of Smog Chamber Photochemical Experiments," Report R74-9, Systems Applications, Incorporated, San Rafael, California.

Hecht, T. A., J. H. Seinfeld, and M. C. Dodge (1974b), "Further Development of Generalized Kinetic Mechanism for Photochemical Smog," Environ. Sci. Technol., Vol. 8, p. 327.

Jeffries, H., D. Fox, and R. Kamens (1974), "Outdoor Smog Chambers," presented at EPA Smog Chamber Conference (October 16-17), Research Triangle Park, North Carolina.

LAAPCD (1971), "Study of Jet Aircraft Emissions and Air Quality in the Vicinity of the Los Angeles International Airport," Los Angeles Air Pollution Control District Report No. CPA22-69-137, Los Angeles, California.

Lozano, E. R., W. W. Melvin, and S. Hochheiser (1968), "Air Pollution Emissions from Jet Engines," J. Air Pollution Control Assoc., Vol. 18, p. 393.

Naugle, D. F. (1974), "Pollution Emission Analysis of Selected Air Force Aircraft," Report No. AFWL-TR-74-507, Weapons Laboratory, Kirtland Air Force Base, New Mexico.

Northern Research and Engineering Corporation (1968), "Nature and Control of Aircraft Engine Exhaust Emissions," CFSTI No. PB-187771 (November).

O'Neal, H. E., and C. Blumstein (1973), Int. J. Chem. Kinetics, Vol. 5., pp. 397-413.

Project Clean Air (1970), Task Force Assessments Vol. 4, University of California.

Rasmussen, R. A. (1972), "What Do the Hydrocarbons From Trees Contribute to Air Pollution?" J. Air Pollution Control Assoc., Vol. 22, pp. 537-543.

Roberts, P.J.W. and P. M. Roth (1971), Appendix E of "Development of a Simulation Model for Estimating Ground Level Concentrations of Photochemical Pollutants," Report 71 SAI-7, Systems Applications, Inc., San Rafael, California.

Rote, D. M., R. W. Hecht, I. T. Wong, R. R. Cirillo, L. E. Wanger, and J. Pratapas (1973), "Airport Vicinity Air Pollution Study," Report No. FAA-RD-73-113, Argonne National Laboratory, Argonne, Illinois.

Segal, H. M. (1975), "Realistic Mixing Depths for Above Ground Aircraft Emissions," J. Air Pollution Control Assoc., Vol. 25, p. 1054.